

# A GENERALIZED GEOMETRIC THEORETICAL FRAMEWORK OF CENTROID DISCRIMINANT ANALYSIS FOR LINEAR CLASSIFICATION OF MULTI-DIMENSIONAL DATA

008 **Anonymous authors**

009 Paper under double-blind review

## ABSTRACT

014 With the advent of the neural network era, traditional machine learning methods  
 015 have increasingly been overshadowed. Nevertheless, continuing to research about  
 016 the role of geometry for learning in data science is crucial to envision and un-  
 017 derstand new principles behind the design of efficient machine learning. Linear  
 018 classifiers are favored in certain tasks due to their reduced susceptibility to over-  
 019 fitting and their ability to provide interpretable decision boundaries. However,  
 020 achieving both scalability and high predictive performance in linear classification  
 021 remains a persistent challenge. Here, we propose a theoretical framework named  
 022 geometric discriminant analysis (GDA). GDA includes the family of linear clas-  
 023 sifiers that can be expressed as function of a centroid discriminant basis (CDB0)  
 024 - the connection line between two centroids - adjusted by geometric corrections  
 025 under different constraints. We demonstrate that linear discriminant analysis (LDA)  
 026 is a subcase of the GDA theoretical framework, and we show its convergence to  
 027 CDB0 under certain conditions. Then, based on the GDA framework, we propose  
 028 an efficient linear classifier named centroid discriminant analysis (CDA) which  
 029 is defined as a special case of GDA under a 2D plane geometric constraint. CDA  
 030 training is initialized starting from CDB0 and involves the iterative calculation of  
 031 new adjusted centroid discriminant lines whose optimal rotations on the associated  
 032 2D planes are searched via Bayesian optimization. CDA has good scalability  
 033 (quadratic time complexity) which is lower than LDA and support vectors machine  
 034 (SVM) (cubic complexity). Results on 27 real datasets across classification tasks  
 035 of standard images, medical images and chemical properties, offer empirical evi-  
 036 dence that CDA outperforms other linear methods such as LDA, SVM and logistic  
 037 regression (LR) in terms of scalability, performance and stability. Furthermore,  
 038 we show that linear CDA can be generalized to nonlinear CDA via kernel method,  
 039 demonstrating improvements on the linear version with tests on [three](#) challenging  
 040 datasets of images and chemical data. GDA general validity as a new theoretical  
 041 framework may inspire the design of new classifiers under the definition of different  
 042 geometric constraints, paving the way towards more deeper understanding of the  
 043 role of geometry in learning from data.

## 1 INTRODUCTION

044 Linear classifiers are often favored over nonlinear models, such as neural networks, for certain tasks  
 045 due to their comparable performance in high-dimensional data spaces, faster training speeds, reduced  
 046 tendency to overfit, and greater interpretability in decision-making (Varoquaux et al. (2017); Yuan  
 047 et al. (2012)). Notably, linear classifiers have demonstrated performance on par with convolutional  
 048 neural networks (CNNs) in medical classification tasks, such as predicting Alzheimer’s disease from  
 049 structural or functional brain MRI images (Schulz et al. (2020); Varoquaux & Cheplygina (2022)).

050 These linear classifiers can be categorized into several types based on the principles they use to define  
 051 the decision boundary or classification discriminant, as described below, where  $N$  is the number of  
 052 samples,  $M$  is the number of features and  $k$  denotes an iteration term:

- The minimum distance classifier (MDC) (Duda et al. (2001)) which is a prototype-based classifier that assigns points according to the perpendicular bisector boundary between the centroids of two groups. This classifier has  $O(NM)$  training time complexity.
- Fisher’s linear discriminant analysis (LDA, specifically refer to Fisher’s LDA in this study) is a variance-based classifier which can be trained in cubic time complexity  $O(NM^2 + M^3)$ . While faster implementations like spectral regression discriminant analysis (SRDA) (Cai et al. (2008)) claim lower training time complexity, their efficiency depends on specific conditions, such as a sufficiently small iterative term and sparsity in the data. These constraints limit SRDA’s applicability in real-world classification tasks.
- Support vector machine (SVM) (Cortes & Vapnik (1995)) with a linear kernel is a maximum-margin classifier, which has a training time complexity of  $O(N^3)$ . Fast implementations include Liblinear (referred to as fast SVM) and SVM-SGD, which use coordinate descent and stochastic gradients respectively, achieving quasi-quadratic time complexity  $O(kNM)$ .
- Perceptron (Minsky & Papert (1969)) is a misclassification-triggered ruled-based classifier. Its training time complexity is  $O(kNM)$ .
- Logistic regression (LR) (Panda et al. (2022)) is a statistics-based classifier. It can be trained using either maximum likelihood estimation (MLE) or iteratively reweighted least squares, with time complexity of  $O(NM^2 + M^3)$  and  $O(NM^2)$  respectively, and with  $O(kNM)$  using the same coordinate descent technique in Liblinear.

Among linear classifiers, MDC offers the lowest training time complexity but suffers from limited performance due to its overly simplified decision boundary. Widely used methods such as LDA and SVM are often favored for their strong predictive capabilities. However, these methods can be computationally expensive, particularly for large-scale datasets. Hence, achieving both high scalability and strong predictive performance remains a challenging tradeoff, highlighting the need for new approaches that balance these competing demands.

To address this challenge, this paper makes the following **3 key contributions**:

- **A geometric theoretical framework for classifiers:** (See Appendix. A.1 for explanation of the term theoretical framework.) This study introduces a geometric framework, geometric discriminant analysis (GDA), to unify certain linear classifiers under a common theoretical model. GDA leverages a special type of centroid discriminant basis (CDB0), a vector connecting the centroids of two classes, which serves as the foundation for constructing classifier decision boundaries. The GDA framework adjusts the CDB0 through geometric corrections under various constraints, enabling the derivation of classifiers with desirable properties. Notably, we show that: MDC is a special case of GDA, where geometric corrections are not applied to CDB0; linear discriminant analysis (LDA) is a special case of GDA, where the CDB0 is corrected by maximizing the projection variance ratio.
- **A high-performance and scalable linear geometric classifier:** Building upon the GDA framework, we propose centroid discriminant analysis (CDA), a novel geometric classifier that iteratively adjusts the CDB through performance-dependent rotations on 2D planes. These rotations are optimized via Bayesian optimization, enhancing the decision boundary’s adaptability efficiently. CDA achieves lower training time complexity (quadratic) and is more efficient than LDA and SVM. Experimental evaluations on 27 real-world datasets of standard images, medical images and chemical property data, reveal that CDA consistently outperforms LDA, SVM and and LR in predictive performance, scalability, and stability.
- **Nonlinear geometric classification via kernel method:** For complex data where linear models are not enough, CDA supports nonlinear classification via kernel method. We demonstrated with challenging image and chemical datasets that kernel CDA improved over linear CDA and outperformed kernel SVM and kernel LDA. While the core CDA algorithm is efficient, the kernelized version inherits the standard computational bottleneck of kernel matrix construction. Nonetheless, while kernel CDA offers greater expressiveness and improved capability, linear CDA remains highly valuable for real-world tasks due to its superior training efficiency, interpretability, and reduced risk of overfitting.

More importantly, we emphasize that CDA not only achieves robust predictive performance but also offers superior computational efficiency. Unlike traditional methods such as LDA and SVM,

108 which typically exhibit cubic time complexity, CDA operates with quadratic complexity, resulting  
 109 in significantly faster runtimes in practice. These advantages make CDA particularly attractive for  
 110 real-world applications, where scalability, interpretability, and efficiency are essential. As linear  
 111 classifiers remain widely used across scientific domains for their transparency and speed, CDA  
 112 represents a valuable advancement for practitioners seeking reliable and computationally lightweight  
 113 solutions. Lastly, the GDA theoretical framework, from which CDA is derived, may inspire new  
 114 classifiers under the definition of different geometric constraints.

## 2 GEOMETRIC DISCRIMINANT ANALYSIS (GDA)

118 In this study, we propose a generalized geometric theoretical framework for centroid-based linear  
 119 classifiers. In geometry, the generalized definition of centroid is the weighted average of points. For  
 120 binary classification problem, training a linear classifier involves finding a discriminant (perpendicular  
 121 to the decision boundary) and a bias. In GDA, we focus on the centroid discriminant basis (CDB)  
 122 which is defined as the unit vector from the centroid of negative class to positive class. Specifically, we  
 123 focus on a particular discriminant termed as CDB0, which is constructed from centroids with uniform  
 124 sample weights. GDA theoretical framework incorporates all the classifiers whose classification  
 125 discriminant is CDB0 adjusted by geometric corrections on CDB0, which is described in details in  
 126 the following using an instance with LDA. Moreover, in the GDA theoretical framework, the classifier  
 127 discriminants are scaling-invariant, which is explained in Appendix. A.2. Thus, throughout,  $\gamma \neq 0$   
 128 denotes a generic constant independent of the variable of interest. **The bias is also excluded from the**  
 129 **analysis since it can be naturally determined after the discriminant is fixed (see Appendix. A.3).**

130 Without loss of generality, assume a two-dimensional space (see Appendix. E for any-dimensional  
 131 proofs). We derive the GDA theoretical framework as a generalization of Fisher's LDA (hereafter  
 132 referred to simply as LDA) and includes it under a certain geometric constraint. In LDA, the linear  
 133 discriminant (LD) is derived as the maximization of between-class variance to within-class variance:

$$134 \quad S = \frac{\sigma_b^2}{\sigma_w^2} = \frac{(\mathbf{w}^T \boldsymbol{\nu}_1 - \mathbf{w}^T \boldsymbol{\nu}_0)^2}{\mathbf{w}^T \boldsymbol{\Sigma}_0 \mathbf{w} + \mathbf{w}^T \boldsymbol{\Sigma}_1 \mathbf{w}} = \frac{(\mathbf{w}^T \boldsymbol{\nu}_1 - \mathbf{w}^T \boldsymbol{\nu}_0)^2}{\mathbf{w}^T (\boldsymbol{\Sigma}_0 + \boldsymbol{\Sigma}_1) \mathbf{w}} \quad (1)$$

136 where  $\boldsymbol{\nu}_0$  and  $\boldsymbol{\nu}_1$  are the means of negative and positive class,  $\boldsymbol{\Sigma}_0$  and  $\boldsymbol{\Sigma}_1$  are their covariance  
 137 matrices,  $\mathbf{w}$  is the projection coefficient. The maximum is obtained when  $N\boldsymbol{\Sigma}\mathbf{w} = \boldsymbol{\nu}_1 - \boldsymbol{\nu}_0$  (Fisher  
 138 (1936)), or  $N\boldsymbol{\Sigma}\gamma\mathbf{w}_{LD} = \boldsymbol{\nu}_1 - \boldsymbol{\nu}_0$ , where  $\mathbf{w}_{LD}$  is the normalized LDA discriminant in the GDA  
 139 theoretical framework with a normalizing constant  $\gamma$ ,  $N$  is the total number of samples.  $\boldsymbol{\Sigma}$  is the sum  
 140 of within-class covariance matrices of each class  $\boldsymbol{\Sigma}_0 + \boldsymbol{\Sigma}_1$ :

$$141 \quad \boldsymbol{\Sigma} = \begin{bmatrix} \sigma_{xx}^2 & \sigma_{xy}^2 \\ \sigma_{yx}^2 & \sigma_{yy}^2 \end{bmatrix} + \begin{bmatrix} \sigma_{xx}^2 & \sigma_{xy}^2 \\ \sigma_{yx}^2 & \sigma_{yy}^2 \end{bmatrix} = \begin{bmatrix} \sigma_{xx}^2 & \sigma_{xy}^2 \\ \sigma_{yx}^2 & \sigma_{yy}^2 \end{bmatrix} \quad (2)$$

143 And the inverse of the covariance matrix  $\boldsymbol{\Sigma}$  is:

$$145 \quad \boldsymbol{\Sigma}^{-1} = \frac{\text{adj}(\boldsymbol{\Sigma})}{|\boldsymbol{\Sigma}|} = \frac{1}{\sigma_{xx}^2 \sigma_{yy}^2 - \sigma_{xy}^2 \sigma_{yx}^2} \begin{bmatrix} \sigma_{yy}^2 & -\sigma_{xy}^2 \\ -\sigma_{yx}^2 & \sigma_{xx}^2 \end{bmatrix} = \frac{\sigma_{yy}^2}{\sigma_{xx}^2 \sigma_{yy}^2 - \sigma_{xy}^2 \sigma_{yx}^2} \begin{bmatrix} 1 & -\frac{\sigma_{xy}^2}{\sigma_{yy}^2} \\ -\frac{\sigma_{yx}^2}{\sigma_{yy}^2} & \frac{\sigma_{xx}^2}{\sigma_{yy}^2} \end{bmatrix} \quad (3)$$

148 where  $\text{adj}(\boldsymbol{\Sigma})$  is the adjugate of  $\boldsymbol{\Sigma}$ . Let  $\Delta\boldsymbol{\mu}$  denote the unit vector of  $\Delta\boldsymbol{\nu}$ , then  $\boldsymbol{\nu}_1 - \boldsymbol{\nu}_0 = \gamma(\boldsymbol{\mu}_1 - \boldsymbol{\mu}_0) = \gamma\Delta\boldsymbol{\mu} = \gamma[\Delta\mu_x, \Delta\mu_y]^T$ , and  $\mathbf{w}_{LD} = \gamma\boldsymbol{\Sigma}^{-1}(\boldsymbol{\nu}_1 - \boldsymbol{\nu}_0) = \gamma\boldsymbol{\Sigma}^{-1}(\boldsymbol{\mu}_1 - \boldsymbol{\mu}_0)$ . Further,

$$151 \quad \mathbf{w}_{LD} = \frac{\gamma\sigma_{yy}^2}{\sigma_{xx}^2 \sigma_{yy}^2 - \sigma_{xy}^2 \sigma_{yx}^2} \begin{bmatrix} 1 & -\frac{\sigma_{xy}^2}{\sigma_{yy}^2} \\ -\frac{\sigma_{yx}^2}{\sigma_{yy}^2} & \frac{\sigma_{xx}^2}{\sigma_{yy}^2} \end{bmatrix} \begin{bmatrix} \Delta\mu_x \\ \Delta\mu_y \end{bmatrix} = \gamma \left( \begin{bmatrix} 1 & 0 \\ 0 & 1 \end{bmatrix} + \begin{bmatrix} 0 & -\frac{\sigma_{xy}^2}{\sigma_{yy}^2} \\ -\frac{\sigma_{yx}^2}{\sigma_{yy}^2} & \frac{\sigma_{xx}^2}{\sigma_{yy}^2} - 1 \end{bmatrix} \right) \begin{bmatrix} \Delta\mu_x \\ \Delta\mu_y \end{bmatrix} \\ 154 \quad = \gamma([\Delta\mu_x, \Delta\mu_y]^T + \mathbf{C}_{\text{correction}}[\Delta\mu_x, \Delta\mu_y]^T) \quad (4)$$

156 where  $\mathbf{C}_{\text{correction}}$  is a correction matrix that acts as the second-order term associated with the sum  
 157 of covariance matrices. Since  $\mathbf{w}_{CDB0}$  is the unit vector constructed from centroids with uniform sample  
 158 weights (i.e., arithmetic means), it can be written as  $\mathbf{w}_{CDB0} = [\Delta\mu_x, \Delta\mu_y]^T$ . As in the covariance  
 159 matrix,  $\sigma_{xy}^2 = \sigma_{yx}^2$ , and let  $c_{xy} = \sigma_{xy}^2 / \sigma_{yy}^2$ ,  $c_{xx/yy} = \sigma_{xx}^2 / \sigma_{yy}^2 - 1$ , the linear discriminant in Eq. 4  
 160 can be compressed into the following general form (Fig. 4a-c, general case):

$$161 \quad \mathbf{w}_{GD} = \mathbf{w}_{LD} = \gamma \left( \begin{bmatrix} \Delta\mu_x \\ \Delta\mu_y \end{bmatrix} + \begin{bmatrix} 0 & -c_{xy} \\ -c_{xy} & c_{xx/yy} \end{bmatrix} \begin{bmatrix} \Delta\mu_x \\ \Delta\mu_y \end{bmatrix} \right) = \gamma(\mathbf{w}_{CDB0} + \mathbf{C}_{\text{correction}}\mathbf{w}_{CDB0}). \quad (5)$$

162 Since from [Eq. 5](#),  $w_{LD}$  can be decomposed into the basis  $w_{CDB0}$  and a correction on the basis, we  
 163 write out  $w_{GD}$  to indicate that  $w_{LD}$  is a geometrical discriminant (GD), a discriminant geometrically  
 164 modified from  $w_{CDB0}$ . This geometrical modification can be intuitively interpreted as performing  
 165 rotations on  $w_{CDB0}$ .

166 Starting from [Eq. 5](#), we have the following special cases to consider, which represent different forms  
 167 of geometrical modification applied to  $w_{CDB0}$ :

168 **Special case 1.** If we assume two variables have the same variance ( $\sigma_{xx}^2 = \sigma_{yy}^2$ ), then  $c_{xx/yy} = 0$ .  
 169 [Eq. 5](#) becomes (Fig. 4, special case 1):

$$171 \quad w_{LD} = \gamma \left( \begin{bmatrix} \Delta\mu_x \\ \Delta\mu_y \end{bmatrix} + \begin{bmatrix} 0 & -c_{xy} \\ -c_{xy} & 0 \end{bmatrix} \begin{bmatrix} \Delta\mu_x \\ \Delta\mu_y \end{bmatrix} \right) = \gamma(w_{CDB0} + C_{\text{correction}} w_{CDB0}) \quad (6)$$

174 From [Eq. 6](#), there are two special cases:

175 **Special case 1.1.** If two covariance matrices are same ( $\Sigma_0 = \Sigma_1$ ), then the following also holds:  
 176  $c_{xy} = \frac{\sigma_{xy}^2}{\sigma_{yy}^2} = \frac{\mathbb{E}[(x-\mu_x)(y-\mu_y)]}{\sigma_x \sigma_y} = r_{xy}$  where  $r_{xy}$  is the Pearson correlation coefficient (PCC) between  
 177 x and y of the samples in each class. Equation 6 becomes (Fig. 4, special case 1.1):

$$179 \quad w_{LD} = \gamma \left( \begin{bmatrix} \Delta\mu_x \\ \Delta\mu_y \end{bmatrix} + \begin{bmatrix} 0 & -r_{xy} \\ -r_{xy} & 0 \end{bmatrix} \begin{bmatrix} \Delta\mu_x \\ \Delta\mu_y \end{bmatrix} \right) = \gamma(w_{CDB0} + C_{\text{correction}} w_{CDB0}) \quad (7)$$

182 **Special case 1.1.1.** From [Eq. 7](#), if there is no correlation between x and y variables (e.g.,  $r_{xy} = 0$ ),  
 183 then the equation becomes (Fig. 4, special case 1.1.1):

$$185 \quad w_{LD} = \gamma([\Delta\mu_x, \Delta\mu_y]^T) = [\Delta\mu_x, \Delta\mu_y]^T = w_{CDB0} \quad (8)$$

186 which is equivalent to MDC method except for the bias. The second equal mark is from the fact that  
 187  $[\Delta\mu_x, \Delta\mu_y]^T$  is already a unit vector, thus  $\gamma = 1$ .

189 **Special case 1.2.** From [Eq. 6](#), if two classes are symmetric about one variable, i.e.,  $\sigma_0^2_{xy} = -\sigma_1^2_{xy} \neq$   
 190 0, then  $c_{xy} = \frac{\sigma_{xy}^2}{\sigma_{yy}^2} = 0$ . In this case, the obtained discriminant is the same as in Special case 1.1.1  
 191 (Fig. 4, special case 1.2):

$$193 \quad w_{LD} = \gamma[\Delta\mu_x, \Delta\mu_y]^T = [\Delta\mu_x, \Delta\mu_y]^T = w_{CDB0} \quad (9)$$

195 Fig. 4c shows how LDA applies geometric modifications to  $w_{CDB0}$  as a shape adjustment for different  
 196 shapes of data. When two covariance matrices are similar (Special case 1.1), the correction term acts  
 197 only when the variables x and y have a certain extent of correlation and increases with this correlation  
 198 (Fig. 4, the third row). Interestingly, when further assumptions are made that two variables have no  
 199 correlation (Special case 1.1.1), or when two classes are symmetric about one variable (Special case  
 200 1.2), we can see from [Eq. 8-9](#) that  $w_{LD}$  will approach  $w_{CDB0}$ , which is indeed what we observe in  
 201 the last two rows of Fig. 4. Videos showing these special cases using 2D simulated data can be found  
 202 from this link<sup>1</sup>.

203 The demonstrations of all these cases for higher-dimensional space are in the Appendix. E.

204 From the above derivation, [Eq. 5-9](#) show that the solution of LDA can be represented by  $w_{CDB0}$   
 205 superimposed with a geometric correction on  $w_{CDB0}$ , and the geometric correction term is obtained  
 206 under the constraint of [Eq. 1](#), which solves the maximization of the projection variance ratio. Without  
 207 loss of generality, the conclusion can be extended to other linear classifiers with different constraints  
 208 imposed on the geometric correction term, for instance MDC, where the correction terms are all zero.

209 Here, we propose the generalized GDA theoretical framework in which not only the geometric  
 210 correction term can impose any constraint based on different principles, but also any number of  
 211 correction terms can act together on  $w_{CDB0}$  to create the classification discriminant, given by:  
 212

$$213 \quad w_{GD} = \gamma(w_{CDB0} + C_1 w_{CDB0} + C_2 w_{CDB0} + \dots + C_n w_{CDB0}) \quad (10)$$

214 in which LDA only involves the first order base term  $w_{CDB0}$  and the second order correction  $C_1$ ,  
 215 while higher order terms  $C_2, C_3, \dots$  become 0. Fig. 1 shows that LDA is derived by the general GD

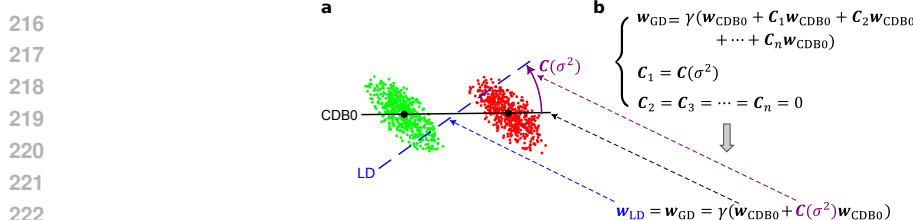


Figure 1: (a) A 2D instance showing that LD (blue dashed) can be constructed from CDB0 (black solid) using covariance correction which is a geometrical correction. (b) The evolution from CDB0 to LD. The first equation is the general form of geometrical discriminants (GD) that can be constructed by CDB0 with geometric corrections. If only one correction exists and this correction is a covariance-related matrix, LD can be derived from the general expression.  $\gamma$  denotes a normalizing factor. LD: Linear Discriminant; CDB0: Centroid Discriminant Basis 0.

equation imposing one variance-based geometric correction in Fig. 1b, shown in Fig. 1a using an instance of 2d artificial data with specific covariance.

Since GDA is a framework rather than a specific algorithm, it does not itself provide global theoretical guarantees on performance or convergence. Instead, such guarantees must be established for each concrete classifier instantiated within the framework. Therefore, in Section D we provide a section on CDA convergence proof, where we provide a formal mathematical proposition showing that, under the defined fitness function, CDA is guaranteed to converge. This convergence relies solely on the monotonicity and boundedness of the objective sequence and therefore holds independently of the specific 1D optimizer employed (e.g., BO, Brent’s method, etc).

### 3 CENTROID DISCRIMINANT ANALYSIS (CDA)

Based on the GDA theoretical framework, in this study we propose an efficient geometric centroid-based linear classifier named centroid discriminant analysis (CDA), then introduce the extension to nonlinear classification via kernel method in section 5. As described by Eq. 10 in the GDA theory, the model of a geometric classifier can be expressed by the basis CDB0 imposed by geometric corrections on this basis. We first give the conclusion that the final discriminant of CDA after  $n$  rotations is in the form  $\mathbf{w}_{\text{CDA}}^{(n)} = \gamma(\mathbf{w}_{\text{CDB0}} + \mathbf{C}_1 \mathbf{w}_{\text{CDB0}}) = \mathbf{w}_{\text{GD}}$ , where  $\mathbf{C}_1 = \mathbf{I} - \prod^n \mathbf{A}_{\text{cda}}$  is the geometric correction operator term,  $\mathbf{I}$  is the identity operator, and  $\mathbf{A}_{\text{cda}}$  is the operator of a single CDA rotation). The complete derivation of CDA in GDA theoretical framework can be found in Appendix. F.

From the geometric point of view, CDA is built on the basis CDB0 in the GDA theoretical framework, then subjected to a series of geometric constraints guiding the rotations of the discriminant CDB in high-dimensional spaces. CDA follows a performance-dependent training that starting from CDB0 involves the iterative calculation of new adjusted centroid discriminant lines whose optimal rotations on the associated 2D planes are searched via Bayesian optimization. The following parts together with Figure. 5 describe the CDA workflow, mechanisms and principles in detail.

**Performance-associated CDB Classifier:** In GDA theoretical framework, CDB is defined as the unit vector pointing from the geometric centroid of the negative class to positive class. The geometric centroid is defined in a general sense which considers the weights of the data. The space of CDB consists of unit vectors obtained with all possible weights.

Apart from the discriminant line, a bias is further required to realize classification by offering a decision boundary for data projected onto the discriminant. We perform a search for this bias by checking the middle points of every two consecutive sorted projections. Thus, given  $N$  samples, there are  $N - 1$  candidates. We name the best candidate as optimal operating point (OOP) and select OOP according to a performance-score, defined as  $(F\text{score}^{\text{pos}} + F\text{score}^{\text{neg}} + AC\text{score})/3$  (see Appendix. G for definitions), where pos and neg means evaluating the metric for each class. The

<sup>1</sup><https://drive.google.com/drive/folders/1E3QqNzkBz7hdTwpBhEIA75px1AY4xxw3?usp=sharing>

270 performance score is a comprehensive metric that simultaneously considers sensitivity, recall, and  
 271 specificity, providing a fair evaluation that accounts for biased models trained on imbalanced data,  
 272 owing to the more conservative AC-score metric (Wu & Cannistraci (2025)). With this OOP search  
 273 strategy, any vector in the space of CDB is associated with a performance-score. The OOP search can  
 274 be performed efficiently in  $O(N \log N)$  time (see Alg. 3 for pseudocode). Importantly, during each  
 275 rotation within the 2D plane, CDA explicitly selects the direction that maximizes the performance  
 276 score, and progressively refines this choice through continuous rotations. Because the optimization  
 277 target is transparent at every step, CDA offers an inherently explainable learning process.

278 **CDA as Consecutive Geometric Rotations of CDB in 2D planes:** Our idea is to start the optimization  
 279 path from CDB0, continuously rotate the classification discriminant on 2D planes on which there  
 280 is a high probability of having a classification discriminant with better performance. To construct  
 281 such a 2D plane with another vector, a key observation is that the samples, whose projections onto  
 282 CDB are close to the decision boundary (i.e. OOP), should have more weights, because these samples  
 283 are prone to overlapping with samples from the other class, causing misclassification. Thus, we  
 284 compute another CDB using centroids with shifted sample weights toward OOP (see next part). On  
 285 the plane formed by these two CDBs, the best rotation is found by Bayesian optimization. For clarity,  
 286 we have the following definition: the first vector in each rotation is termed as CDB1, the second  
 287 vector in each rotation is termed as CDB2, the CDB searched with the best performance is termed as  
 288 CDA, and at the end of each rotation CDA becomes CDB1 for the next rotation. CDA rotation is used  
 289 to refer to this rotation process. Figure 5a shows the diagram for the first CDA rotation, where CDB1  
 290 equals to CDB0 calculated using uniform sample weights. The CDA training stops when meeting  
 291 any of the two criteria: (1) Reach the maximum 50 iterations. (2) the coefficient of variation (CV) of  
 292 the last 10 performance-score is less than a threshold, indicating that the training has converged (see  
 293 Alg. 1,2 and 4 for pseudocode).

294 **Sample Weights Update Strategy:** Given CDB1 and the associated OOP in each CDA rotation,  
 295 the distance of all projections to OOP can be obtained by  $d_i = |q_i - oop|$ ,  $\forall i \in \{1, 2, \dots, N\}$ ,  
 296 which is then reversed by  $d_r = |\mathbf{d} - \min(\mathbf{d}) - \max(\mathbf{d})|$ , in align with the purpose that points close  
 297 to decision boundary should have larger weights. Since only the relative information of sample  
 298 weights is important, they are L2-normalized and decay smoothly from previous sample weights by  
 299  $\alpha = \alpha \odot d_r / \|\alpha \odot d_r\|_2$ , where  $\odot$  indicates the Hadamard (element-wise) product. Specifically, in  
 300 the first CDA rotation, the CDB1 is obtained with uniform sample weights, which corresponds to  
 301 CDB0 in the GDA theoretical framework.

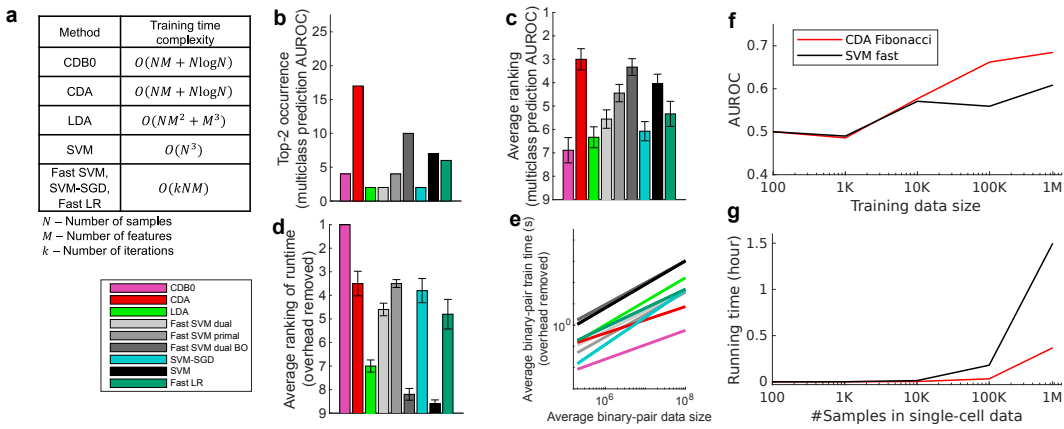
302 **Rotation Optimization:** The CDA rotation aims to search for a unit vector CDB with the best  
 303 performance-score in a 2d plane spanned by CDB1 and CDB2. There are several optimizers that  
 304 can realize this single-parameter search of rotation angle. Based on our findings in Section L, we  
 305 make the following recommendations. For maximum speed, Fibonacci search is the preferred choice,  
 306 and BO is a strong second option. Be aware that BO seems to prefer log-transform of the data. For  
 307 large-scale datasets, Fibonacci search remains the most efficient and still reliable method. In the main  
 308 article, we proceed with BO since due to its high performance. BO is a statistical-based technique to  
 309 estimate the global minimum of a function with as fewer evaluations as possible. CDA leverages this  
 310 high-efficiency characteristic of BO to achieve fast training. BO has  $O(Z^3)$  time complexity when it  
 311 searches a single parameter, where  $Z$  is the number of sampling-and-evaluations. CDA employs a  
 312 strategy that grows BO sampling times from 4 to the maximum 10 with CDA iterations (see Appendix  
 313 C.1). Figure 5b shows an instance of BO working process. Alg. 5 shows the pseudocode for the CDA  
 314 rotation as the black box function to optimize by BO.

315 **Finalization:** As a finalization step, on the best plane CDA refines the discriminant with a null-model  
 316 statistical test using 100 random CDB lines drawn from the plane (see Appendix. C.2 and Alg. 6).

317 **Multiclass Prediction:** Error-correcting output codes (ECOC) (Allwein et al. (2001)) is a  
 318 vodte/penalization-based method to make multiclass predictions from trained binary classifiers.  
 319 To predict the class of a new sample, multiple scores can be obtained from the set of trained binary  
 320 classifiers. These scores are interpreted as they either vote for or are against a particular class.  
 321 Depending on the coding matrix and the loss function chosen, ECOC takes the class with the highest  
 322 overall reward or lowest overall penalty as the predicted class. In this study, the coding matrix for  
 323 one-versus-one training scheme is selected, as it creates more linear separability (Acevedo et al.  
 324 (2022; 2024)). For the type of loss function, hinge-loss is chosen, as our internal tests suggested that  
 325 this loss leads to the best classification performance for all tested linear classifiers.

## 324 4 EXPERIMENTAL EVIDENCES ON LINEAR CLASSIFICATION OF REAL DATA

326 In this section, we compared the proposed CDA with other linear classifiers including LDA, SVM and  
 327 LR. The 5 tested SVM variants includes the original SVM, dual and primal fast SVM implemented  
 328 by Liblinear, SVM-SGD, and one fast SVM with BO hyperparameter search. LR uses fast imple-  
 329 mentation by Liblinear (fast SVM and fast LR refers to the dual version unless otherwise specified).  
 330 Additionally, we include the baseline method, CDB0 (equivalent to MDC equipped with OOP bias),  
 331 to quantify the improvements made by CDA over a simplistic centroid-based classification approach.  
 332 Their theoretical time complexity is shown in Fig. 2a. Experiment details are in Appendix J. [An](#)  
 333 [additional comparison with Partial Least Squares Discriminant Analysis \(PLSDA, Barker & Rayens](#)  
 334 [\(2003\)\) - a widely used and competitive linear method especially in chemometrics, genomics, and](#)  
 335 [other high-dimensional applications - with both binary-version and inherent-multiclass version can](#)  
 336 [be accessed in Section T\).](#)



351 Figure 2: (a) Theoretical training time complexity of linear classifiers. (b-e) Performance on 27  
 352 real datasets. (b) Top-2 occurrences and (c) average ranking of classifiers according to multiclass  
 353 AUROC. Error bars represent standard errors. (d) Average ranking of training time on large datasets  
 354 with average class-pair data size  $N \times M > 10^7$ . (e) Lines of linear regression between training  
 355 times and dataset sizes averaged across binary-pairs in each dataset, in the log-log scale to reveal  
 356 the scalability. (f-g) Large-scale data test. (f) Test set AUROC and (g) training time on large-scale  
 357 single-cell data with varying sizes of training samples by CDA-Fibonacci and fast SVM. CDB0:  
 358 Centroid Discriminant Basis 0; CDA: Centroid Discriminant Analysis; LDA: Linear Discriminant  
 359 Analysis; SVM: Support Vector Machine; LR: Logistic Regression; BO: Bayesian Optimization.

360 **Classification Performance on Real Data:** We assessed linear classification performance across  
 361 27 datasets, including standard image classification (Coates et al. (2011); Cohen et al. (2017); Hull  
 362 (1994); Krizhevsky (2009); LeCun et al. (1998); Netzer & Wang (2011); Nilsback & Zisserman  
 363 (2008); Stallkamp et al. (2011); Xiao et al. (2017)), medical image classification (Yang et al. (2023)),  
 364 and chemical property prediction tasks (Wu et al. (2018)). These datasets represent a broad range  
 365 of real-world applications and varying data sizes, enabling evaluations for both training speed and  
 366 predictive performance. Image data were used in their original value flattened to 1d vectors; chemical  
 367 formula were processed by simplified molecular input line entry system (SMILES) tokenized encoding  
 368 (see Appendix K). Each dataset was split into a 4:1 ratio for training and test sets. The final model for  
 369 each method was an unweighted ensemble of the five cross-validated models on the training set. [We](#)  
 370 [used one-versus-one training scheme and use external framework to realize multiclass prediction,](#)  
 371 [instead of the native multiclass approaches \(See reasons in Section T\).](#)

372 Fig. 2b-e show the test set multiclass prediction performance. In Fig. 2b, CDA achieved a top-  
 373 2 occurrence of AUROC on 17 out of 27 datasets, outperforming all the other linear classifiers,  
 374 indicating its stability and competitiveness. Fig. 2c shows that CDA achieved the highest average  
 375 ranking around 3.3, followed by fast SVM BO and SVM, however, their extremely low average  
 376 ranking of training speed in Fig. 2d indicates the impracticality for large-scale datasets (Panel (d)  
 377 shows results on large datasets with average class-pair data size  $N \times M > 10^7$ , because in practice  
 we care more about the time consumption on large datasets rather than small ones). [See Section N](#)

378 for other metrics and Section S for complete performance tables. These results of CDA is with BO  
 379 optimizer and log-transform to stabilize training, while the comparison for different optimizers are in  
 380 Section L, and for the efficient variant CDA-Fibonacci see Fig. N.

381 In Fig. 2e we performed linear regressions between training times and data sizes averaged across  
 382 binary pairs within each dataset with overhead deducted (See Fig. 8a for original data points,  
 383 and Fig. 8b-c for results with overhead kept). The regression results show that CDB0 exhibits  
 384 the best scalability due to its simplicity. SVM primal and SVM-SGD are fast for small data size,  
 385 however, CDA outperforms them when data size gets large. CDA not only improves significantly  
 386 over CDB0 in performance but also retains similar scalability. This improvement is driven by three  
 387 key components: generalized centroids with non-uniform weights, sample weight shift strategy, and  
 388 rotations by Bayesian optimization. The weighted average number of iterations required by CDA  
 389 per dataset was 29.33 - a small constant that does not contribute to time complexity. In contrast,  
 390 the iterations required by SVM variants increase significantly with more challenging datasets to  
 391 achieve a reasonable classification performance. Considering the diversity of tested datasets, CDA  
 392 demonstrates itself as a generic classifier with strong performance and scalability, making it applicable  
 393 to large-scale classification tasks across various domains.

394 We further test CDA on a large-scale dataset, the 1.3-million-cell mouse brain dataset (10x Genomics  
 395 (2017)), with the largest two classes (See Section. H for details). We applied CDA-Fibonacci as a  
 396 faster version for large data (See Section L). The results show that with growing sample sizes, CDA  
 397 outperforms fast SVM on both classification AUROC (Fig. 2f and Appendix Fig. 6), and training  
 398 speed (Fig. 2g). These results indicate that linear CDA is even more efficient and scalable than  
 399 the flagship SVM method in efficiency. Hence, CDA as a fast approach has the potential to drive  
 400 large-scale real-world applications in fields such as biomedicine and autonomous driving.

401 In addition, we made a comparison between CDA with two prevalent neural network architectures  
 402 - MLP and ResNet (See Appendix. U.1). In addition, we found that it is feasible to incorporate  
 403 neural networks in CDA, using their extracted features to train CDA, which improves linear CDA  
 404 performance. **Importantly, CDA can be used to initialize linear layers or MLP in the final layers of a**  
 405 **neural network architecture, outperforming their randomly initialized versions (See Appendix U.2).**

406 **CDA’s Convergence Property:** We analyzed the relationship between the actual stopping iteration  
 407 of CDA and the average binary classification performance (ps-score) across different datasets and  
 408 iteration limits. The results revealed two distinct regimes. In the right half of Fig. 3, for tasks  
 409 converging before 50 iterations, we observed a significant negative correlation (Pearson’s  $R = -0.48$ ),  
 410 indicating that datasets with lower performance required more iterations to converge. This highlights  
 411 the importance of allowing at least 50 iterations, as early stopping before this point may prevent  
 412 convergence for more challenging tasks. In contrast, for tasks exceeding 50 iterations, the correlation  
 413 was weak and positive (Pearson’s  $R = 0.184$ ), suggesting that beyond this threshold, the number  
 414 of iterations no longer plays a significant role in ensuring convergence. This indicates that once  
 415 50 iterations are reached, CDA can stabilize regardless of the underlying task performance. To  
 416 further validate this observation, in the left half of Fig. 3, we compared the distributions of ps-scores  
 417 obtained under maximum iteration limits of 50 and 150. The estimated probability densities were  
 418 nearly identical, and the Wilcoxon signed-rank test confirmed no significant difference between the  
 419 two conditions ( $p=0.398$ ). This result supports the conclusion that extending the maximum number  
 420 of iterations beyond 50 does not provide systematic benefits in terms of classification performance.  
 421 We also provide a similar convergence analysis for fast version CDA-Fibonacci in Appendix O.

## 422 5 PRELIMINARY TEST ON NONLINEAR KERNEL CDA

423 When data exhibit strong nonlinearity, linear classifiers often underperform. To address this problem,  
 424 models must exploit these nonlinear patterns to enhance expressiveness and improve classification  
 425 performance. In fact, linear CDA can be naturally extended to a nonlinear variant using kernel method  
 426 while retaining efficiency (see Appendix C.4). The main computational bottleneck lies in the kernel  
 427 matrix computation, which is a common cost shared by all kernel-based classifiers.

428 To compare the performance of nonlinear CDA and other nonlinear classifiers, we performed tests  
 429 on 3 challenging datasets, image dataset SVHN, chemical property dataset ClinTox and medical  
 430 image dataset fracturemnist3d (see Appendix. K for data processing). We choose these datasets

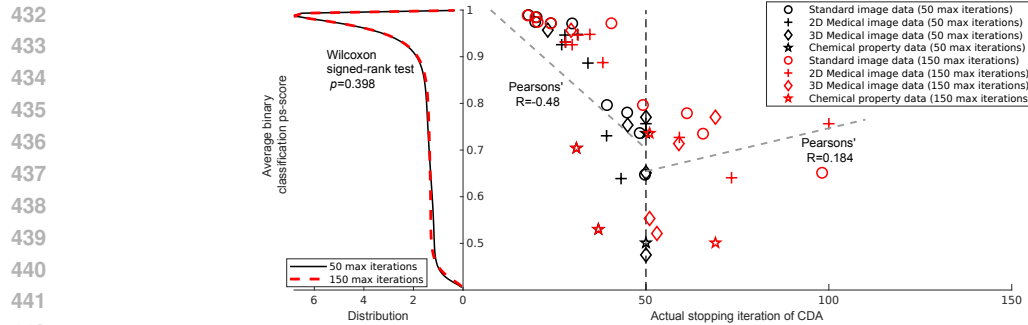


Figure 3: CDA-BO convergence. The right half shows relationship between classification performance and the actual stopping iteration of CDA across datasets under two maximum iteration limits (50 and 150). A negative correlation was observed for tasks converging before 50 iterations (Pearson’s  $R = -0.48$ ), while a weak positive correlation was found for tasks converging after 50 iterations (Pearson’s  $R = 0.184$ ). The gray dash lines show linear regression of points till 50 and points between 51 and 150. The black vertical line indicates the 50-iteration threshold. In the left half, probability density distributions of ps-scores under 50 and 150 maximum iterations show substantial overlap.

because they are difficult to classify with linear classifiers, and we are interested in to what extent can nonlinear classifiers improve over linear ones. We used a subset of SVHN samples (24,000) due to the time limitation to test with kernel method. We compared linear/Gaussian CDA (nCDA), SVM/nSVM and LDA/nLDA. For kernel methods, we performed hyperparameter search for the gaussian parameter  $\sigma$ . The data were divided into train, validation and test set, where on the validation set the hyperparameter was tuned. The training specifics can be found in Appendix J.2. The multiclass test set results (on ClinTox binary results since it is a binary task) in Table 1 show that kernel CDA outperforms on 2 out of 3 datasets, while the performance gap compared to the best one (nLDA) is not large. Importantly, kernel CDA improves on linear CDA substantially, suggesting the potential of applying kernel methods on linear CDA for complex data. Despite the fact that gaussian CDA improves substantially over linear CDA in tasks such as the SVHN image classification, we emphasize that linear CDA is still very useful and important, with high efficiency and low resource requirement in computation, among other merits.

Table 1: Test set classification performance on SVHN subset and ClinTox.

Dataset	Method	AUROC	AUPR	Fscore	ACscore
SVHN subset (image)	CDA	0.615 $\pm$ 0.02	0.63 $\pm$ 0.02	0.619 $\pm$ 0.02	0.423 $\pm$ 0.05
	nCDA	0.777 $\pm$ 0.01	0.782 $\pm$ 0.01	0.78 $\pm$ 0.01	0.731 $\pm$ 0.02
	SVM	0.555 $\pm$ 0.01	0.568 $\pm$ 0.007	0.551 $\pm$ 0.006	0.273 $\pm$ 0.05
	nSVM	0.736 $\pm$ 0.02	0.776 $\pm$ 0.009	0.756 $\pm$ 0.008	0.654 $\pm$ 0.03
	nLDA	<b>0.786<math>\pm</math>0.01</b>	<b>0.79<math>\pm</math>0.01</b>	<b>0.789<math>\pm</math>0.01</b>	<b>0.743<math>\pm</math>0.02</b>
		0.567	0.561	0.56	0.351
ClinTox (chemical)	nCDA	<b>0.625</b>	<b>0.627</b>	<b>0.627</b>	<b>0.46</b>
	SVM	0.565	0.578	0.575	0.294
	nSVM	0.500	0.481	0.480	0.000
	nLDA	0.605	0.612	0.611	0.409
		0.518 $\pm$ 0.01	0.526 $\pm$ 0.02	0.486 $\pm$ 0.02	0.279 $\pm$ 0.05
Fracture 3D (medical image)	nCDA	<b>0.625<math>\pm</math>0.04</b>	0.62 $\pm$ 0.04	<b>0.607<math>\pm</math>0.04</b>	<b>0.577<math>\pm</math>0.08</b>
	SVM	0.576 $\pm$ 0.009	0.579 $\pm$ 0.008	0.577 $\pm$ 0.008	0.505 $\pm$ 0.05
	nSVM	0.608 $\pm$ 0.06	0.591 $\pm$ 0.07	0.586 $\pm$ 0.07	0.44 $\pm$ 0.2
	nLDA	0.608 $\pm$ 0.03	<b>0.626<math>\pm</math>0.02</b>	0.605 $\pm$ 0.02	0.491 $\pm$ 0.1

## 6 CONCLUSIONS AND DISCUSSIONS

Linear classifiers, while inherently simpler, are favored in certain contexts due to their reduced tendency to overfit and their interpretability in decision-making. However, achieving both high scalability and robust predictive performance simultaneously remains a significant challenge.

486 In this study, the introduction of the Geometric Discriminant Analysis (GDA) framework marks a  
 487 notable step forward in addressing this challenge. By leveraging the geometric properties of centroids  
 488 – a fundamental concept in multiple disciplines – GDA provides a unifying framework for certain  
 489 linear classifiers. The core innovation lies in a special type of Centroid Discriminant Basis (CDB0),  
 490 which serves as the foundation for deriving discriminants. These discriminants, when augmented  
 491 with geometric corrections under varying constraints, extend the theoretical flexibility of GDA.  
 492 Notably, Minimum Distance Classifier (MDC) and Linear Discriminant Analysis (LDA) are shown  
 493 to be a subset of this broader framework, demonstrating how they converge to CDB0 under specific  
 494 conditions. This theoretical generalization not only validates the GDA framework but also sets the  
 495 stage for novel classifier designs.

496 A key practical contribution of this work is the Centroid Discriminant Analysis (CDA), a specialized  
 497 implementation of GDA. CDA employs geometric rotations of the CDB within planes defined by  
 498 centroid-vectors with shifted sample weights. These rotations, combined with Bayesian optimization  
 499 techniques, enhance the method’s scalability, achieving quadratic time complexity  $O(NM + N\log N)$ .  
 500 Across diverse datasets—including standard images, medical images, and chemical property clas-  
 501 sifications—CDA demonstrated superior performance in scalability, predictive performance, and  
 502 stability. We emphasize that CDA not merely robustly outperforms most of existing linear classifica-  
 503 tion methods, but crucially, it achieves this with superior computational efficiency. Specifically, CDA  
 504 exhibits a quadratic time complexity in the worst-case scenario, compared to the cubic complexity  
 505 typical of established methods such as LDA and SVM, with significantly shorter runtimes that high-  
 506 light its practical advantage in real-world applications. These findings hold particular relevance for  
 507 the broader machine learning community, as linear classifiers remain widely used across numerous  
 508 scientific domains where interpretability, scalability, and computational efficiency are critical. In  
 509 such contexts, practitioners often prefer models that are not only robust and fast but also transparent  
 510 and easy to deploy in real-world decision-making scenarios.

511 For data exhibiting complex nonlinear structures that linear classifiers cannot adequately capture,  
 512 linear CDA can be extended to nonlinear form via kernel methods. This generalization significantly  
 513 broadens the applicability of CDA by enabling it to handle nonlinear patterns in the data. Together,  
 514 linear and kernel-based CDA form a complementary toolkit for classifications. A practical strategy  
 515 is to begin with linear CDA to see whether the predictions are satisfying, which offers fast and  
 516 interpretable results. Our preliminary results also suggest that extending CDA with nonlinear kernels  
 517 is a promising direction for future research, since the variety of available kernels broadens the  
 518 opportunity to tailor the mapping of original data onto higher-dimensional spaces according to the  
 519 specific structure of the data - where it may become more easily separable. **Another future work is to**  
 520 **explore an inherent multiclass extension of CDA (see Section T), especially given that other classifiers**  
 521 **such as LDA and SVM have their inherent multiclass approach. In the cases where  $C$  is large and**  
 522 **not negligible, inherent multiclass approaches offer attractive lower computational complexity with**  
 523 **respect to the number of classes ( $C$  versus  $C(C - 1)/2$  discriminants in pairwise schemes).**

524 One limitation of this study is that the current CDA does not have a natively multiclass approach,  
 525 hence it can be interesting to investigate how to formulate CDA in a natively multiclass way. However,  
 526 in Section T we showed that using inherently multiclass LDA, SVM, and PLS-DA the performance  
 527 does not improve and even drops significantly for SVM, a reason for which in this study we decided  
 528 to focus on binary CDA classification and leveraging external multiclass framework. In addition, in  
 529 this study, the GDA framework is used to show that LDA is a special centroid-based method case, and  
 530 then is adopted to design CDA. CDA itself is presented as a single, highly effective derivative, but  
 531 the GDA framework’s utility in systematically generating other novel classifiers is not investigated  
 532 enough. Since GDA in the current formulation is a framework that can include only centroid based  
 533 classifiers, methods such as SVM that are based on large margin classification are not included in the  
 534 GDA framework to explain and design classifiers based on linear centroid-based separability. The  
 535 mission to investigate the extent to which GDA framework may inspire the design of new classifiers  
 536 will be a not trivial point to expand in future studies.

537 In conclusion, the GDA framework and its CDA implementation represent a paradigm shift in classifier  
 538 design, combining the interpretability of geometric principles with state-of-the-art computational  
 539 efficiency. This work not only advances the field of classification but also lays groundwork for  
 innovative approaches to supervised learning.

## 540 REFERENCES

541

542 10x Genomics. 1.3 million brain cells from e18 mice. [https://support.10xgenomics.com/single-cell-gene-expression/datasets/1.3.0/1M\\_neurons](https://support.10xgenomics.com/single-cell-gene-expression/datasets/1.3.0/1M_neurons), 2017. Accessed: May 2025.

543

544

545 Aldo Acevedo, Claudio Duran, Ming-Ju Kuo, Sara Ciucci, Michael Schroeder, and Carlo Vittorio Cannistraci. Measuring group separability in geometrical space for evaluation of pattern recognition and dimension reduction algorithms. *IEEE Access*, 10:22441–22471, 2022. ISSN 2169-3536. doi: 10.1109/access.2022.3152789. URL <http://dx.doi.org/10.1109/access.2022.3152789>.

546

547

548

549

550 Aldo Acevedo, Yue Wu, Fabio Lorenzo Traversa, and Carlo Vittorio Cannistraci. Geometric separability of mesoscale patterns in embedding representation and visualization of multidimensional data and complex networks. *PLOS Complex Systems*, 1:1–28, 1 2024. doi: 10.1371/journal.pcsy.0000012. URL <https://doi.org/10.1371/journal.pcsy.0000012>.

551

552

553

554

555 Erin L. Allwein, Robert E. Schapire, and Yoram Singer. Reducing multiclass to binary: A unifying approach for margin classifiers. *Journal of Machine Learning Research*, 1, 2001. ISSN 15324435.

556

557 M. Barker and W. Rayens. Partial least squares for discrimination. *Journal of Chemometrics*, 17(3):166–173, 2003. doi: 10.1002/cem.785.

558

559

560 Deng Cai, Xiaofei He, and Jiawei Han. Training linear discriminant analysis in linear time. In *Proceedings - International Conference on Data Engineering*, 2008. doi: 10.1109/ICDE.2008.4497429.

561

562

563 Adam Coates, Honglak Lee, and Andrew Y. Ng. An analysis of single-layer networks in unsupervised feature learning. In *Journal of Machine Learning Research*, volume 15, 2011.

564

565 Gregory Cohen, Saeed Afshar, Jonathan Tapson, and Andre Van Schaik. Emnist: Extending mnist to handwritten letters. In *Proceedings of the International Joint Conference on Neural Networks*, volume 2017-May, 2017. doi: 10.1109/IJCNN.2017.7966217.

566

567

568 Corinna Cortes and Vladimir Vapnik. Support-vector networks. *Machine Learning*, 20, 1995. ISSN 15730565. doi: 10.1023/A:1022627411411.

569

570

571 Richard O. Duda, Peter E Hart, and David G. Stork. Pattern classification, second edition. *NY: Wiley-Interscience*, 2001.

572

573

574 R. A. Fisher. The use of multiple measurements in taxonomic problems. *Annals of Eugenics*, 7, 1936. ISSN 2050-1420. doi: 10.1111/j.1469-1809.1936.tb02137.x.

575

576

577 Jonathan J. Hull. A database for handwritten text recognition research. *IEEE Transactions on Pattern Analysis and Machine Intelligence*, 16, 1994. ISSN 01628828. doi: 10.1109/34.291440.

578

579 Alex Krizhevsky. Learning multiple layers of features from tiny images. . . . *Science Department, University of Toronto, Tech. . . .*, 2009. ISSN 1098-6596. doi: 10.1.1.222.9220.

580

581 Yann LeCun, Léon Bottou, Yoshua Bengio, and Patrick Haffner. Gradient-based learning applied to document recognition. *Proceedings of the IEEE*, 86, 1998. ISSN 00189219. doi: 10.1109/5.726791.

582

583

584 Marvin L. Minsky and Seymour Papert. *Perceptrons, Expanded Edition An Introduction to Computational Geometry*. 1969.

585

586

587 Masaya Misaki, Youngmoon Kim, Peter A Bandettini, and Nikolaus Kriegeskorte. Comparison of multivariate classifiers and response normalizations for pattern-information fmri. *NeuroImage*, 53(1):103–118, 2010. doi: 10.1016/j.neuroimage.2010.05.051.

588

589

590 Yuval Netzer and Tao Wang. Reading digits in natural images with unsupervised feature learning. *Nips*, 2011.

591

592

593 Maria Elena Nilsback and Andrew Zisserman. Automated flower classification over a large number of classes. In *Proceedings - 6th Indian Conference on Computer Vision, Graphics and Image Processing, ICVGIP 2008*, 2008. doi: 10.1109/ICVGIP.2008.47.

594 Nihar Ranjan Panda, Jitendra Kumar Pati, Jatindra Nath Mohanty, and Ruchi Bhuyan. A review on  
 595 logistic regression in medical research, 2022. ISSN 22296816.  
 596

597 Marc Andre Schulz, B. T.Thomas Yeo, Joshua T. Vogelstein, Janaina Mourao-Miranada, Jakob N.  
 598 Kather, Konrad Kording, Blake Richards, and Danilo Bzdok. Different scaling of linear models  
 599 and deep learning in ukbiobank brain images versus machine-learning datasets. *Nature Communications*, 11, 2020. ISSN 20411723. doi: 10.1038/s41467-020-18037-z.  
 600

601 Xi Shen, Emily S Finn, Dustin Scheinost, Monica D Rosenberg, Maria M Chun, Xenophon  
 602 Papademetris, and R. Todd Constable. Using connectome-based predictive modeling to pre-  
 603 dict individual behavior from brain connectivity. *Nature Protocols*, 12:506–518, 2017. doi:  
 604 10.1038/nprot.2016.178.

605 Johannes Stallkamp, Marc Schlipsing, Jan Salmen, and Christian Igel. The german traffic sign recog-  
 606 nition benchmark: A multi-class classification competition. In *Proceedings of the International*  
 607 *Joint Conference on Neural Networks*, 2011. doi: 10.1109/IJCNN.2011.6033395.  
 608

609 Gaël Varoquaux and Veronika Cheplygina. Machine learning for medical imaging: methodological  
 610 failures and recommendations for the future, 2022. ISSN 23986352.  
 611

612 Gaël Varoquaux, Pradeep Reddy Raamana, Denis A. Engemann, Andrés Hoyos-Idrobo, Yannick  
 613 Schwartz, and Bertrand Thirion. Assessing and tuning brain decoders: Cross-validation, caveats,  
 614 and guidelines. *NeuroImage*, 145, 2017. ISSN 10959572. doi: 10.1016/j.neuroimage.2016.10.038.  
 615

616 Yue Wu and Carlo Vittorio Cannistraci. Accuracy score for evaluation of classification on imbalanced  
 617 data. *Preprints*, 1 2025. doi: 10.20944/preprints202501.2178.v1. URL <https://doi.org/10.20944/preprints202501.2178.v1>.  
 618

619 Zhenqin Wu, Bharath Ramsundar, Evan N. Feinberg, Joseph Gomes, Caleb Geniesse, Aneesh S.  
 620 Pappu, Karl Leswing, and Vijay Pande. Moleculenet: A benchmark for molecular machine learning.  
 621 *Chemical Science*, 9, 2018. ISSN 20416539. doi: 10.1039/c7sc02664a.  
 622

623 Han Xiao, Kashif Rasul, and Roland Vollgraf. Fashion-mnist: a novel image dataset for benchmarking  
 624 machine learning algorithms, 2017. URL <https://arxiv.org/abs/1708.07747>.  
 625

626 Jiancheng Yang, Rui Shi, Donglai Wei, Zequan Liu, Lin Zhao, Bilian Ke, Hanspeter Pfister, and  
 627 Bingbing Ni. Medmnist v2 - a large-scale lightweight benchmark for 2d and 3d biomedical image  
 628 classification. *Scientific Data*, 10, 2023. ISSN 20524463. doi: 10.1038/s41597-022-01721-8.  
 629

630 Guo Xun Yuan, Chia Hua Ho, and Chih Jen Lin. Recent advances of large-scale linear classification.  
 631 *Proceedings of the IEEE*, 100, 2012. ISSN 00189219. doi: 10.1109/JPROC.2012.2188013.  
 632

633

634

635

636

637

638

639

640

641

642

643

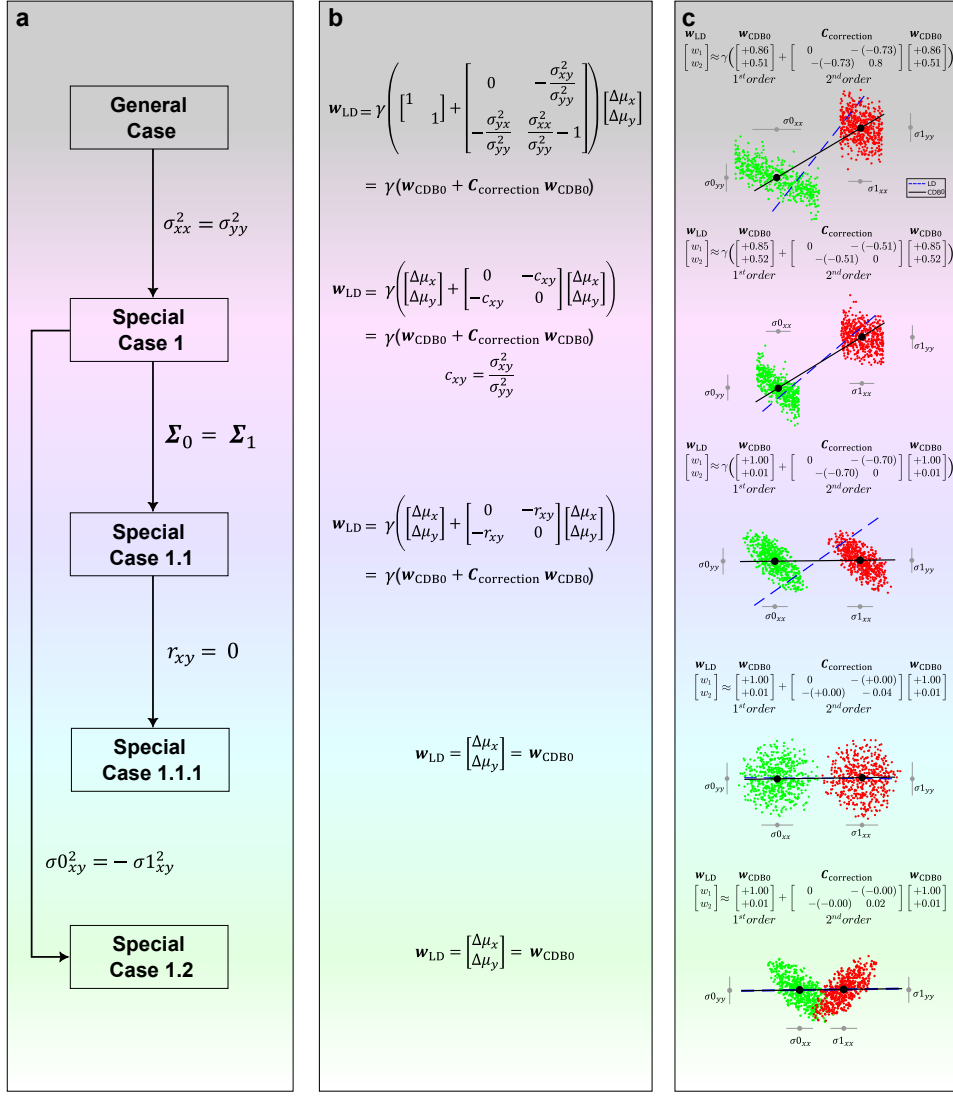
644

645

646

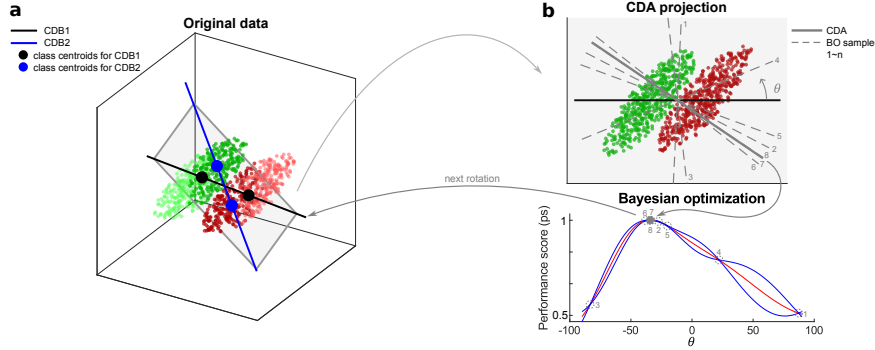
647

648 A SUPPLEMENTARY: GDA THEORETICAL FRAMEWORK  
649650 A.1 DIFFERENCE BETWEEN THEORY AND THEORETICAL FRAMEWORK  
651652 We emphasize that GDA does not constitute a new theory, but rather a theoretical framework. A  
653 theory in data science and machine learning provides a foundational explanation often accompanied  
654 by rigorous mathematical derivations, such as performance bounds or convergence guarantees. In  
655 contrast, a theoretical framework offers a structured set of concepts and assumptions, typically  
656 formalized through equations, that guide the design of methods and the interpretation of results -  
657 without necessarily proving theoretical performance guarantees. Within this clarified scope, GDA  
658 serves as the framework under which we define and motivate an efficient geometric, centroid-based  
659 linear classification method: Centroid Discriminant Analysis (CDA), which is discussed in Section 3.  
660661 A.2 SCALING INVARIANCE OF THE DISCRIMINANTS IN THE GDA FRAMEWORK  
662663 GDA is a geometrical projection-based theoretical framework. In this framework, the discriminant  
664 (the high-dimensional vector orthogonal to the classification boundary) of the involved classifiers  
665 (including CDA), is normalized to a unit vector before projecting data. The final classification  
666 depends solely on these projections; scaling the discriminant length by any factor (including terms  
667 like  $\sigma_{yy}^2/|\Sigma|$  in the derivation of GDA by LDA) uniformly scales all projections without changing  
668 their relative positions. Consequently, the optimal threshold (which can be found by search) and  
669 classification results remain unchanged. This normalization is explicitly implemented in CDA (see,  
670 for example, Appendix C.3, Algorithm 1, line 4: “Normalize  $w_{\text{CDB1}} \dots$ ”), ensuring that only the  
671 direction is refined during iterations.672 This property distinguishes GDA and CDA from approaches like SVM, where the magnitude of the  
673 discriminant vector is tied to the margin width during training. However, even for SVM, once the  
674 model is trained, scaling  $w$  and  $b$  together leaves predictions unchanged because the decision function  
675  $y = H(w^T x + b)$  is homogeneous in  $w$  and  $b$ . ( $y$ : predicted class;  $H(\cdot)$ : Heaviside function;  $x$ :  
676 sample;  $b$ : bias). In CDA training, magnitude carries no interpretive meaning - only direction matters.  
677 These also reflect that GDA reinterprets certain existing classifiers from the geometric projection  
678 perspective, which is an innovation that inherently differs from their own interpretations.679 A.3 EXPLANATION OF THE DISCRIMINANT BIAS IN THE GDA FRAMEWORK  
680681 In practice, GDA-based methods—including CDA—explicitly normalize the discriminant to unit  
682 length before projection (see Algorithm 1, line 4). This normalization ensures that the training process  
683 refines only the direction of the discriminant, while the bias can always be computed afterwards  
684 by placing a threshold between the projected class distributions. For binary classification, the bias  
685 may be chosen using a variety of monotonic criteria—e.g., the midpoint between class means, the  
686 empirical risk minimizer on the projected line, or a direct search for the threshold optimizing AUROC,  
687 accuracy, or any other performance metric. Because projection preserves the ordering of samples, all  
688 of these methods yield a valid bias once the discriminant direction is fixed.689 This perspective also clarifies that the discriminant and the bias play fundamentally different roles:  
690 the discriminant determines the orientation of the separating hyperplane, while the bias determines  
691 its position. The former is geometrically meaningful in GDA; the latter can always be adjusted post  
692 hoc without altering the interpretation of the discriminant.693  
694  
695  
696  
697  
698  
699  
700  
701

702 A.4 GDA DEMONSTRATION WITH 2D ARTIFICIAL DATA  
703  
704

742 Figure 4: The GDA theoretical framework in 2 dimensions showing how the relation between LD  
743 and CDB0 evolves under specific conditions. (a) The relations between LD and CDB0 proceeding  
744 from the general case to different special cases under the conditions shown along each arrow.  
745 (b) The specific expressions of LD in terms of CDB0 and corrections corresponding to each case in column  
746 (c) Binary classification models of LD (blue dashed) and CDB0 (black solid) on different 2D  
747 data corresponding to each case in column (a). The lines show the direction instead of the unit vector  
748 of the discriminants. LD: Linear Discriminant; CDB0: Centroid Discriminant Basis 0.  $\gamma$  denotes a  
749 generic normalizing factor.

750  
751  
752  
753  
754  
755

756 **B CDA SCHEMATIC DIAGRAM**  
757

771 Figure 5: Diagram for the first CDA rotation. (a) CDB1 is obtained from specific sample weights.  
772 CDB2 is obtained from centroids with a shifted sample weights toward the decision boundary.  
773 Darker points represent larger sample weights. CDB1 and CDB2 form a 2d plane on which BO is  
774 performed to estimate the best classification discriminant. (b) The process of BO to estimate the best  
775 discriminant. The rotation angle  $\theta$  from CDB1 is the only independent variable to search in BO. The  
776 estimated optimal line CDA servers as the new CDB1 in the next CDA rotation. CDB: Centroid  
777 Discriminant Basis; CDA: Centroid Discriminant Analysis.

778 **C THE CDA ALGORITHM**  
779780 **C.1 BAYESIAN OPTIMIZATION**

781 One factor related to the effectiveness of CDA is the estimation with varying precision in BO. We set  
782 the number of BO sampling times to  $\min(3 + rot, 10)$  as default parameter during the CDA rotation,  
783 where  $rot$  is the  $rot$ -th rotation. During the first few CDA rotations, the BO estimation has relatively  
784 less precision. This gives CDA enough randomness to first enter a large region in which there are  
785 more discriminants with high performance, under the hypothesis that regions close to global optimum  
786 or suboptimum have more high-performance solutions that are more likely to be randomly selected.  
787 Starting from this large region, BO precision is gradually enhanced to refine the search in or close to  
788 this region in terms of Euclidean distance, and force CDA to converge. The upper limit of 10 CDA  
789 rotations still creates a small level of imprecision, in order to make CDA escape from small-size local  
790 minimum, to acquire higher performance, and improve training efficiency.

791 **C.2 REFINING CDA WITH STATISTICAL EXAMINATION ON 2D PLANE**

792 In CDA, the plane associated with the best performance is selected, but it is uncertain whether there  
793 are higher-performance discriminants on this plane, since the precision might not be high enough  
794 with 10 BO samplings and even lower for less samplings. To determine whether the BO is precise  
795 enough, a statistical examination using p-value with respect to null-model is performed. On this  
796 best plane, we generate 100 random CDBs, run BO in turn for 10, 20 and to the maximum 30 BO  
797 samplings, until the p-value of training performance-score of the BO-estimated CDB with regard  
798 to the null model is 0, otherwise using the best random CDB. In this way, we are able to give a  
799 confidence level of the BO estimated discriminant in the best CDA rotation plane. Alg. 6 shows the  
800 pseudocode for the refining finalization step.

801 **C.3 LINEAR CDA PSEUDOCODE**

802 This study deals with a supervised binary classification problem on labeled data  $\{X, y\} =$   
803  $\{\mathbf{x}_i, y_i\}_{i=1}^N$  with  $N$  samples and  $M$  features. The samples consist of positive and negative class  
804 data  $\chi_1$  and  $\chi_2$  with sizes  $N_1$  and  $N_2$ , respectively, and the corresponding labels are tokenized as 1  
805 and 0, respectively. The sample features are flattened to 1D if they have higher dimensions, such as

810 image data. The following section introduces CDA in pseudo-code. CDA rotations, BO sampling  
 811 and p-value computing involve constant numbers, thus, they do not contribute to the time complexity.  
 812

---

**813 Algorithm 1** CDA Main Algorithm (CDA)  $O(NM + N\log N)$ 


---

814 **Input:**  $N \times M$  data matrix  $\mathbf{X}$ ,  $N \times 1$  labels  $\mathbf{y}$   
 815 Initialize  $\boldsymbol{\alpha} = [1; 1; \dots; 1]^{N \times 1} / \sqrt{N}$   $\{O(N)\}$   
 816 Compute  $\mathbf{w}_{\text{CDB1}} = \sum_{c=1}^2 (-1)^{c+1} \frac{1}{N_c} \sum_{\mathbf{x}_i \in \mathcal{X}_c} \alpha_i \mathbf{x}_i$   $\{O(NM)\}$   
 817 Normalize  $\mathbf{w}_{\text{CDB1}} = \mathbf{w}_{\text{CDB1}} / \|\mathbf{w}_{\text{CDB1}}\|_2$   $\{O(M)\}$   
 818 Initialize  $ps^* = 0$   $\{O(1)\}$   
 819 **for**  $i = 1$  **to** 50 **do**  
 820      $\boldsymbol{\alpha} = \text{updateSampleWeights}(\mathbf{X}, \mathbf{y}, \boldsymbol{\alpha}, \mathbf{w}_{\text{CDB1}})$   $\{O(NM + N\log N)\}$   
 821     Compute  $\mathbf{w}_{\text{CDB2}} = \sum_{c=1}^2 (-1)^{c+1} \frac{1}{N_c} \sum_{\mathbf{x}_i \in \mathcal{X}_c} \alpha_i \mathbf{x}_i$   $\{O(NM)\}$   
 822     Normalize  $\mathbf{w}_{\text{CDB2}} = \mathbf{w}_{\text{CDB2}} / \|\mathbf{w}_{\text{CDB2}}\|_2$   $\{O(M)\}$   
 823     Set  $N_{\text{BO}} = \min(i + 3, 10)$   $\{O(1)\}$  Number of BO sampling  
 824      $(\mathbf{w}_{\text{CDA}}, ps) = \text{CdaRotation}(\mathbf{w}_{\text{CDB1}}, \mathbf{w}_{\text{CDB2}}, \mathbf{X}, \mathbf{y}, N_{\text{BO}})$   $\{O(NM + N\log N)\}$   
 825     **if**  $ps > ps^*$  **then**  
 826          $(\mathbf{w}_{\text{CDB1}}^*, \mathbf{w}_{\text{CDB2}}^*, ps^*) = (\mathbf{w}_{\text{CDB1}}, \mathbf{w}_{\text{CDB2}}, ps)$   $\{O(M)\}$   
 827     **end if**  
 828     **if** coefficient of variation of the last 10  $ps < 0.001$  **then**  
 829         **break**  $\{\text{Early stop convergence}\}$   
 830     **end if**  
 831     Update  $\mathbf{w}_{\text{CDB1}} = \mathbf{w}_{\text{CDA}}$   $\{O(M)\}$   
 832 **end for**  
 833 Compute  $(\mathbf{w}_{\text{CDA}}, oop) = \text{refineOnBestPlane}(\mathbf{w}_{\text{CDB1}}^*, \mathbf{w}_{\text{CDB2}}^*, \mathbf{X}, \mathbf{y})$   $\{O(NM + N\log N)\}$   
 834 **Output:**  $\mathbf{w}_{\text{CDA}}, oop$ 


---

---

**835 Algorithm 2** Update Sample Weights (updateSampleWeights)  $O(NM + N\log N)$ 


---

836 **Input:**  $N \times M$  data matrix  $\mathbf{X}$ ,  $N \times 1$  labels  $\mathbf{y}$ ,  $N \times 1$  sample weights  $\boldsymbol{\alpha}$ ,  $1 \times M$  vector  $\mathbf{w}_{\text{CDB1}}$   
 837 Initialize  $oop = \text{searchOOP}(\mathbf{X}, \mathbf{w})$   $\{O(N\log N)\}$   
 838 Compute  $\mathbf{q} = \mathbf{X} \mathbf{w}_{\text{CDB1}}^T$   $\{O(NM)\}$   
 839 Compute  $d_i = |q_i - oop|$ ,  $\forall i \in \{1, 2, \dots, N\}$   $\{O(N)\}$   
 840 Compute  $\mathbf{d}_r = |\mathbf{d} - \min(\mathbf{d}) - \max(\mathbf{d})|$   $\{O(N)\}$   
 841 Update  $\boldsymbol{\alpha} = \boldsymbol{\alpha} \odot \mathbf{d}_r / \|\boldsymbol{\alpha} \odot \mathbf{d}_r\|_2$   $\{O(N)\}$ ,  $\odot$  is Hadamard product  
 842 **Output:**  $\boldsymbol{\alpha}$ 


---

---

**843 Algorithm 3** Search Optimal Operating Point (searchOOP)  $O(N\log N)$ 


---

844 **Input:**  $N \times 1$  projected points  $\mathbf{q}$ ,  $N \times 1$  labels  $\mathbf{y}$   
 845 Sort  $(\mathbf{q}, \mathbf{y})$   $\{O(N\log N)\}$ , sort according to  $\mathbf{q}$   
 846 Initialize  $\mathbf{cm} = \text{evaluateMetrics}(\mathbf{y}, [0; 0; \dots; 0]^{N \times 1})$   $\{O(N)\}$  initial confusion matrix  
 847 **for**  $i = 1$  **to**  $N - 1$  **do**  
 848     Update  $\mathbf{cm} = \text{updateCM}(y_i, \mathbf{cm})$   $\{O(1)\}$  scan each label and adjust cm  
 849     Compute  $ps_i = \text{evaluateMetrics}(\mathbf{cm})$   $\{O(1)\}$   
 850 **end for**  
 851 Compute  $idx = \arg \max_i ps_i$   $\{O(N)\}$   
 852 Compute  $ps = \max(\mathbf{ps})$   $\{O(N)\}$   
 853 Compute  $oop = \frac{q_{idx} + q_{(idx+1)}}{2}$   $\{O(1)\}$   
 854 **Output:**  $oop, ps$ 


---

855  
 856  
 857  
 858  
 859  
 860  
 861  
 862  
 863

---

864 **Algorithm 4** Approximate Optimal Line by BO (CdaRotation)  $O(NM + N\log N)$

865 **Input:**  $1 \times M$  lines  $\mathbf{w}_{\text{CDB1}}, \mathbf{w}_{\text{CDB2}}, N \times M$  data matrix  $\mathbf{X}, N \times 1$  labels  $\mathbf{y}$ , total BO iteration  
866  $N_{\text{BO}}$

867 Compute  $\mathbf{w}_{\text{orth}} = \mathbf{w}_{\text{CDB2}} - \mathbf{w}_{\text{CDB1}}^T \mathbf{w}_{\text{CDB2}} \mathbf{w}_{\text{CDB1}}$   $\{O(M)\}$

868 Normalize  $\mathbf{w}_{\text{orth}} = \mathbf{w}_{\text{orth}} / \|\mathbf{w}_{\text{orth}}\|_2$   $\{O(M)\}$

869 Estimate  $\hat{\theta} = \text{BayesianOptimization}(\text{evaluateRotation}(\theta, \mathbf{w}_{\text{CDB1}}, \mathbf{w}_{\text{orth}}, \mathbf{X}, \mathbf{y}), N_{\text{BO}})$ ,  $\theta \in [-\frac{\pi}{2}, \frac{\pi}{2}]$   $\{O(NM + N\log N)\}$

870 Compute  $\mathbf{w}_{\text{CDA}} = \mathbf{w}_{\text{CDB1}} \cos \hat{\theta} + \mathbf{w}_{\text{orth}} \sin \hat{\theta}$   $\{O(M)\}$

871 Compute  $\mathbf{q} = \mathbf{X} \mathbf{w}_{\text{CDA}}^T$   $\{O(NM)\}$

872 Get the mean of  $(oop, ps) = \text{searchOOP}(\mathbf{q}, \mathbf{y})$  with 5-fold cross-validation  $\{O(N\log N)\}$

873 **Output:**  $\mathbf{w}_{\text{CDA}}, oop, ps$

---

876 **Algorithm 5** Evaluate the Line with Rotation Angle (evaluateRotation)  $O(NM + N\log N)$

877 **Input:** Rotation angle  $\theta, 1 \times M$  lines  $\mathbf{w}_{\text{CDB1}}, \mathbf{w}_{\text{orth}}, N \times M$  data matrix  $\mathbf{X}, N \times 1$  labels  $\mathbf{y}$

878 Compute  $\mathbf{w}_{\text{CDA}} = \mathbf{w}_{\text{CDB1}} \cos \theta + \mathbf{w}_{\text{orth}} \sin \theta$   $\{O(M)\}$

879 Compute  $\mathbf{q} = \mathbf{X} \mathbf{w}_{\text{CDA}}^T$   $\{O(NM)\}$

880 Get mean  $ps = \text{searchOOP}(\mathbf{q}, \mathbf{y})$  with 5-fold cross-validation scheme  $\{O(N\log N)\}$

881 **Output:**  $ps$

---

884 **Algorithm 6** Refine on the Best Model (refineOnBestPlane)  $O(NM + N\log N)$

885 **Input:**  $1 \times M$   $\mathbf{w}_{\text{CDB1}}$  and its orthogonal vector  $\mathbf{w}_{\text{orth}}, N \times M$  data matrix  $\mathbf{X}, N \times 1$  labels  $\mathbf{y}$

886 **for**  $i = 1$  **to** 100 **do**

887 Randomly choose  $\theta \in [-\frac{\pi}{2}, \frac{\pi}{2}]$   $\{O(1)\}$

888 Compute  $\mathbf{w}_r = \mathbf{w}_{\text{CDB1}} \cos \theta + \mathbf{w}_{\text{orth}} \sin \theta$   $\{O(M)\}$

889 Compute  $\mathbf{q} = \mathbf{X} \mathbf{w}_r^T$   $\{O(NM)\}$

890 Get mean  $(oop_r, ps_r)_i = \text{searchOOP}(\mathbf{q}, \mathbf{y})$  with 5-fold cross-validation  $\{O(N\log N)\}$

891 **end for**

892 Sort  $idx = \text{sortIdx}([ps, ps_r])$   $\{O(1)\}$  sort returning position indices

893 Compute  $p = 1 - \frac{(idx(1)-1)}{N_r}$   $\{O(1)\}$

894 Initialize  $N_{\text{BO}} = 0$

895 **while**  $p \neq 0$  and  $N_{\text{BO}} < 30$  **do**

896 Increment  $N_{\text{BO}} = N_{\text{BO}} + 10$

897 Compute  $(\mathbf{w}_{\text{CDA}}, oop, ps) = \text{CdaRotation}(\mathbf{w}_{\text{CDB1}}, \mathbf{w}_{\text{CDB2}}, \mathbf{X}, \mathbf{y}, N_{\text{BO}})$   $\{O(NM + N\log N)\}$

898 Sort  $idx = \text{sortIdx}([ps, ps_r])$   $\{O(1)\}$  sort returning position indices

899 Compute  $p = 1 - \frac{(idx(1)-1)}{N_r}$   $\{O(1)\}$

900 **end while**

901 **if**  $p \neq 0$  **then**

902 Compute  $i = \arg \min_i ps_{r,i}$   $\{O(1)\}$

903 Set  $(\mathbf{w}_{\text{CDA}}, oop, ps) = (\mathbf{w}_r, oop_r, ps_r)_i$   $\{O(1)\}$

904 **end if**

905 **Output:**  $\mathbf{w}_{\text{CDA}}, oop, ps$

---

#### C.4 NONLINEAR KERNEL CDA

910 The CDA algorithm involves computing the CDBs using the equation provided in Appendix. C.3,  
911 Algorithm 1:

912

$$\mathbf{w}_{\text{CDB}} = \sum_{c=1}^2 (-1)^{c+1} \cdot \frac{1}{N_c} \sum_{\mathbf{x}_i \in \chi_c} \alpha_i \mathbf{x}_i \quad (11)$$

913

914 Combining this with the normalization step for each CDB  $\mathbf{w}_{\text{CDB}} \leftarrow \mathbf{w}_{\text{CDB}} / \|\mathbf{w}_{\text{CDB}}\|_2$ , the equation  
915 can be rewritten as:

918  
919  
920

$$\mathbf{w}_{\text{CDB}} = (\boldsymbol{\alpha} \odot \mathbf{n} \odot \mathbf{y}_t \cdot k)^\top \mathbf{X} = \boldsymbol{\beta}^\top \mathbf{X}, \quad (12)$$

921 where  $\boldsymbol{\alpha}$  is the vector of sample weights;  $\mathbf{n} = [1/N_{\text{map}(i)}]$  for all  $i \in \{1, 2, \dots, N\}$  is the weight  
922 sum division for each class, and  $\text{map}(i)$  maps sample index  $i$  to class index  $c$ ;  $\mathbf{y}_t = (-1)^{c+1}$  are the  
923 tokenized labels (+1 or -1);  $k$  is the factor to normalize each CDB as a unit vector.

924 For the rotated CDBs used in Bayesian optimization (Appendix B, Algorithms 4–5), they can be  
925 expressed as linear combinations of CDB1 and orthogonalized CDB2, mixing their corresponding  $\boldsymbol{\beta}$   
926 vectors. Thus, the sample coefficient  $\boldsymbol{\beta}$  is tracked throughout the training process for each CDB.  
927

928 The data projection can be expressed as:

929  
930  
931

$$\mathbf{q} = \mathbf{X} \mathbf{w}_{\text{CDB}}^\top = \mathbf{X} (\boldsymbol{\beta}^\top \mathbf{X})^\top = \mathbf{X} \mathbf{X}^\top \boldsymbol{\beta} \quad (13)$$

932 With this expression, the data projection can incorporate kernel methods to realize nonlinear classifi-  
933 cation, shown by the following equation.

934  
935  
936

$$\mathbf{q} = \text{Ker}(\mathbf{X}, \mathbf{X}^\top) \boldsymbol{\beta} \quad (14)$$

937 In fact, kernel methods implicitly projects data into a high-dimensional space, then applying linear  
938 classifiers in the transformed feature space.

939  
940  
941  
942  
943  
944  
945  
946  
947  
948  
949  
950  
951  
952  
953  
954  
955  
956  
957  
958  
959  
960  
961  
962  
963  
964  
965  
966  
967  
968  
969  
970  
971

972 D CDA CONVERGENCE PROOF  
973974 In the Section we provide a mathematical proof with a proposition showing that, under the defined  
975 fitness function, CDA is guaranteed to converge. This convergence relies solely on the monotonicity  
976 and boundedness of the objective sequence and therefore holds independently of the specific 1D  
977 optimizer employed (e.g., BO, Brent’s method).978 **Proposition.** Let  $w_{\text{CDB1}}^{(k)} \in \mathbb{R}^M$  be the CDB1 vector at iteration  $k$ . In each CDA iteration,  
979  $w_{\text{CDB1}}^{(k)}$  determines the CDB2 vector  $w_{\text{CDB2}}^{(k)}$  via the CDA algorithm with sample weights up-  
980 date strategy  $w_{\text{CDB2}}^{(k)} = g(X, w_{\text{CDB1}}^{(k)})$ . Each discriminant has an associated performance met-  
981 ric  $ps = f(w_{\text{CDB}})$ , bounded above by 1. At the current iteration, the optimal vector is found  
982 in the 2D plane spanned by CDB1 and CDB2 as  $w_{\text{CDB1}}^{(k+1)} = \lambda_1^* w_{\text{CDB1}}^{(k)} + \lambda_2^* w_{\text{CDB2}}^{(k)}$ , where  
983  $(\lambda_1^*, \lambda_2^*) = \arg \max_{\lambda_1, \lambda_2 \in \mathbb{R}} f(\lambda_1 w_{\text{CDB1}}^{(k)} + \lambda_2 w_{\text{CDB2}}^{(k)})$ , which is then used as the new CDB1 at  
984 iteration  $k + 1$ . Since  $w_{\text{CDB1}}^{(k)} \in \{\lambda_1 w_{\text{CDB1}}^{(k)} + \lambda_2 w_{\text{CDB2}}^{(k)}\}$  as a special case with  $\lambda_1 = 1$  and  $\lambda_2 = 0$ ,  
985 it follows that  $ps_{\text{CDB1}}^{(k+1)} \geq ps_{\text{CDB1}}^{(k)}$ . Therefore, the sequence  $ps_{\text{CDB1}}^{(k)} = f(w_{\text{CDB1}}^{(k)})$  is non-decreasing  
986 and bounded above, and hence converges to a finite limit  $ps^*$ .  
987  
988989  
990  
991  
992  
993  
994  
995  
996  
997  
998  
999  
1000  
1001  
1002  
1003  
1004  
1005  
1006  
1007  
1008  
1009  
1010  
1011  
1012  
1013  
1014  
1015  
1016  
1017  
1018  
1019  
1020  
1021  
1022  
1023  
1024  
1025

1026 **E DERIVING LDA IN THE GDA THEORETICAL FRAMEWORK FOR**  
 1027 **M-DIMENSIONS (M>2)**  
 1028

1029 In the GDA theoretical framework, we have demonstrated that linear discriminant (LD) can be  
 1030 expressed by the basis CDB0 with different geometric corrections on CDB0 under different conditions,  
 1031 as shown in Fig. 4. The conclusions are not confined only to the 2-dimensional case but also applicable  
 1032 to the  $m$ -dimensional case ( $m > 2$ ). Here we derive the generalization of the LD coefficient to the  
 1033  $m$ -dimensional case. The discriminant of LDA is given by  $\mathbf{w}_{\text{LD}} = \gamma \Sigma^{-1}(\boldsymbol{\mu}_1 - \boldsymbol{\mu}_0) = \gamma \Sigma^{-1} \mathbf{w}_{\text{CDB0}}$ ,  
 1034 where  $\gamma$  is a constant, and it is assumed that the within-class covariance matrix  $\Sigma$  is invertible, and  
 1035  $\Sigma = \Sigma_0 + \Sigma_1$  is the sum of covariance matrices of individual classes. Denote the elements in  $\Sigma$ ,  
 1036  $\Sigma_0$ , and  $\Sigma_1$  by  $\sigma_{ij}$ ,  $\sigma_{0ij}$ , and  $\sigma_{1ij}$  for all  $i, j \in \{1, 2, \dots, m\}$ , respectively.

1037 **Special Case 1.** Assume that pairwise features have the same covariance  $\alpha$ , and all pairwise features  
 1038 have the same covariance  $\alpha + \beta$  (In experiments, we relax the conditions to have similar variance  
 1039 and similar covariance). Then,  $\Sigma = \beta \mathbf{I} + \alpha \mathbf{1}$ , where  $\mathbf{I}$  is the identity matrix, and  $\mathbf{1}$  is the all-  
 1040 one matrix. According to the Woodbury matrix identity, we have  $\Sigma^{-1} = \frac{1}{\beta} \mathbf{I} - \frac{\alpha}{\beta(m\alpha+\beta)} \mathbf{1} =$   
 1041  $\gamma(\mathbf{I} - \frac{\alpha}{(m-1)\alpha+\beta} \mathbf{1}_N)$ , where  $\mathbf{1}_N$  is the matrix with all ones except on the diagonal. Thus,  $\mathbf{w}_{\text{LD}} =$   
 1042  $\gamma(\mathbf{w}_{\text{CDB0}} - \frac{\alpha}{(m-1)\alpha+\beta} \mathbf{1}_N \mathbf{w}_{\text{CDB0}})$ , which corresponds to the row for special case 1 in Fig. 4.

1043 **Special Case 1.1.** Based on the assumptions in Special Case 1, we further assume that the two  
 1044 covariance matrices are similar, i.e.,  $\Sigma_0 \approx \Sigma_1$ , so that  $\sigma_{0,ij} = \sigma_{1,ij}$  for all  $i, j$ . We further have  
 1045  $\frac{\sigma_{ij}}{\sigma_{ii}} = \frac{2\sigma_{0,ij}}{2\sigma_{0,ii}} = \frac{\sigma_{0,ij}}{\sqrt{\sigma_{0,ii}}\sqrt{\sigma_{0,jj}}} = r_{ij} \quad \forall i \neq j$ , where  $r_{ij}$  is the Pearson correlation coefficient (PCC)  
 1046 between features  $i$  and  $j$ . Based on the assumptions made in this special case, all pairwise PCCs  
 1047 are the same, i.e.,  $r_{ij} = r$  for all  $i \neq j$ . Thus,  $\Sigma^{-1} = \gamma(\mathbf{I} - \frac{r}{(m-2)r+1} \mathbf{1}_N)$ , which shows that  
 1048 the geometric correction part is related to feature correlations. Accordingly,  $\mathbf{w}_{\text{LD}} = \gamma(\mathbf{w}_{\text{CDB0}} -$   
 1049  $\frac{r}{(m-2)r+1} \mathbf{1}_N \mathbf{w}_{\text{CDB0}})$ , which corresponds to the row for special case 1.1 in Fig. 4.

1050 **Special Case 1.1.1.** Based on Special Case 1.1, assume further that all pairwise features have no  
 1051 correlations (i.e.,  $r = 0$ ), then according to the equation,  $\Sigma^{-1} = \gamma \mathbf{I}$ . Thus,  $\mathbf{w}_{\text{LD}} = \gamma \mathbf{w}_{\text{CDB0}} =$   
 1052  $\mathbf{w}_{\text{CDB0}}$ , where  $\gamma = 1$  since  $\mathbf{w}_{\text{CDB0}}$  is already a unit vector, which corresponds to the row for special  
 1053 case 1.1.1 in Fig. 4. By these derivations, we show how LDA converges to CDB0 under specific  
 1054 conditions of the data.

1055 **F DERIVING CDA IN THE GDA THEORETICAL FRAMEWORK**  
 1056

1057 In this section, we give the mathematical demonstration of how CDA is formulated in the GDA  
 1058 theoretical framework. Since the correction matrix for LDA in Section 2 is a special case of a  
 1059 linear operator, we extend to a more general correction term deriving CDA in the GDA theoretical  
 1060 framework. The construction of the geometric discriminant  $\mathbf{w}_{\text{GD}}$  can be realized by continuously  
 1061 rotating CDB0 in planes that satisfy several constraints, shown by:

$$\begin{aligned}
 \mathbf{w}_{\text{CDA}}^{(n)} &= \mathbf{A}_{\text{cda}}(\mathbf{w}_{\text{CDB1}}^{(n)}, \boldsymbol{\alpha}^{(n)}, \mathbf{X}, \mathbf{y}) \\
 &= \mathbf{A}_{\text{cda}}(\mathbf{w}_{\text{CDA}}^{(n-1)}, \boldsymbol{\alpha}^{(n)}, \mathbf{X}, \mathbf{y}) \\
 &= \mathbf{A}_{\text{cda}}(\mathbf{A}_{\text{cda}}(\mathbf{w}_{\text{CDB1}}^{(n-1)}, \boldsymbol{\alpha}^{(n-1)}, \mathbf{X}, \mathbf{y}), \mathbf{X}, \mathbf{y}) \\
 &= \dots = \left( \prod_{i=1}^n \mathbf{A}_{\text{cda}} \right) (\mathbf{w}_{\text{CDB1}}^{(1)}, \boldsymbol{\alpha}^{(1)}, \mathbf{X}, \mathbf{y}) \\
 &= \left( \prod_{i=1}^n \mathbf{A}_{\text{cda}} \right) (\mathbf{w}_{\text{CDB0}}) \\
 &= \mathbf{w}_{\text{CDB0}} + (\mathbf{I} - \prod_{i=1}^n \mathbf{A}_{\text{cda}})(\mathbf{w}_{\text{CDB0}}) \\
 &= \mathbf{w}_{\text{CDB0}} + \mathbf{C}_1 \mathbf{w}_{\text{CDB0}} = \mathbf{w}_{\text{GD}}
 \end{aligned} \tag{15}$$

1080 where  $\mathbf{A}_{\text{CDA}}$  is the CDA rotation operator,  $\mathbf{C}_1 = (\mathbf{I} - \prod^n \mathbf{A}_{\text{cda}})$ , in which  $\mathbf{I}$  is the identity operator.  
 1081 This equation matches with Eq. 10 and involves only one correction term, where  $\gamma = 1$  because  
 1082 both the CDB0 and CDA are unit vectors and  $\mathbf{C}_1$  is an overall matrix of high-dimensional rotation.  
 1083 For a given dataset  $\mathbf{X}, \mathbf{y}$  are fixed, it is simplified by:  $(\mathbf{w}_{\text{CDA}}, \boldsymbol{\alpha}) = \mathbf{A}_{\text{cda}}(\mathbf{w}_{\text{CDB1}}, \boldsymbol{\alpha}, \mathbf{X}, \mathbf{y}) =$   
 1084  $\mathbf{A}_{\text{cda}}(\mathbf{w}_{\text{CDB1}}, \boldsymbol{\alpha}) : \mathbb{R}^m \times \mathbb{R}^n \rightarrow \mathbb{R}^m \times \mathbb{R}^n$ , which defines the linear operator that maps the line  
 1085 CDB1 to CDA in each CDA iteration and maps the sample weights  $\boldsymbol{\alpha}$  to the updated sample weights.

1086 In Eq. 15, the second equality holds because  $\mathbf{w}_{\text{CDA}}$  obtained at the end of each rotation is used as  
 1087  $\mathbf{w}_{\text{CDB1}}$  in the next rotation. The fifth equality shows that the final CDA line can be written in a form  
 1088 that only depends on variables of the first iteration. This is because, in the first CDA rotation, the  
 1089 initial sample weights  $\boldsymbol{\alpha}^{(1)}$  are uniform, and CDB1 is the same as CDB0 of the GDA theoretical  
 1090 framework. Thus, from the sixth equality,  $\mathbf{X}, \mathbf{y}, \boldsymbol{\alpha}^{(1)}$  are omitted. The last three equalities show that  
 1091 the final CDA discriminant is a subcase of the generalized GDA theoretical framework.

1092 The operator  $\mathbf{A}_{\text{cda}}$  can be decomposed as two sequential operators:  
 1093

$$\begin{aligned} 1094 \mathbf{A}_{\text{cda}} &= \mathbf{A}_{\text{BO}} \left( \mathbf{w}_{\text{CDB1}}, \mathbf{A}_{\text{cda}}(\mathbf{w}_{\text{CDB1}}, \mathbf{A}_{\text{swu}}(\mathbf{w}_{\text{CDB1}}, \boldsymbol{\alpha}, \mathbf{X}, \mathbf{y}), \mathbf{X}, \mathbf{y}), \mathbf{X}, \mathbf{y} \right) \\ 1095 \\ 1096 \\ 1097 &= \mathbf{A}_{\text{BO}} \left( \mathbf{w}_{\text{CDB1}}, \boldsymbol{\alpha} \right) \end{aligned} \quad (16)$$

1098 where  $\mathbf{A}_{\text{cda}}(\mathbf{w}_{\text{CDB1}}, \boldsymbol{\alpha}) : \mathbb{R}^m \times \mathbb{R}^n \rightarrow \mathbb{R}^m \times \mathbb{R}^n$  is the linear operator that maps CDB1 to CDB2  
 1099 and updates sample weights by  $\mathbf{A}_{\text{swu}}(\mathbf{w}_{\text{CDB1}}, \boldsymbol{\alpha}) : \mathbb{R}^m \times \mathbb{R}^n \rightarrow \mathbb{R}^n$  which corresponds to Appendix  
 1100 C.3 Algorithm 2.  $\mathbf{A}_{\text{BO}}(\mathbf{w}_{\text{CDB1}}, \boldsymbol{\alpha}) : \mathbb{R}^m \times \mathbb{R}^n \rightarrow \mathbb{R}^m \times \mathbb{R}^n$  is the linear operator that maps two  
 1101 vectors CDB1 and CDB2 to the BO-estimated discriminant on the plane spanned by CDB1 and  
 1102 CDB2, and updates samples weights.  
 1103

1104  $\mathbf{A}_{\text{cda}}$  performs the mapping to CDB2 through the following equation:  
 1105

$$1107 \tilde{\mathbf{w}}_{\text{CDB2}} = \sum_{c=0}^1 (-1)^{c+1} \frac{\sum_{i=1}^N \alpha_i \mathbf{x}_i \delta(y_i - c)}{\sum_{i=1}^N \alpha_i \delta(y_i - c)} \quad (17)$$

$$1111 \mathbf{w}_{\text{CDB2}} = \tilde{\mathbf{w}}_{\text{CDB2}} / \|\tilde{\mathbf{w}}_{\text{CDB2}}\|_2 \quad (18)$$

1112 The operator  $\mathbf{A}_{\text{BO}}$  does the mapping to CDA through the following equation:  
 1113

$$1116 \tilde{\mathbf{w}}_{\text{orth}} = \mathbf{w}_{\text{CDB2}} - \mathbf{w}_{\text{CDB1}} \mathbf{w}_{\text{CDB2}}^T \mathbf{w}_{\text{CDB1}} \quad (19)$$

$$1120 \mathbf{w}_{\text{orth}} = \tilde{\mathbf{w}}_{\text{orth}} / \|\tilde{\mathbf{w}}_{\text{orth}}\|_2 \quad (20)$$

$$1123 \hat{\theta}^* \approx \arg \max_{\theta} \mathbf{A}_{\text{ps}}(\cos \theta \mathbf{w}_{\text{CDB1}} + \sin \theta \mathbf{w}_{\text{CDB2}}) \quad (21)$$

$$1126 \mathbf{w} = (\cos \hat{\theta}^* \mathbf{w}_{\text{CDB1}} + \sin \hat{\theta}^* \mathbf{w}_{\text{CDB2}}) \quad (22)$$

1128 Where the first two equations find the unit orthogonal vector to CDB1 by the Gram-Schmidt process.  
 1129 The orthogonalization process ensures an efficient search in the space of CDBs during the rotation.  
 1130 The last two equations estimate the optimal rotation angle using Bayesian optimization and the  
 1131 corresponding discriminant.  
 1132

1133  $ps = \mathbf{A}_{\text{ps}}(\mathbf{w}_{\text{CDB}}) : \mathbb{R}^m \rightarrow \mathbb{R}$  is the operator that outputs the performance score given a classification  
 1134 discriminant, which projects all data onto the discriminant and performs the OOP search of the score.

---

## 1134 G CLASSIFICATION PERFORMANCE EVALUATION

1135  
 1136 The datasets used in this study span standard image classification, medical image classification, and  
 1137 chemical property classification, most of which involve multiclass data. To comprehensively assess  
 1138 classification performance across these diverse tasks, we employed four key metrics: AUROC, AUPR,  
 1139 F-score, and AC-score. Accuracy was excluded due to its limitations in reflecting true performance,  
 1140 especially on imbalanced data. Though data augmentation can make data balanced, it introduces  
 1141 uncertainty due to the augmentation strategy and the data quality.

1142 Since we do not prioritize any specific class (as designing a dataset-specific metric is beyond this  
 1143 study’s scope), we perform two evaluations—one assuming each class as positive—and take the  
 1144 average. This approach applies to AUPR and F-score, whereas AUROC and AC-score, being  
 1145 symmetric about class labels, require only a single evaluation.

1146 For multiclass prediction, a  $C$ -dimensional confusion matrix is obtained by comparing predicted  
 1147 labels with true labels. This is converted to  $C$  binary confusion matrices by each time taking one  
 1148 class as positive and all the others as negative, and the final evaluation is the average of evaluations  
 1149 on these individual confusion matrices.

1150 To interpret this evaluation scheme, consider the MNIST dataset and the AUPR metric as an example.  
 1151 In binary classification, for the pair of digits “1” and “2”, it calculates the sensitivity-recall for  
 1152 detecting “1” and the sensitivity-recall for detecting “2”, then takes the average. For other pairs, the  
 1153 calculation follows the same pattern. In the multiclass scenario, it considers the sensitivity-recall  
 1154 for detecting “1” and the sensitivity-recall for detecting “not 1”, then takes the average. The same  
 1155 approach applies to other pairs.

### 1157 INDIVIDUAL METRICS

#### 1159 (A) AUROC

1160 Area Under the Receiver Operating Characteristic curve involves the true positive rate (TPR) and  
 1161 false positive rate (FPR) as follows:

$$1163 \quad AUROC = \int_{x=0}^1 TPR \times FPR^{-1}(x)dx \quad (23)$$

1164 This measure indicates how well the model distinguishes between classes. A high score means that  
 1165 the model can identify most positive cases with few false positives.

#### 1168 (B) AUPR

1169 Area Under the Precision-Recall curve considers two complementary indices: precision ( $prec$ ) and  
 1170 recall ( $rec$ ), defined as:

$$1172 \quad AUPR = \int_{x=0}^1 prec \times rec^{-1}(x)dx \quad (24)$$

1173 AUPR measures whether the classifier retrieves most positive cases.

#### 1176 (C) F-SCORE

1177 F-score (using F1-score in this study) is the harmonic mean of precision and recall which contribute  
 1178 equally:

$$1180 \quad F_{score} = 2 \times \frac{prec \times rec}{prec + rec} \quad (25)$$

#### 1182 (D) AC-SCORE

1183 An accuracy-related metric AC-score (Wu & Cannistraci (2025)) addresses the limitations of tra-  
 1184 ditional accuracy for imbalanced data. It imposes a stronger penalty for deviations from optimal  
 1185 performance on imbalanced data and is defined as:

$$1187 \quad AC_{score} = \frac{2 \times TPR \times TNR}{TPR + TNR} \quad (26)$$

1188 This metric assigns equal importance to both classes and penalizes imbalanced performance by  
 1189 ensuring that if one class is poorly classified, the overall score remains low. Thus, AC-score provides  
 1190 a more conservative but reliable evaluation of classifier performance.  
 1191

1192 (E) PERFORMANCE-SCORE (PS)  
 1193

1194 The proposed CDA classifier employs performance-dependent learning, guided by a performance  
 1195 score (ps):

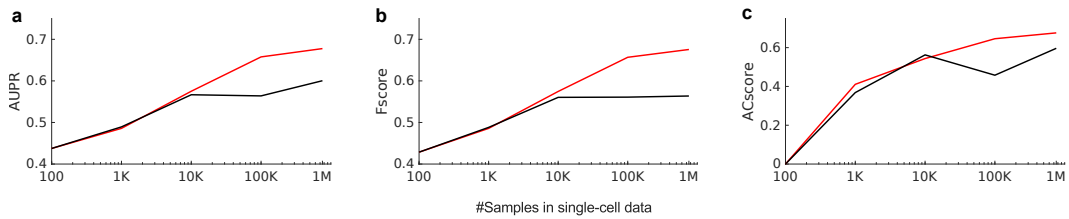
$$1196 ps = (F_{score}^{pos} + F_{score}^{neg} + AC_{score})/3 \quad (27)$$

1197 This formulation ensures a balanced consideration of both F-score and AC-score.

1198 Though CDA as a generic classifier utilizes a relatively balanced metric, it can be customized to  
 1199 specific applications as needed.  
 1200

1201 **H EXPERIMENT ON LINEAR CLASSIFICATION OF LARGE-SCALE DATA**  
 1202

1203 There are real-world problems where the samples are at million-level in addition to plenty of features,  
 1204 posing a significant challenge to train classifiers in reasonable time. One of these problems is omics  
 1205 data classification such as single-cell sequencing data. We collected the 1.3-million-cell mouse brain  
 1206 dataset (10x Genomics (2017)) and took the largest two classes to create a binary classification task  
 1207 (757,526 samples and 27,998 features), with varying number of samples by random subsampling  
 1208 till all samples were included. We compared CDA and fast SVM (dual optimizer), which is one  
 1209 of the most efficient and scalable linear SVM, with regard to performance and speed. **We applied**  
 1210 **CDA with Fibonacci optimizer as the fast version for large data.** Original data of sequencing counts  
 1211 were used, and the training and test sets were created using a 4:1 split. The results show that with  
 1212 growing sample sizes, linear CDA outperforms fast SVM not only on classification performance  
 1213 AUROC (Figure 2a and Appendix Figure 6), but also on the single-core training speed (Figure 2b).  
 1214 These results indicate that linear CDA is even more efficient and scalable than the flagship SVM  
 1215 method in efficiency. Hence, CDA as a fast approach has the potential to drive large-scale real-world  
 1216 applications in fields such as biomedicine and autonomous driving.



1217  
 1218 Figure 6: Test set performance with varying sizes of training samples in single-cell mouse brain data,  
 1219 evaluated by (a) AUPR, (b) Fscore and (c) ACscore. CDA: Centroid Discriminant Analysis; SVM:  
 1220 Support Vector Machine; AUPR: Area under precision-recall curve; ACscore: Accuracy score.  
 1221

1222 **I SUPPLEMENTAL TRAINING SPEED RESULTS**  
 1223

1224  
 1225  
 1226  
 1227  
 1228  
 1229  
 1230  
 1231  
 1232  
 1233  
 1234  
 1235  
 1236  
 1237  
 1238  
 1239  
 1240  
 1241

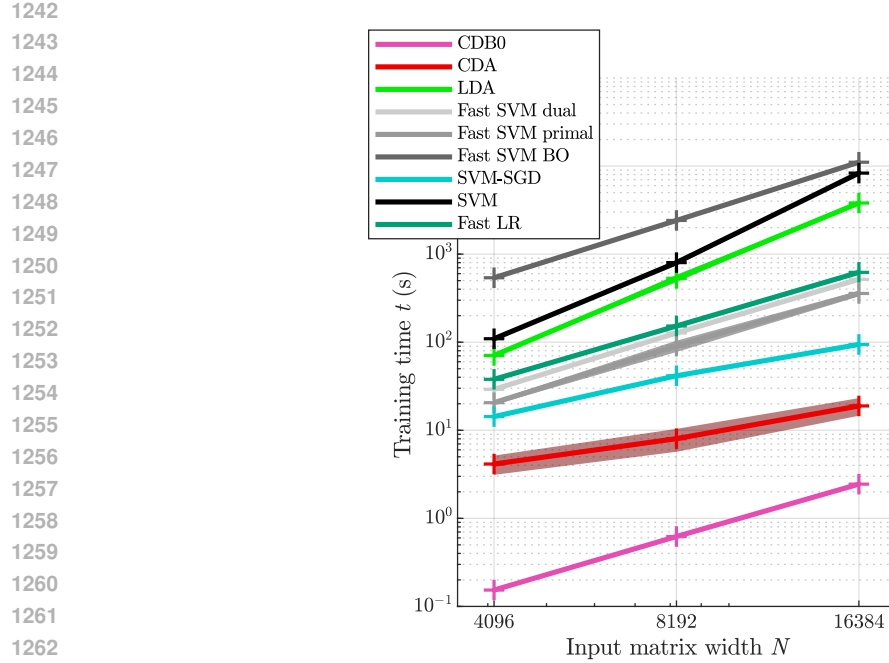


Figure 7: The training time with constant overhead kept. The training time of linear classifiers with increasing input matrix sizes. The number of features were set the same as number of samples  $N$ . Shaded area represents standard error. Log-scale is used for both axes to reveal the scalability of algorithms. CDB0: Centroid Discriminant Basis 0; CDA: Centroid Discriminant Analysis; LDA: Linear Discriminant Analysis; SVM: Support Vector Machine; BO: Bayesian Optimization; SGD: Stochastic Gradient Descent; LR: Logistic Regression.

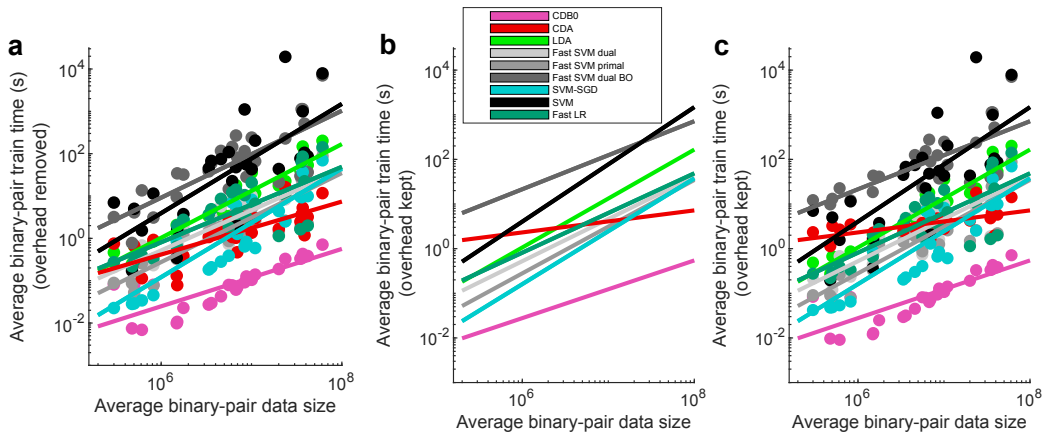


Figure 8: Running time results of linear classifiers on 27 real datasets. (a) Linear regression fit of the running time against data sizes, together with original running time data shown by the circles. Overhead is removed. (b-c) Running time and speed results with overhead kept. (b) Linear regression fit of the running time against data sizes. (c) The same as (b) with original running time data shown by the circles. The log-log scale is applied then linear regression is performed in (a-c) to reflect scaling behavior. CDB0: Centroid Discriminant Basis 0; CDA: Centroid Discriminant Analysis; LDA: Linear Discriminant Analysis; SVM: Support Vector Machine; BO: Bayesian Optimization; SGD: Stochastic Gradient Descent; LR: Logistic Regression.

1296 **J IMPLEMENTATION DETAILS**  
12971298 All data samples were converted into 1d representations without feature extraction or standardization  
1299 throughout the paper, as the focus of this study is to compare the general performance of various  
1300 classifiers on common tasks, rather than optimizing feature extraction for specific applications such  
1301 as image classification.  
13021303 **J.1 LINEAR CLASSIFIERS**  
13041305 Linear classifiers compared in this study include LDA, SVM, and fast SVM. Data were input to  
1306 classifiers in their original values without standardization.  
13071308 For CDA, the threshold for the coefficient of variation (CV) of performance-score was set to 0.001.  
1309 5-fold cross-validation is applied on the OOP search.  
13101311 For LDA, the MATLAB toolbox function `fitcdiscr` was applied, with `pseudolinear` as  
1312 the discriminant type, which solves the pseudo-inverse with SVD to adapt to poorly conditioned  
1313 covariance matrices.  
13141315 For SVM, the MATLAB toolbox function `fitcsvm` was applied, with sequential minimal  
1316 optimization (SMO) as the optimizer. The cost function used the L2-regularized (margin) L1-loss  
1317 (misclassification) form. The misclassification cost coefficient was set to  $C = 1$  by default. The  
1318 maximum number of iterations was linked to the number of training samples in the binary pair as  
1319  $100 \times N_{\text{train}}$ . The convergence criteria were set to the default values.  
13201321 For fast SVM, the LIBLINEAR MATLAB `mex` function was applied. For the dual form SVM  
1322 using dual coordinate descent (DCD), the cost function used the L2-regularized (margin) L1-loss  
1323 (misclassification) form; For the primal form SVM, both regularization and loss are in L2 form.  
1324 The misclassification cost coefficient was set to  $C = 1$  by default. A bias term was added, and  
1325 correspondingly, the data had an additional dimension with a value of 1. The convergence criteria  
1326 were set to the default values. Training epochs were set to 300 in general tasks and 100 in large-scale  
1327 single-cell test.  
13281329 For SVM-SGD, the passes of all training data are 10; batchsize is 10; learning rate is  
1330  $1/\sqrt{1 + \max_i \|\mathbf{x}_i\|_2}$ .  
13311332 Hyperparameter tuning was performed for fast SVM to achieve the its best performance. CDA, as  
1333 well as CDB0, do not require parameter tuning.  
13341335 Speed tests and performance test were from different computational conditions. To obtain classifica-  
1336 tion performance in a reasonable time span, GPU was enabled for SVM, and multicore was enabled  
1337 for CDA and LDA. To compare speed fairly, all linear classifiers used single-core computing mode.  
13381339 **J.2 NONLINEAR CLASSIFIERS**  
13401341 For the experiments on the nonlinear kernel-based approaches, on SVHN subset and chemical ClinTox,  
1342 the data were first divided into train+validation and test set with 5:1 and 4:1 ratio respectively, then  
1343 the train+validation set was further divided into train set and validation set with a 4:1 ratio.  
13441345 The gaussian kernel parameter sigma was tuned on the validation set by Bayesian optimiza-  
1346 tion with 30 sampling. For the tuned gaussian parameter, on SVHN subset gaussian CDA  
1347 has  $\text{coeff} = 0.2$  and gaussian SVM has  $\text{coeff} = 0.134$ ; on ClinTox gaussian CDA has  
1348  $\text{coeff} = 1.34$  and gaussian SVM has  $\text{coeff} = 68.9$ , where in gaussian kernel  $\sigma^2 = \text{coeff} * \text{median}(\text{pairwiseSquareEuclideanDistance}(\mathbf{X}_{\text{train}}))$ .  
13491350 For CDA, the threshold for the coefficient of variation (CV) of performance-score was set to 0.001.  
1351 For SVM, libSVM was implemented with L2-regularized (margin) L1-loss (misclassification) cost  
1352 function and with default misclassification cost coefficient  $C = 1$ .  
1353

## 1350 K DATASET DESCRIPTION

1352 The datasets tested in this study encompass standard image classification, medical image classification,  
 1353 and chemical property prediction, described in details in Table. 1.

1356 **Table 2: Dataset description**

1357 Dataset	1358 #Samples	1359 #Features	1360 #Classes	1361 Balancedness	1362 Modality/source	1363 Classification task
<b>1358 Standard images</b>						
MNIST	70000	400	10	imbalanced	image	digits
USPS	9298	256	10	imbalanced	image	digits
EMNIST	145600	784	26	balanced	image	letters
CIFAR10	60000	3072	10	balanced	image	objects
SVHN	99289	3072	10	imbalanced	image	house numbers
flower	3670	1200	5	imbalanced	image	flowers
GTSRB	26635	1200	43	imbalanced	image	traffic signs
STL10	13000	2352	10	balanced	image	objects
FMNIST	70000	784	10	balanced	image	fashion objects
<b>1365 Medical images</b>						
dermamnist	10015	2352	7	imbalanced	dermatoscope	dermal diseases
pneumoniamnist	5856	784	2	imbalanced	chest X-Ray	pneumonia
retinamnist	1600	2352	5	imbalanced	fundus camera	diabetic retinopathy
breastmnist	780	784	2	imbalanced	breast ultrasound	breast diseases
bloodmnist	17092	2352	8	imbalanced	blood cell microscope	blood diseases
organamnist	58830	784	11	imbalanced	abdominal CT	human organs
organcmnist	23583	784	11	imbalanced	abdominal CT	human organs
organsmnist	25211	784	11	imbalanced	abdominal CT	human organs
organmnist3d	1472	21952	11	imbalanced	abdominal CT	human organs
nodulemnist3d	1633	21952	2	imbalanced	chest CT	nodule malignancy
fracturemnist3d	1370	21952	3	imbalanced	chest CT	fracture types
adrenalmnist3d	1584	21952	2	imbalanced	shape from abdominal CT	adrenal gland mass
vesselmnist3d	1908	21952	2	imbalanced	shape from brain MRA	aneurysm
synapsemnist3d	1759	21952	2	imbalanced	electron microscope	excitatory/inhibitory
<b>1375 Chemical formula</b>						
bace	1513	198	2	imbalanced	chemical formula	BACE1 enzyme
BBBP	2050	400	2	imbalanced	chemical formula	blood-brain barrier permeability
clintox	1484	339	2	imbalanced	chemical formula	clinical toxicity
HIV	41127	575	2	imbalanced	chemical formula	HIV drug activity
<b>1379 Large-scale single-cell sequencing data</b>						
Mouse brain	1306127	27998	10	imbalanced	single-cell sequencing	cell type

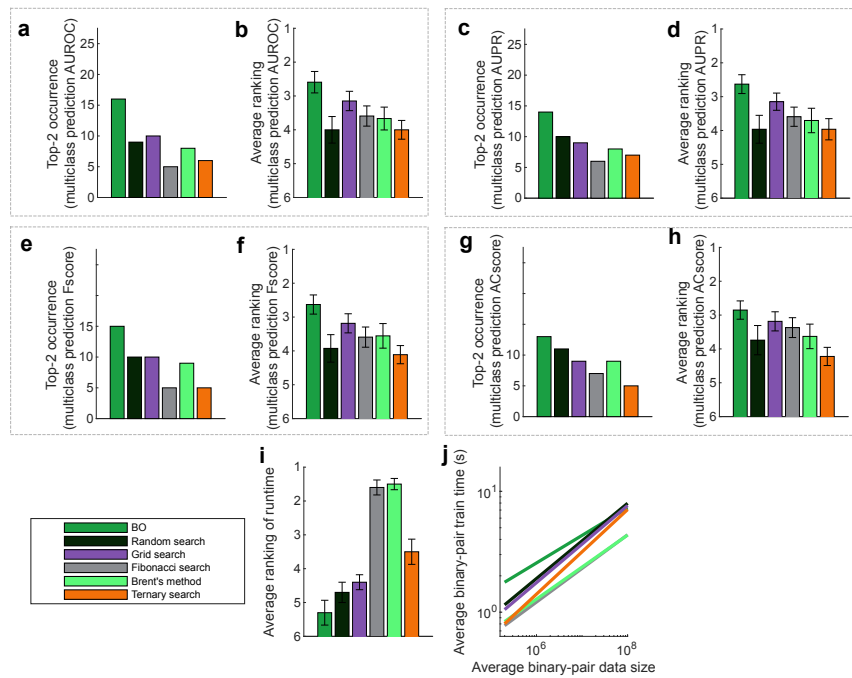
1380 **1381 Data processing:** Image data were used in their original value flattened to 1d vectors; chemical for-  
 1382 mula were processed by simplified molecular input line entry system (SMILES) tokenized encoding.  
 1383 SMILES is a line notation for describing the structure of chemical entities using short ASCII strings.  
 1384 Chemical formula were stacked and aligned from the left since they have different SMILES lengths.  
 1385 The strings were mapped to natural numbers using a predefined dictionary, and those missing string  
 1386 positions were filled with 0. On these converted data we performed different classifiers.

## 1404 L OPTIMIZER COMPARISON FOR CDA ROTATION

1406 In this section we provide an expanded justification and empirical assessment of the one-dimensional  
 1407 (1D) optimizer used within the CDA iterative update. Although Bayesian Optimization (BO) was  
 1408 originally adopted, a 1D optimization problem does not inherently require BO; several classical  
 1409 black-box optimizers can also be applied with low implementation overhead. To rigorously assess the  
 1410 optimizer choice, we conducted a meticulous study comparing BO with five alternative 1D optimizers:  
 1411 (1) random search, (2) grid search, (3) Fibonacci search, (4) Brent’s method, and (5) ternary search.  
 1412 All methods were evaluated under identical settings.

1413 Figure L summarizes the comparative performance of CDA under six different 1D optimization  
 1414 strategies across 27 real datasets, reported using AUPR, Fscore, and ACscore. CDA with Fibonacci  
 1415 and BO achieves the most frequent top-ranked positions, further confirming the empirical robustness  
 1416 of the proposed recommendations.

1417 Based on these findings, several practical recommendations emerge. For maximum computational  
 1418 efficiency, Fibonacci search is the preferred choice and provides the most favorable balance between  
 1419 speed and stability. BO remains a competitive secondary option, particularly when log-transformed  
 1420 data are used, as BO tends to exploit smoothness more effectively in this domain. For large-scale  
 1421 datasets, Fibonacci search consistently offers the most robust and efficient solution.



1447 Figure 9: Performance comparison of CDA using six different one-dimensional optimizers: Bayesian  
 1448 Optimization (BO), random search, grid search, Fibonacci search, Brent’s method, and ternary search.  
 1449 Panels (a–b) show AUROC, (c–d) AUPR, (e–f) F-score, and (g–h) AC-score, reporting both top-2  
 1450 occurrences and average ranking of multiclass performance across 27 real datasets. Panels (i–j)  
 1451 show the average ranking of running speed and the corresponding runtime plot. Error bars represent  
 1452 standard errors. CDA: Centroid Discriminant Analysis.

1453 Table 3 reports the results on the same experiments with (i) final CDA performance, (ii) average  
 1454 running time, (iii) average number of CDA iterations, and (iv) average runtime per iteration, as  
 1455 summarized in the table below. Notably, across all optimizers, CDA consistently converges to a  
 1456 similar performance level, demonstrating that CDA algorithm is well-posed and stable, regardless  
 1457 of the choice of 1D optimizer. For runtime per iteration (iv), random search is the fastest due  
 1458 to minimal structural overhead, whereas BO is the slowest because of the cost associated with

1458 maintaining its surrogate model. CDA employs an early-stop strategy, monitoring the stability of  
 1459 training performance across iterations. Among the tested optimizers, Fibonacci search provides the  
 1460 most stable training, yielding the lowest average running time and the fewest CDA iterations.

1461 To further validate this conclusion, CDA with Fibonacci search was applied to a large-scale mouse-  
 1462 brain single-cell dataset containing up to one million samples for multiclass cell-type classification  
 1463 (see Section H). The resulting performance and running time demonstrate that the Fibonacci-based  
 1464 CDA significantly improves computational efficiency while maintaining high predictive accuracy,  
 1465 whereas even optimized SVM implementations require substantially longer runtimes.

1466 The CDA convergence analysis with Fibonacci optimizer is provided in Section O.

1467

1468

1469 Table 3: CDA performance and efficiency across six 1D optimizers for original and log-transformed  
 1470 data.

	BO	Random search	Grid search	Fibonacci search	Brent's method	Ternary search
<b>Original data</b>						
Avg. performance (AUROC)	0.758	0.755	0.751	0.757	0.753	<b>0.760</b>
Avg. runtime (s)	4.681	4.339	4.137	<b>2.473</b>	2.838	3.230
Avg. number of rotations	36.278	46.330	43.811	<b>29.689</b>	29.252	35.441
Time per iteration (s)	0.136	<b>0.096</b>	0.099	0.099	0.107	0.114
<b>Log-transformed data</b>						
Avg. performance (AUROC)	<b>0.764</b>	0.745	0.761	0.755	0.754	0.758
Avg. runtime (s)	4.693	4.313	4.003	<b>2.503</b>	2.546	3.355
Avg. number of rotations	35.796	46.330	43.507	30.244	<b>26.178</b>	35.759
Time per iteration (s)	0.134	<b>0.095</b>	0.098	0.098	0.113	0.108

1483

1484

1485

1486

1487

1488

1489

1490

1491

1492

1493

1494

1495

1496

1497

1498

1499

1500

1501

1502

1503

1504

1505

1506

1507

1508

1509

1510

1511

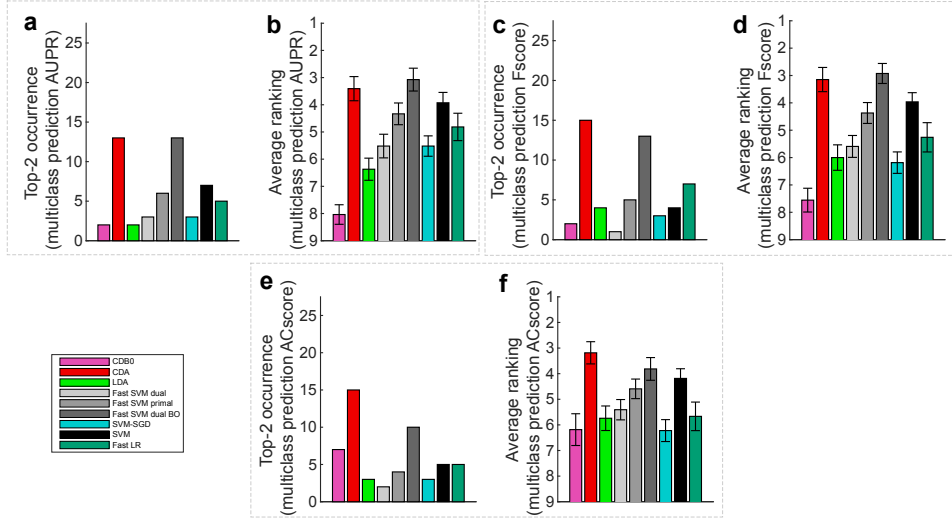
1512 M STABILITY OF BO IN CDA WITH INITIAL FEW SAMPLING  
1513

1514 To assess the stability of the BO-driven rotation process when only a few initial samples are available,  
 1515 we compared two BO schemes that differ only in the number of initial samples (all other BO  
 1516 hyperparameters and total BO budget were kept the same). In the first BO sampling scheme, the  
 1517 number of sampling is set to  $\min(10, \max(4, \text{Iter}))$  that gradually increase the number of sampling  
 1518 from 4 to 10 according to the current CDA iteration. In the second BO sampling scheme, the  
 1519 number of sampling is set to always 10. The goal is to test whether the early-stage sampling scarcity  
 1520 destabilizes convergence or substantially degrades multiclass performance.

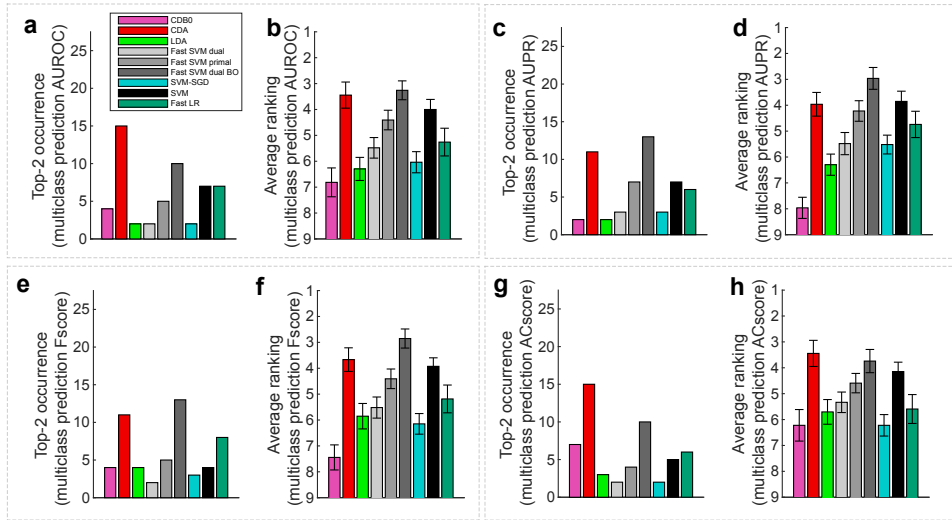
1521 The results in Table 4 show that, across a wide set of image, medical and chemical datasets, perfor-  
 1522 mance is essentially unchanged between the two schemes (average AUROC 0.758 vs 0.754). The  
 1523 absolute average difference is 0.004, which is negligible for our tasks and indicates that BO-driven  
 1524 rotations are stable even when the initial sampling budget is small. It is even beneficial to use fewer  
 1525 sampling at initial CDA iterations.

1527 Table 4: [Multiclass AUROC for CDA with different BO sampling schemes.](#)

	BO with few initial sampling	BO control with high initial sampling
Average AUROC	<b>0.758</b>	0.754

1566 N SUPPLEMENTAL PERFORMANCES ON REAL DATASETS OF LINEAR CDA  
1567  
1568  
1569

1587 Figure 10: Multiclass prediction performance on 27 real datasets of CDA-BO. Panels (a–b) show  
1588 AUPR, (c–d) Fscore, (e–f) ACscore, reporting both top-2 occurrences and average ranking of  
1589 multiclass performance across 27 real datasets. Error bars represent standard errors. CDB0: Centroid  
1590 Discriminant Basis 0; CDA: Centroid Discriminant Analysis; LDA: Linear Discriminant Analysis;  
1591 SVM: Support Vector Machine; LR: Logistic Regression; BO: Bayesian Optimization

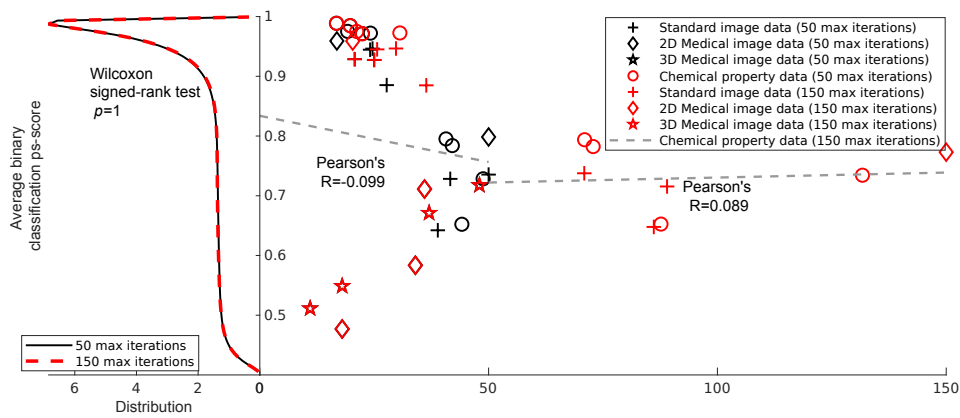


1611 Figure 11: Multiclass prediction performance on 27 real datasets of CDA-Fibonacci. Panels (a–b)  
1612 show AUROC, (c–d) AUPR, (e–f) F-score, and (g–h) AC-score, reporting both top-2 occurrences  
1613 and average ranking of multiclass performance across 27 real datasets. Error bars represent standard  
1614 errors. CDB0: Centroid Discriminant Basis 0; CDA: Centroid Discriminant Analysis; LDA: Linear  
1615 Discriminant Analysis; SVM: Support Vector Machine; LR: Logistic Regression; BO: Bayesian  
1616 Optimization

1620 **O CDA-FIBONACCI CONVERGENCE**  
1621

1622 We analyzed the relationship between the actual stopping iteration of CDA and the average binary  
1623 classification performance (ps-score) across different datasets and iteration limits. The results  
1624 revealed two distinct regimes. In the right half of Fig. 12, for tasks converging before 50 iterations,  
1625 we observed a significant negative correlation (Pearson’s  $R = -0.099$ ), indicating that datasets with  
1626 lower performance required more iterations to converge. This highlights the importance of allowing at  
1627 least 50 iterations, as early stopping before this point may prevent convergence for more challenging  
1628 tasks. In contrast, for tasks exceeding 50 iterations, the correlation was weak and positive (Pearson’s  $R$   
1629 = 0.089), suggesting that beyond this threshold, the number of iterations no longer plays a significant  
1630 role in ensuring convergence. This indicates that once 50 iterations are reached, CDA can stabilize  
1631 regardless of the underlying task performance.

1632 To further validate this observation, in the left half of Fig. 12, we compared the distributions  
1633 of ps-scores obtained under maximum iteration limits of 50 and 150. The estimated probability  
1634 densities were identical, and the Wilcoxon signed-rank test confirmed no difference between the  
1635 two conditions ( $p=1$ ). This result supports the conclusion that extending the maximum number of  
1636 iterations beyond 50 does not provide systematic benefits in terms of classification performance. Note  
1637 that the correlation before 50 in CDA-Fibonacci is weaker than CDA-BO in Figure 3, indicating that  
1638 the Fibonacci optimizer helps CDA converge faster.

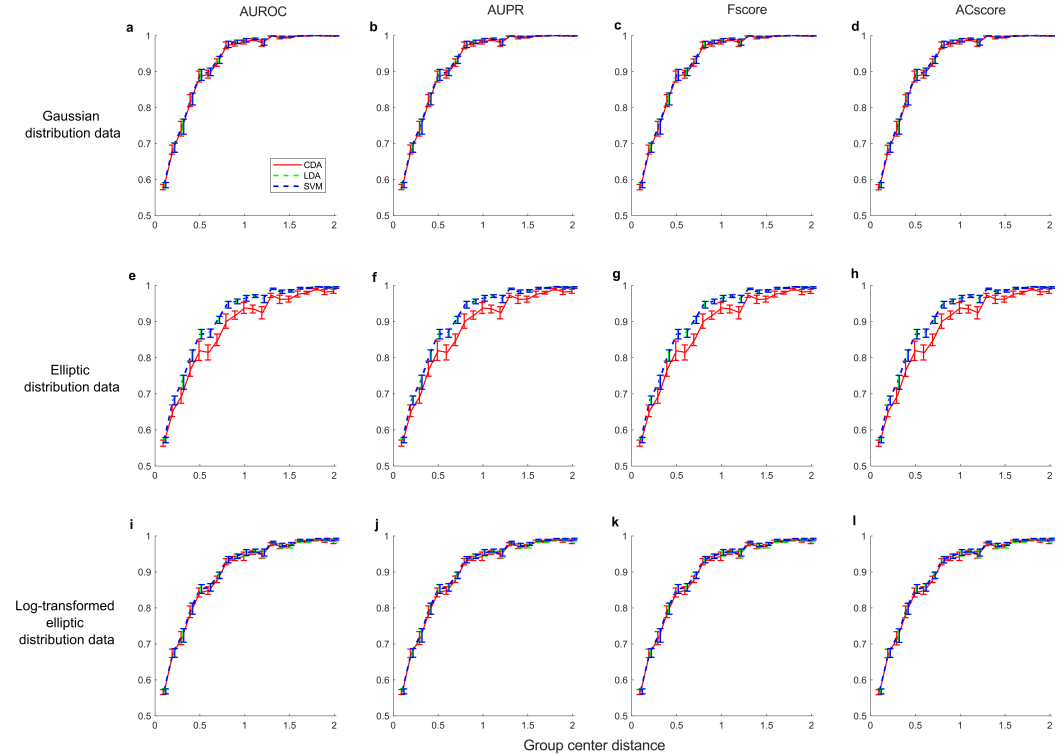


1639  
1640  
1641  
1642  
1643  
1644  
1645  
1646  
1647  
1648  
1649  
1650  
1651  
1652  
1653 Figure 12: Convergence characterization of CDA-Fibonacci. In the right half, relationship between  
1654 average binary classification ps-score and the actual stopping iteration of CDA across four dataset  
1655 categories (standard images, 2D medical images, 3D medical images, and chemical property data)  
1656 under two maximum iteration limits (50 and 150). A negative correlation was observed for tasks  
1657 converging before 50 iterations (Pearson’s  $R = -0.099$ ), while a weak positive correlation was found  
1658 for tasks converging after 50 iterations (Pearson’s  $R = 0.089$ ). The gray dash lines show linear  
1659 regression of points till 50 and points between 51 and 150. The black vertical line indicates the  
1660 50-iteration threshold. In the left half, probability density distributions of ps-scores under 50 and  
1661 150 maximum iterations show substantial overlap. The Wilcoxon signed-rank test confirmed no  
1662 difference ( $p=1$ ), demonstrating that increasing the maximum iteration limit beyond 50 does not  
1663 improve classification performance.

1664  
1665  
1666  
1667  
1668  
1669  
1670  
1671  
1672  
1673

1674 **P LOG-TRANSFORMING THE DATA FOR CDA TO HANDLE OUTLIERS**  
1675

1676 We performed controlled simulations under three conditions: Gaussian data, elliptic data, and log-  
1677 transformed elliptic data. Each simulation consisted of 10,000 samples with 10 features, and the  
1678 covariance structure was specified using a Toeplitz matrix. The distance between group centers  
1679 was gradually increased to generate different levels of class separability. We included SVM in the  
1680 comparison, since its margin-based formulation is known to provide a degree of robustness to outliers.  
1681

1682 The results shown in Figure 13 indicate that for Gaussian data, CDA performs comparably to LDA  
1683 and SVM, confirming that it does not lose predictive power under ideal Gaussian conditions. For  
1684 elliptic distributions, CDA is affected by outliers, as expected. However, applying a log-transform to  
1685 the features effectively mitigates the influence of extreme values. After log-transforming the elliptic  
1686 data, the performance of CDA improves substantially, and this preprocessing step benefits CDA more  
1687 than it benefits LDA or SVM.  
1688

1712 Figure 13: Controlled simulation results comparing CDA, LDA, and SVM under different data  
1713 distributions. Panels (a-d) correspond to Gaussian data, (e-h) to elliptic data, and (i-l) to log-  
1714 transformed elliptic data. Within each group, the metrics shown are AUROC (a, e, i), AUPR (b,  
1715 f, j), F-score (c, g, k), and AC-score (d, h, l). The simulations consist of 10,000 samples with 10  
1716 features, and the covariance structure is specified using a Toeplitz matrix. Group center distances were  
1717 gradually increased to evaluate performance under varying class separability. These results illustrate  
1718 that CDA maintains comparable performance to LDA and SVM for Gaussian data, is affected by  
1719 outliers under elliptic distributions, and benefits substantially from log-transforming features.  
1720

1721 We further applied the log-transform to 27 real datasets, with results summarized in Table 5. For  
1722 CDA, both the winning rate (from 0.519 to 0.741) and the average performance increased. For  
1723 LDA, although the winning rate improved, the average performance decreased, while for SVM, the  
1724 log-transform led to an overall decline in performance. These results suggest that the log-transform is  
1725 well suited for variance stabilization and outlier control, and that CDA uniquely benefits from this  
1726 preprocessing step, yielding enhanced overall performance. Based on these findings, we recommend  
1727 incorporating a log-transform preprocessing step when applying CDA to data with heavy-tailed or  
1728 elliptic distributions.  
1729

1728  
 1729  
 1730  
 1731  
 1732  
 1733  
 1734  
 1735  
 1736  
 1737  
 1738  
 1739  
 1740  
 1741  
 1742  
 1743  
 1744  
 1745  
 1746  
 1747  
 1748  
 1749  
 1750  
 1751  
 1752

1753 Table 5: Binary classification performance comparison under original and log-transformed data.

	CDA		LDA		SVM fast	
	Original	Log	Original	Log	Original	Log
Average performance	0.800	<b>0.805</b>	<b>0.758</b>	0.742	<b>0.765</b>	0.757
Winning rate	0.519	<b>0.741</b>	0.481	<b>0.688</b>	<b>0.704</b>	0.407

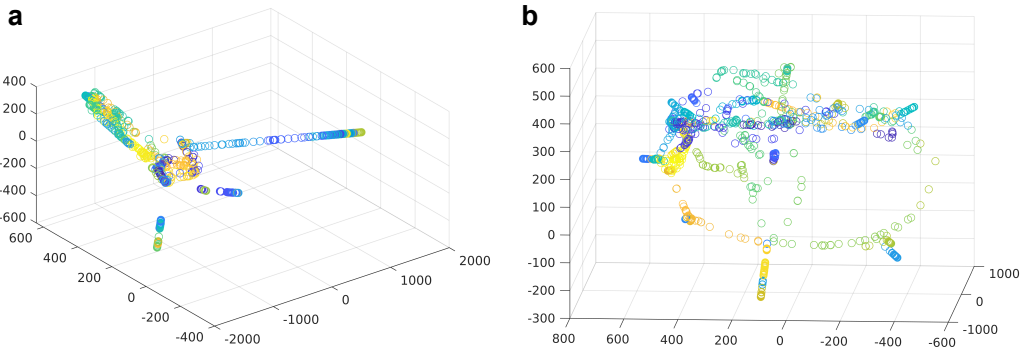
1758  
 1759  
 1760  
 1761  
 1762  
 1763  
 1764  
 1765  
 1766  
 1767  
 1768  
 1769  
 1770  
 1771  
 1772  
 1773  
 1774  
 1775  
 1776  
 1777  
 1778  
 1779  
 1780  
 1781

1782  
 1783 **Q PERFORMANCE OF CENTROID-BASED METHODS IN DATASETS WITH**  
 1784 **MULTIPLE SUBCLASSES**

1785 We analyzed a dataset in which each class naturally decomposes into several subclasses, for example,  
 1786 due to illumination changes or rotations. To illustrate this, we selected two classes from the GTSRB  
 1787 dataset and applied Isomap dimensionality reduction (k-nearest neighbors, k=3), marking the ground-  
 1788 truth subclasses in the same color. The resulting embeddings are shown in Figure 14 for the two  
 1789 groups.

1790 We first applied a log-transform to the data to assess the potential impact of outliers. As indicated by  
 1791 the results in Table 6 using CDA with Bayesian Optimization, the log-transform did not produce a  
 1792 significant difference, ruling out outliers as the primary source of variability. Therefore, the challenges  
 1793 in modeling this dataset can be attributed to the presence of multiple subclusters within each class.

1794 We then compared CDA, CDB0, LDA, and SVM on the GTSRB dataset. The results in Table 7  
 1795 show that the purely centroid-based baseline CDB0 performs poorly (AUROC = 0.589, close to  
 1796 random), confirming that a single centroid is insufficient for classes with multiple subclusters. In  
 1797 contrast, CDA—while still centroid-driven—incorporates adaptive discriminant corrections and  
 1798 achieves AUROC = 0.878, outperforming LDA (AUROC = 0.821). This demonstrates that, among  
 1799 centroid-based methods, CDA is substantially more robust to intra-class multimodality. While all  
 1800 SVM variants achieve AUROC > 0.90, CDA remains competitive, offering a strong balance between  
 1801 robustness and computational efficiency in datasets with multiple subclusters per class.



1815 Figure 14: Isomap dimension reduction results of two classes in GTSRB dataset (Pictures of different  
 1816 traffic signs). The same subclasses are marked with the same color according to the ground truth,  
 1817 which shows there are obvious subclusters.

1821 **Table 6: Multiclass prediction performance (AUROC) of CDA with Bayesian Optimization on the**  
 1822 **GTSRB dataset under original and log-transformed data.**

Data	CDA BO
Original	0.878±0.01
Log-transformed	<b>0.887±0.01</b>

1828 **Table 7: Multiclass prediction performance (AUROC) on the GTSRB dataset.**

Method	CDB0	CDA	LDA	SVM
AUROC	0.589±0.01	0.878±0.01	0.821±0.02	<b>0.983±0.003</b>

1836 R MORE ABOUT LINEAR CDA CLASSIFICATION  
1837

1838 While the core CDA algorithm is efficient, the kernelized version inherits the standard computational  
 1839 bottleneck of kernel matrix construction. This bottleneck is not specific to CDA, but is an inherent  
 1840 limitation of all kernel-based linear classifiers. When any linear method (e.g., LDA, SVM) is  
 1841 kernelized, the dominant cost comes from constructing and storing the  $N \times N$  kernel matrix, which  
 1842 scales quadratically with the sample size. Thus, the kernelized CDA inherits the standard kernel-  
 1843 matrix bottleneck shared universally by kernel methods, rather than introducing a new one. Although,  
 1844 we provide preliminary results that CDA can be formulated in the nonlinear versions via the kernel  
 1845 trick, we stress that in this paper we focused on linear CDA classification, because linear methods  
 1846 remain widely used in several scientific domains - particularly neuroscience, biomedicine, and social  
 1847 sciences - where explainability, stability, interpretability, and transparent decision boundaries are  
 1848 essential. In many neuroimaging studies, for example, linear classifiers are preferred Shen et al.  
 1849 (2017); Misaki et al. (2010) because they provide direct insight into which brain regions contribute  
 1850 to a behavioral or cognitive prediction, making them a standard analytical tool despite the inherent  
 1851 nonlinearity of the data. To further assess the capability of CDA under nonlinear data distributions,  
 1852 we conducted an additional experiment on a real fMRI-behavior prediction task, where the goal is to  
 1853 classify human subjects into four behavioral score categories (fluid intelligence (gF); 4 groups are low  
 1854 gF, low-middle gF, middle-high gF and high gF). Although the underlying neurobiological patterns  
 1855 are highly nonlinear, this setting reflects a realistic domain where linear models are still favored for  
 1856 interpretability and reproducibility Shen et al. (2017); Misaki et al. (2010). The results (Table 8) show  
 1857 that CDA consistently outperforms all other linear classifiers, including LDA, logistic regression,  
 1858 and several SVM variants. This demonstrates that CDA can better capture discriminative structures  
 1859 even when the data distribution is nonlinear, while maintaining the transparency advantages of linear  
 1860 models.

1861 Table 8: Test set multiclass prediction performance on fMRI-behavior dataset (N=1076, M=64620, 4  
 1862 classes).

Method	AUROC	AUPR	Fscore	ACscore
CDA	<b>0.577±0.02</b>	<b>0.574±0.02</b>	<b>0.571±0.02</b>	<b>0.495±0.04</b>
LDA	0.538±0.02	0.558±0.03	0.536±0.03	0.384±0.07
SVM fast	0.534±0.005	0.536±0.005	0.532±0.007	0.4±0.04
SVM SGD	0.544±0.005	0.547±0.007	0.545±0.007	0.424±0.04
SVM	0.538±0.006	0.539±0.007	0.538±0.007	0.419±0.03
LR fast	0.537±0.004	0.539±0.005	0.536±0.006	0.4±0.05

1890 **S FULL CLASSIFICATION PERFORMANCE ON REAL DATASETS OF LINEAR**  
 1891 **CDA**  
 1892

1893 In the below tables we give full classification performance on 27 real datasets based on 4 metrics  
 1894 with binary classification (Table. 1-4) and multiclass prediction (Table. 5-8). In multiclass prediction,  
 1895 the performances on datasets with only two classes were filled with the one of binary classification.  
 1896

1897 **S.1 BINARY CLASSIFICATION**  
 1898

1900 **Table 9: AUROC (Binary Classification Performance)**

Dataset	CDB0	CDA	LDA	Fast SVM dual	Fast SVM primal	Fast SVM BO	SVM SGD	SVM	Fast LR
<b>Standard images</b>									
MNIST	0.957±0.004	0.985±0.002	0.981±0.002	0.985±0.002	<b>0.986±0.002</b>	<b>0.986±0.002</b>	<b>0.986±0.002</b>	<b>0.986±0.002</b>	<b>0.986±0.002</b>
USPS	0.966±0.005	0.989±0.001	0.982±0.002	0.99±0.002	0.99±0.002	0.99±0.001	<b>0.991±0.001</b>	0.99±0.002	<b>0.991±0.001</b>
EMNIST	0.928±0.003	0.972±0.001	0.964±0.001	0.97±0.001	0.97±0.001	<b>0.973±0.001</b>	0.97±0.002	0.97±0.001	0.97±0.002
CIFAR10	0.696±0.01	0.797±0.01	0.741±0.01	0.754±0.01	0.784±0.01	<b>0.807±0.01</b>	0.762±0.01	0.787±0.01	0.757±0.02
SVHN	0.528±0.003	<b>0.667±0.005</b>	0.555±0.003	0.55±0.004	0.578±0.004	0.592±0.005	0.537±0.003	0.591±0.004	0.57±0.008
flower	0.703±0.02	0.739±0.02	0.571±0.01	0.71±0.03	0.705±0.03	<b>0.754±0.03</b>	0.722±0.03	0.71±0.03	0.734±0.02
GTSRB	0.767±0.003	0.972±0.001	0.942±0.002	<b>0.995±0.0004</b>	<b>0.995±0.0003</b>	<b>0.995±0.0004</b>	0.99±0.0006	<b>0.995±0.0004</b>	0.994±0.0004
STL10	0.723±0.02	0.781±0.02	0.667±0.01	0.758±0.02	0.757±0.02	<b>0.791±0.02</b>	0.766±0.02	0.761±0.02	0.712±0.03
FMNIST	0.937±0.01	0.975±0.006	0.973±0.006	0.976±0.006	0.976±0.006	<b>0.978±0.005</b>	0.975±0.006	0.976±0.006	0.976±0.006
<b>Medical images</b>									
ermammist	0.682±0.01	<b>0.753±0.02</b>	0.684±0.02	0.676±0.02	0.708±0.02	0.698±0.02	0.608±0.02	0.712±0.02	0.663±0.03
pneumoniamnist	0.837±0	0.933±0	0.912±0	0.941±0	0.943±0	0.941±0	0.942±0	0.941±0	<b>0.944±0</b>
retinamnist	0.63±0.03	<b>0.662±0.04</b>	0.616±0.02	0.631±0.03	0.626±0.02	0.632±0.03	0.615±0.03	0.622±0.03	0.619±0.03
breastmnist	0.66±0	<b>0.763±0</b>	0.703±0	0.726±0	0.757±0	0.705±0	0.734±0	0.709±0	0.688±0
bloodmnist	0.89±0.02	0.947±0.01	0.898±0.02	0.951±0.01	0.955±0.01	0.955±0.01	0.946±0.01	<b>0.957±0.01</b>	0.955±0.01
organamnist	0.897±0.009	0.948±0.008	0.95±0.008	0.928±0.01	0.953±0.008	<b>0.958±0.008</b>	0.939±0.01	0.957±0.008	0.954±0.008
organcmnist	0.89±0.01	0.925±0.01	0.908±0.01	0.895±0.01	0.913±0.01	<b>0.928±0.01</b>	0.911±0.01	0.919±0.01	0.902±0.02
organsmnist	0.831±0.01	0.886±0.01	0.866±0.01	0.842±0.02	0.871±0.01	<b>0.888±0.01</b>	0.853±0.02	0.88±0.01	0.844±0.03
organnmnist3d	0.924±0.01	0.957±0.008	0.953±0.008	0.965±0.007	<b>0.966±0.007</b>	0.962±0.007	<b>0.966±0.007</b>	0.937±0.02	
nodulemnist3d	0.715±0	<b>0.781±0</b>	0.732±0	0.687±0	0.702±0	0.735±0	0.691±0	0.724±0	0.743±0
fracturemnist3d	<b>0.671±0.06</b>	0.556±0.03	0.525±0.04	0.576±0.007	0.578±0.008	0.6±0.004	0.592±0.004	0.612±0.007	0.592±0.01
adrenalmnist3d	0.653±0	<b>0.756±0</b>	0.692±0	0.697±0	0.619±0	0.647±0	0.637±0	0.665±0	0.641±0
vesselmnist3d	0.605±0	<b>0.685±0</b>	0.681±0	0.61±0	0.648±0	0.628±0	0.604±0	0.6±0	0.584±0
synapsemnist3d	0.539±0	<b>0.544±0</b>	0.508±0	0.518±0	0.527±0	0.518±0	0.525±0	0.539±0	0.517±0
<b>Chemical formula</b>									
bace	0.621±0	<b>0.705±0</b>	0.684±0	0.618±0	0.677±0	0.697±0	0.639±0	0.637±0	0.693±0
BBBP	0.711±0	<b>0.743±0</b>	0.693±0	0.667±0	0.707±0	0.71±0	0.646±0	0.697±0	0.712±0
clintox	<b>0.65±0</b>	0.575±0	0.543±0	0.517±0	0.515±0	0.519±0	0.508±0	0.514±0	0.515±0
HIV	0.6±0	<b>0.616±0</b>	0.537±0	0.51±0	0.506±0	0.51±0	0.505±0	0.506±0	0.51±0

1919  
 1920  
 1921  
 1922  
 1923  
 1924  
 1925  
 1926  
 1927  
 1928  
 1929  
 1930  
 1931  
 1932  
 1933  
 1934  
 1935  
 1936  
 1937  
 1938  
 1939  
 1940  
 1941  
 1942  
 1943

1944

1945

1946

1947

1948

1949

1950

1951

1952

1953

1954

1955

1956

1957

1958

1959

1960

1961

1962

1963

1964

1965

1966

1967

1968

1969

1970

1971

1972

1973

1974

1975

1976

1977

1978

1979

1980

1981

1982

1983

1984

1985

1986

1987

1988

1989

1990

1991

1992

1993

1994

1995

1996

1997

Table 10: AUPR (Binary Classification Performance)

Dataset	CDB0	CDA	LDA	Fast SVM dual	Fast SVM primal	Fast SVM BO	SVM SGD	SVM	Fast LR
<b>Standard images</b>									
MNIST	0.957±0.004	0.985±0.002	0.981±0.002	0.985±0.002	<b>0.986±0.002</b>	<b>0.986±0.002</b>	<b>0.986±0.002</b>	<b>0.986±0.002</b>	<b>0.986±0.002</b>
USPS	0.966±0.005	0.989±0.001	0.983±0.002	0.99±0.002	0.99±0.002	0.99±0.001	<b>0.991±0.001</b>	0.99±0.002	<b>0.991±0.001</b>
EMNIST	0.928±0.003	0.972±0.001	0.964±0.001	0.97±0.001	0.97±0.001	<b>0.973±0.001</b>	0.97±0.002	0.97±0.001	0.97±0.002
CIFAR10	0.697±0.01	0.797±0.01	0.741±0.01	0.762±0.01	0.784±0.01	<b>0.807±0.01</b>	0.774±0.01	0.787±0.01	0.757±0.02
SVHN	0.528±0.003	<b>0.682±0.006</b>	0.559±0.003	0.577±0.005	0.604±0.004	0.638±0.006	0.566±0.005	0.634±0.006	0.587±0.009
flower	0.704±0.02	0.741±0.02	0.571±0.01	0.712±0.03	0.707±0.03	<b>0.759±0.03</b>	0.73±0.03	0.712±0.03	0.736±0.02
GTSRB	0.757±0.003	0.973±0.001	0.934±0.002	0.995±0.0003	<b>0.996±0.0003</b>	<b>0.996±0.0003</b>	0.991±0.0005	0.995±0.0003	0.995±0.0003
STL10	0.724±0.02	0.782±0.02	0.667±0.01	0.759±0.02	0.757±0.02	<b>0.791±0.02</b>	0.772±0.02	0.762±0.02	0.713±0.03
FMNIST	0.937±0.01	0.975±0.006	0.973±0.006	0.976±0.006	0.976±0.006	<b>0.978±0.005</b>	0.975±0.006	0.976±0.006	0.977±0.006
<b>Medical images</b>									
dermamnist	0.653±0.01	0.743±0.02	0.681±0.02	0.729±0.02	0.746±0.02	0.744±0.02	0.646±0.03	<b>0.752±0.02</b>	0.717±0.03
pneumoniamnist	0.817±0	0.931±0	0.922±0	0.937±0	0.944±0	<b>0.946±0</b>	0.927±0	0.945±0	<b>0.946±0</b>
retinamnist	0.614±0.03	<b>0.649±0.03</b>	0.612±0.02	0.641±0.02	0.634±0.02	0.637±0.03	0.622±0.03	0.632±0.03	0.631±0.03
breastmnist	0.653±0	0.759±0	0.694±0	0.743±0	<b>0.766±0</b>	0.718±0	0.726±0	0.725±0	0.736±0
bloodmnist	0.889±0.02	0.947±0.01	0.895±0.02	0.953±0.01	0.955±0.01	<b>0.957±0.01</b>	0.945±0.01	<b>0.957±0.01</b>	0.956±0.01
organamnist	0.902±0.009	0.95±0.007	0.951±0.008	0.929±0.01	0.953±0.008	<b>0.959±0.008</b>	0.941±0.01	0.957±0.008	0.955±0.008
organcmnist	0.901±0.009	0.931±0.009	0.908±0.01	0.893±0.01	0.911±0.01	<b>0.932±0.009</b>	0.913±0.01	0.918±0.01	0.902±0.02
organsmnist	0.839±0.01	0.892±0.01	0.867±0.01	0.84±0.02	0.87±0.01	<b>0.894±0.01</b>	0.86±0.02	0.88±0.01	0.845±0.03
organmnist3d	0.924±0.009	0.958±0.008	0.954±0.008	0.965±0.007	0.966±0.007	<b>0.967±0.007</b>	0.963±0.007	<b>0.967±0.007</b>	0.937±0.02
nodeulemnist3d	0.7±0	<b>0.771±0</b>	0.745±0	0.695±0	0.709±0	0.749±0	0.711±0	0.732±0	0.752±0
fracturemnist3d	<b>0.663±0.05</b>	0.566±0.02	0.531±0.05	0.583±0.003	0.586±0.008	0.606±0.004	0.6±0.006	0.618±0.01	0.608±0.01
adrenalmnist3d	0.65±0	<b>0.774±0</b>	0.705±0	0.708±0	0.627±0	0.663±0	0.657±0	0.689±0	0.665±0
vesselmnist3d	0.582±0	0.671±0	0.694±0	0.627±0	<b>0.7±0</b>	0.692±0	0.668±0	0.646±0	0.661±0
synapsemnist3d	0.537±0	0.542±0	0.544±0	0.533±0	0.558±0	0.533±0	0.538±0	<b>0.572±0</b>	0.546±0
<b>Chemical formula</b>									
bace	0.62±0	<b>0.704±0</b>	0.685±0	0.643±0	0.679±0	0.699±0	0.652±0	0.64±0	0.695±0
BBBP	0.701±0	0.747±0	0.734±0	0.712±0	0.743±0	<b>0.751±0</b>	0.701±0	0.723±0	0.742±0
clintox	<b>0.602±0</b>	0.57±0	0.548±0	0.553±0	0.54±0	0.575±0	0.514±0	0.53±0	0.54±0
HIV	0.565±0	0.583±0	0.558±0	<b>0.612±0</b>	0.578±0	0.584±0	0.601±0	0.585±0	0.596±0

1998

1999

2000

Table 11: F-score (Binary Classification Performance)

Dataset	CDB0	CDA	LDA	Fast SVM dual	Fast SVM primal	Fast SVM BO	SVM SGD	SVM	Fast LR
<b>Standard images</b>									
2001	MNIST	0.957±0.004	0.985±0.002	0.981±0.002	0.985±0.002	<b>0.986±0.002</b>	<b>0.986±0.002</b>	<b>0.986±0.002</b>	<b>0.986±0.002</b>
2002	USPS	0.966±0.005	0.989±0.001	0.983±0.002	0.99±0.002	0.99±0.002	0.99±0.001	<b>0.991±0.001</b>	0.99±0.002
2003	EMNIST	0.928±0.003	0.972±0.001	0.964±0.001	0.97±0.001	0.97±0.001	<b>0.973±0.001</b>	0.97±0.002	0.97±0.001
2004	CIFAR10	0.696±0.01	0.797±0.01	0.741±0.01	0.747±0.01	0.784±0.01	<b>0.807±0.01</b>	0.751±0.02	0.787±0.01
2005	SVHN	0.523±0.003	<b>0.664±0.005</b>	0.555±0.003	0.51±0.01	0.568±0.005	0.574±0.007	0.471±0.01	0.577±0.006
2006	flower	0.701±0.02	0.738±0.02	0.57±0.01	0.709±0.03	0.705±0.03	<b>0.754±0.03</b>	0.715±0.03	0.709±0.03
2007	GTSRB	0.743±0.003	0.972±0.001	0.931±0.002	0.995±0.0003	<b>0.996±0.0003</b>	<b>0.996±0.0003</b>	0.99±0.0005	0.995±0.0003
2008	STL10	0.722±0.02	0.781±0.02	0.666±0.01	0.756±0.02	0.756±0.02	<b>0.791±0.02</b>	0.76±0.02	0.761±0.02
2009	FMNIST	0.937±0.01	0.975±0.006	0.973±0.006	0.976±0.006	0.976±0.006	<b>0.978±0.005</b>	0.975±0.006	0.976±0.006
<b>Medical images</b>									
2010	dermammist	0.621±0.02	<b>0.736±0.02</b>	0.677±0.02	0.682±0.03	0.726±0.02	0.722±0.02	0.595±0.03	0.731±0.02
2011	pneumoniamnist	0.812±0	0.931±0	0.921±0	0.937±0	0.944±0	0.945±0	0.925±0	0.944±0
2012	retinammnist	0.594±0.02	<b>0.639±0.03</b>	0.61±0.02	0.611±0.04	0.611±0.04	0.631±0.03	0.586±0.04	0.623±0.03
2013	breastammnist	0.651±0	0.759±0	0.684±0	0.739±0	<b>0.765±0</b>	0.716±0	0.725±0	0.722±0
2014	bloodammnist	0.888±0.02	0.947±0.01	0.894±0.02	0.952±0.01	0.955±0.01	<b>0.957±0.01</b>	0.943±0.01	<b>0.957±0.01</b>
2015	organammnist	0.899±0.01	0.949±0.008	0.951±0.008	0.923±0.02	0.953±0.008	<b>0.959±0.008</b>	0.939±0.01	0.957±0.008
2016	organcmmnist	0.896±0.01	0.929±0.009	0.908±0.01	0.892±0.02	0.911±0.01	<b>0.932±0.009</b>	0.911±0.01	0.918±0.01
2017	organsmmnist	0.834±0.01	0.89±0.01	0.866±0.01	0.834±0.02	0.869±0.01	<b>0.893±0.01</b>	0.85±0.02	0.88±0.01
2018	organmmnist3d	0.92±0.01	0.957±0.008	0.953±0.008	0.964±0.007	<b>0.966±0.007</b>	<b>0.966±0.007</b>	0.962±0.007	<b>0.966±0.007</b>
2019	nodulemmnist3d	0.695±0	<b>0.769±0</b>	0.743±0	0.694±0	0.708±0	0.747±0	0.706±0	0.731±0
2020	fracturemmnist3d	<b>0.651±0.05</b>	0.523±0.03	0.514±0.05	0.577±0.007	0.579±0.007	0.602±0.003	0.594±0.004	0.615±0.009
2021	adrenalmnist3d	0.65±0	<b>0.771±0</b>	0.703±0	0.707±0	0.625±0	0.659±0	0.651±0	0.681±0
2022	vesselmmnist3d	0.56±0	0.669±0	<b>0.693±0</b>	0.623±0	0.681±0	0.663±0	0.635±0	0.625±0
2023	synapsemmnist3d	0.534±0	<b>0.539±0</b>	0.45±0	0.493±0	0.501±0	0.493±0	0.511±0	0.522±0
<b>Chemical formula</b>									
2024	bace	0.619±0	<b>0.704±0</b>	0.684±0	0.569±0	0.678±0	0.698±0	0.634±0	0.637±0
2025	BBBP	0.699±0	<b>0.747±0</b>	0.718±0	0.691±0	0.731±0	0.736±0	0.669±0	0.716±0
2026	clintox	0.54±0	<b>0.569±0</b>	0.547±0	0.517±0	0.515±0	0.52±0	0.506±0	0.513±0
2027	HIV	0.531±0	<b>0.562±0</b>	0.548±0	0.511±0	0.504±0	0.511±0	0.501±0	0.504±0
2028									
2029									
2030									
2031									
2032									
2033									
2034									
2035									
2036									
2037									
2038									
2039									
2040									
2041									
2042									
2043									
2044									
2045									
2046									
2047									
2048									
2049									
2050									
2051									

2052

2053

2054

2055

2056

2057

2058

2059

2060

2061

2062

2063

2064

2065

2066

2067

2068

2069

2070

2071

2072

2073

2074

2075

2076

2077

2078

2079

2080

2081

2082

2083

2084

2085

2086

2087

2088

2089

2090

2091

2092

2093

2094

2095

2096

2097

2098

2099

2100

2101

2102

2103

2104

2105

Table 12: AC-score (Binary Classification Performance)

Dataset	CDB0	CDA	LDA	Fast SVM dual	Fast SVM primal	Fast SVM BO	SVM SGD	SVM	Fast LR
<b>Standard images</b>									
MNIST	0.957±0.004	0.985±0.002	0.981±0.002	0.985±0.002	<b>0.986±0.002</b>	<b>0.986±0.002</b>	<b>0.986±0.002</b>	<b>0.986±0.002</b>	<b>0.986±0.002</b>
USPS	0.966±0.005	0.989±0.001	0.982±0.002	0.99±0.002	0.99±0.002	0.99±0.001	<b>0.991±0.001</b>	0.99±0.002	<b>0.991±0.001</b>
EMNIST	0.927±0.003	0.972±0.001	0.964±0.001	0.97±0.001	0.969±0.001	<b>0.973±0.001</b>	0.969±0.002	0.97±0.001	0.97±0.002
CIFAR10	0.694±0.01	0.796±0.01	0.74±0.01	0.725±0.02	0.784±0.01	<b>0.807±0.01</b>	0.72±0.02	0.787±0.01	0.756±0.02
SVHN	0.524±0.002	<b>0.614±0.004</b>	0.499±0.008	0.352±0.03	0.444±0.02	0.419±0.02	0.302±0.03	0.438±0.02	0.461±0.02
flower	0.698±0.02	0.733±0.02	0.567±0.01	0.701±0.03	0.696±0.03	<b>0.74±0.03</b>	0.678±0.05	0.7±0.03	0.725±0.03
GTSRB	0.753±0.003	0.97±0.002	0.941±0.002	<b>0.995±0.0004</b>	<b>0.995±0.0003</b>	<b>0.995±0.0004</b>	0.99±0.0006	<b>0.995±0.0004</b>	0.994±0.0004
STL10	0.72±0.01	0.779±0.02	0.664±0.01	0.75±0.02	0.755±0.02	<b>0.79±0.02</b>	0.743±0.02	0.76±0.02	0.711±0.03
FMNIST	0.936±0.01	0.975±0.006	0.973±0.006	0.975±0.006	0.976±0.006	<b>0.978±0.005</b>	0.975±0.006	0.976±0.006	0.976±0.006
<b>Medical images</b>									
dermamnist	0.658±0.02	<b>0.72±0.02</b>	0.608±0.04	0.535±0.05	0.602±0.05	0.62±0.05	0.323±0.07	0.606±0.05	0.518±0.05
pneumoniamnist	0.837±0	0.932±0	0.908±0	0.94±0	0.942±0	0.94±0	0.942±0	0.94±0	<b>0.943±0</b>
retinamnist	0.62±0.03	<b>0.639±0.05</b>	0.567±0.03	0.513±0.07	0.543±0.04	0.544±0.05	0.448±0.08	0.518±0.06	0.501±0.06
breastmnist	0.641±0	<b>0.751±0</b>	0.698±0	0.682±0	0.732±0	0.658±0	0.722±0	0.661±0	0.59±0
bloodmnist	0.889±0.02	0.946±0.01	0.897±0.02	0.949±0.01	0.954±0.01	0.954±0.01	0.944±0.01	<b>0.956±0.01</b>	0.953±0.01
organamnist	0.892±0.01	0.946±0.008	0.949±0.008	0.919±0.02	0.952±0.009	<b>0.958±0.008</b>	0.935±0.01	0.956±0.008	0.954±0.008
organcmnist	0.881±0.01	0.92±0.01	0.907±0.01	0.893±0.02	0.913±0.01	<b>0.927±0.01</b>	0.905±0.01	0.919±0.01	0.9±0.02
organsmnist	0.822±0.01	0.88±0.01	0.862±0.01	0.833±0.02	0.868±0.01	<b>0.884±0.01</b>	0.828±0.02	0.877±0.01	0.839±0.03
organmnist3d	0.918±0.01	0.956±0.008	0.952±0.008	0.964±0.007	<b>0.965±0.007</b>	<b>0.965±0.007</b>	0.962±0.007	<b>0.965±0.007</b>	0.937±0.02
nodulemnist3d	0.707±0	<b>0.773±0</b>	0.693±0	0.636±0	0.657±0	0.694±0	0.623±0	0.688±0	0.71±0
fracturemnist3d	<b>0.668±0.06</b>	0.38±0.1	0.351±0.1	0.491±0.06	0.491±0.04	0.535±0.03	0.514±0.03	0.562±0.01	0.485±0.05
adrenalmnist3d	0.602±0	<b>0.718±0</b>	0.631±0	0.642±0	0.52±0	0.553±0	0.526±0	0.57±0	0.528±0
vesselmnist3d	0.547±0	<b>0.615±0</b>	0.58±0	0.43±0	0.488±0	0.434±0	0.376±0	0.375±0	0.313±0
synapsemnist3d	0.498±0	<b>0.506±0</b>	0.0612±0	0.189±0	0.19±0	0.189±0	0.253±0	0.239±0	0.137±0
<b>Chemical formula</b>									
bace	0.62±0	<b>0.704±0</b>	0.678±0	0.483±0	0.673±0	0.694±0	0.583±0	0.621±0	0.688±0
BBBP	0.693±0	<b>0.715±0</b>	0.603±0	0.553±0	0.63±0	0.632±0	0.501±0	0.626±0	0.646±0
clintox	<b>0.634±0</b>	0.365±0	0.238±0	0.0869±0	0.0869±0	0.0869±0	0.0868±0	0.0869±0	0.0869±0
HIV	<b>0.471±0</b>	0.465±0	0.159±0	0.0407±0	0.0273±0	0.0407±0	0.0205±0	0.0273±0	0.0407±0

2106 S.2 MULTICLASS PREDICTION  
2107  
2108

2109 Table 13: AUROC (Multiclass Prediction Performance)

Dataset	CDB0	CDA	LDA	Fast SVM dual	Fast SVM primal	Fast SVM BO	SVM SGD	SVM	Fast LR
<b>Standard images</b>									
MNIST	0.897±0.01	0.963±0.005	0.958±0.006	0.965±0.005	0.965±0.005	<b>0.967±0.004</b>	0.965±0.005	0.966±0.005	<b>0.967±0.004</b>
USPS	0.914±0.01	0.971±0.004	0.969±0.006	0.974±0.005	0.974±0.005	0.973±0.004	0.974±0.004	0.973±0.005	<b>0.976±0.004</b>
EMNIST	0.773±0.01	0.896±0.008	0.879±0.009	0.891±0.008	0.888±0.008	<b>0.895±0.008</b>	0.883±0.01	0.892±0.008	0.878±0.01
CIFAR10	0.594±0.02	0.671±0.02	0.627±0.01	0.641±0.02	0.661±0.02	<b>0.681±0.01</b>	0.645±0.02	0.663±0.02	0.627±0.03
SVHN	0.522±0.006	<b>0.638±0.01</b>	0.531±0.007	0.536±0.01	0.55±0.01	0.551±0.01	0.534±0.008	0.558±0.01	0.543±0.01
flower	0.61±0.03	0.666±0.03	0.554±0.02	0.632±0.03	0.629±0.02	<b>0.669±0.03</b>	0.634±0.03	0.632±0.03	0.652±0.03
GTSRB	0.589±0.01	0.878±0.01	0.821±0.02	0.982±0.003	0.982±0.003	0.982±0.003	0.959±0.005	<b>0.983±0.003</b>	0.972±0.004
STL10	0.607±0.02	0.655±0.02	0.596±0.02	0.648±0.02	0.648±0.02	<b>0.663±0.02</b>	0.648±0.03	0.653±0.02	0.584±0.02
FMNIST	0.836±0.03	0.917±0.02	0.92±0.02	0.924±0.02	0.923±0.02	<b>0.927±0.02</b>	0.918±0.02	0.924±0.02	0.924±0.02
<b>Medical images</b>									
dermamnist	0.614±0.03	<b>0.658±0.03</b>	0.588±0.02	0.595±0.03	0.596±0.02	0.601±0.03	0.531±0.01	0.606±0.03	0.563±0.02
pneumoniamnist	0.837±0	0.933±0	0.912±8e-17	0.941±0	0.943±6e-17	0.941±0	0.942±6e-17	0.941±0	<b>0.944±0</b>
retinamnist	0.575±0.04	<b>0.622±0.04</b>	0.592±0.03	0.596±0.04	0.596±0.04	0.608±0.04	0.61±0.04	0.603±0.04	0.596±0.04
breastmnist	0.66±0	<b>0.763±8e-17</b>	0.703±0	0.726±0	0.757±0	0.705±0	0.734±0	0.709±0	0.688±0
bloodmnist	0.789±0.04	0.88±0.03	0.817±0.03	0.882±0.03	0.893±0.03	0.891±0.03	0.877±0.03	<b>0.895±0.03</b>	0.891±0.03
organamnist	0.815±0.03	0.888±0.02	0.885±0.03	0.854±0.04	0.891±0.03	<b>0.9±0.02</b>	0.866±0.03	0.897±0.02	0.893±0.03
organcmnist	0.809±0.03	<b>0.869±0.03</b>	0.833±0.03	0.811±0.04	0.839±0.03	0.862±0.03	0.833±0.03	0.847±0.03	0.798±0.05
organsmnist	0.694±0.03	<b>0.761±0.03</b>	0.735±0.03	0.7±0.03	0.733±0.03	0.754±0.03	0.732±0.04	0.746±0.03	0.705±0.05
organmnist3d	0.867±0.03	0.913±0.02	0.903±0.03	0.924±0.02	<b>0.93±0.02</b>	0.925±0.02	0.925±0.02	0.925±0.02	0.834±0.06
nodulemnist3d	0.715±0	<b>0.781±0</b>	0.732±8e-17	0.687±0	0.702±6e-17	0.735±6e-17	0.691±6e-17	0.724±0	0.743±0
fracturemnist3d	<b>0.622±0.04</b>	0.518±0.01	0.554±0.04	0.574±0.004	0.579±0.005	0.578±0.01	0.575±0.009	0.576±0.009	0.578±0.01
adrenalmnist3d	0.653±8e-17	<b>0.756±8e-17</b>	0.692±0	0.697±0	0.619±0	0.647±6e-17	0.637±0	0.665±6e-17	0.641±0
vesselmnist3d	0.605±8e-17	<b>0.685±0</b>	0.681±8e-17	0.61±0	0.648±6e-17	0.628±6e-17	0.604±0	0.6±0	0.584±0
synapsemnist3d	0.539±8e-17	<b>0.544±8e-17</b>	0.508±0	0.518±8e-17	0.527±6e-17	0.518±6e-17	0.525±0	0.539±0	0.517±0
<b>Chemical formula</b>									
bace	0.621±8e-17	<b>0.705±0</b>	0.684±8e-17	0.618±8e-17	0.677±6e-17	0.697±0	0.639±6e-17	0.637±6e-17	0.693±6e-17
BBBP	0.711±8e-17	<b>0.743±0</b>	0.693±0	0.667±0	0.707±0	0.71±0	0.646±6e-17	0.697±0	0.712±0
clintox	<b>0.65±0</b>	0.575±0	0.543±0	0.517±0	0.515±0	0.519±6e-17	0.508±0	0.514±6e-17	0.515±0
HIV	0.6±0	<b>0.616±8e-17</b>	0.537±0	0.51±0	0.506±6e-17	0.51±0	0.505±6e-17	0.506±0	0.51±0

2128  
2129  
2130  
2131  
2132  
2133  
2134  
2135  
2136  
2137  
2138  
2139  
2140  
2141  
2142  
2143  
2144  
2145  
2146  
2147  
2148  
2149  
2150  
2151  
2152  
2153  
2154  
2155  
2156  
2157  
2158  
2159

2160

2161

2162

Table 14: AUPR (Multiclass Prediction Performance)

Dataset	CDB0	CDA	LDA	Fast SVM dual	Fast SVM primal	Fast SVM BO	SVM SGD	SVM	Fast LR
<b>Standard images</b>									
MNIST	0.897±0.01	0.963±0.004	0.958±0.005	0.965±0.004	0.965±0.004	<b>0.967±0.004</b>	0.965±0.004	0.966±0.004	<b>0.967±0.004</b>
USPS	0.918±0.01	0.971±0.005	0.969±0.005	0.974±0.004	0.974±0.005	0.974±0.004	0.974±0.004	0.973±0.005	<b>0.976±0.003</b>
EMNIST	0.774±0.01	0.896±0.008	0.888±0.009	0.891±0.008	0.888±0.008	<b>0.898±0.008</b>	0.884±0.009	0.892±0.008	0.878±0.01
CIFAR10	0.6±0.01	0.67±0.01	0.627±0.01	0.64±0.02	0.66±0.01	<b>0.68±0.01</b>	0.651±0.02	0.663±0.02	0.615±0.02
SVHN	0.528±0.009	<b>0.666±0.01</b>	0.533±0.006	0.546±0.005	0.572±0.006	0.589±0.007	0.565±0.01	0.597±0.005	0.552±0.01
flower	0.611±0.02	0.665±0.02	0.554±0.02	0.631±0.02	0.628±0.02	<b>0.671±0.02</b>	0.641±0.03	0.632±0.02	0.652±0.02
GTSRB	0.619±0.01	0.891±0.01	0.805±0.01	0.981±0.003	0.981±0.003	<b>0.982±0.002</b>	0.959±0.005	0.981±0.003	0.975±0.003
STL10	0.604±0.02	0.653±0.02	0.598±0.02	0.648±0.02	0.647±0.02	<b>0.663±0.02</b>	0.65±0.02	0.651±0.02	0.585±0.01
FMNIST	0.836±0.03	0.916±0.02	0.92±0.02	0.923±0.02	0.923±0.02	<b>0.926±0.02</b>	0.918±0.02	0.924±0.02	0.924±0.02
<b>Medical images</b>									
dermammist	0.592±0.02	0.645±0.02	0.603±0.02	0.608±0.03	0.633±0.03	0.629±0.03	0.615±0.03	<b>0.649±0.03</b>	0.596±0.02
pneumoniammist	0.817±0	0.931±0	0.922±0	0.937±0	0.944±0	<b>0.946±0</b>	0.927±0	0.945±0	<b>0.946±0</b>
retinammist	0.568±0.03	0.621±0.04	0.594±0.03	0.589±0.04	0.593±0.04	0.608±0.04	<b>0.632±0.03</b>	0.608±0.04	0.598±0.04
breastmammist	0.653±0	0.759±0	0.69±0	0.743±0	<b>0.766±0</b>	0.718±0	0.726±0	0.725±0	0.736±0
bloodmammist	0.785±0.04	0.878±0.03	0.818±0.03	0.894±0.03	0.895±0.03	0.894±0.03	0.872±0.03	<b>0.897±0.02</b>	0.895±0.03
organammist	0.82±0.03	0.892±0.02	0.889±0.02	0.851±0.03	0.892±0.02	<b>0.903±0.02</b>	0.871±0.03	0.898±0.02	0.895±0.02
organcmmist	0.818±0.03	<b>0.877±0.02</b>	0.838±0.03	0.811±0.04	0.839±0.03	0.87±0.02	0.836±0.03	0.847±0.03	0.793±0.05
organsmmist	0.697±0.02	<b>0.764±0.03</b>	0.741±0.03	0.703±0.03	0.736±0.03	0.763±0.03	0.734±0.03	0.748±0.03	0.698±0.04
organmmnist3d	0.867±0.02	0.913±0.02	0.904±0.03	0.924±0.02	<b>0.93±0.02</b>	0.926±0.02	0.925±0.02	0.926±0.02	0.824±0.05
nodulemmnist3d	0.7±0	<b>0.771±0</b>	0.745±0	0.695±0	0.709±0	0.749±0	0.711±0	0.732±0	0.752±0
fracturemmnist3d	<b>0.617±0.04</b>	0.526±0.02	0.553±0.04	0.578±0.004	0.583±0.003	0.582±0.008	0.579±0.007	0.579±0.008	0.585±0.009
adrenalmnist3d	0.65±0	<b>0.774±0</b>	0.705±0	0.708±0	0.627±0	0.663±0	0.657±0	0.689±0	0.665±0
vesselmmnist3d	0.582±0	0.671±0	0.694±0	0.627±0	<b>0.7±0</b>	0.692±0	0.668±0	0.646±0	0.661±0
synapsemmnist3d	0.537±0	0.542±0	0.544±0	0.533±0	0.558±0	0.533±0	0.538±0	<b>0.572±0</b>	0.546±0
<b>Chemical formula</b>									
bace	0.62±0	<b>0.704±0</b>	0.685±0	0.643±0	0.679±0	0.699±0	0.652±0	0.64±0	0.695±0
BBBP	0.701±0	0.747±0	0.734±0	0.712±0	0.743±0	<b>0.751±0</b>	0.701±0	0.723±0	0.742±0
clintox	<b>0.602±0</b>	0.57±0	0.548±0	0.553±0	0.54±0	0.575±0	0.514±0	0.53±0	0.54±0
HIV	0.565±0	0.583±0	0.558±0	<b>0.612±0</b>	0.578±0	0.584±0	0.601±0	0.585±0	0.596±0

2179

2180

2181

2182

2183

2184

2185

2186

2187

2188

2189

2190

2191

2192

2193

2194

2195

2196

2197

2198

2199

2200

2201

2202

2203

2204

2205

2206

2207

2208

2209

2210

2211

2212

2213

2214

2215

2216

Table 15: F-score (Multiclass Prediction Performance)

Dataset	CDB0	CDA	LDA	Fast SVM dual	Fast SVM primal	Fast SVM BO	SVM SGD	SVM	Fast LR
<b>Standard images</b>									
MNIST	0.896±0.01	0.963±0.004	0.958±0.005	0.965±0.004	0.965±0.004	<b>0.967±0.004</b>	0.965±0.004	0.966±0.004	<b>0.967±0.004</b>
USPS	0.917±0.01	0.971±0.005	0.969±0.005	0.974±0.004	0.973±0.005	0.973±0.004	0.974±0.004	0.973±0.005	<b>0.976±0.003</b>
EMNIST	0.773±0.01	0.896±0.008	0.879±0.009	0.891±0.008	0.888±0.008	<b>0.898±0.008</b>	0.883±0.009	0.892±0.008	0.878±0.01
CIFAR10	0.59±0.01	0.67±0.01	0.627±0.01	0.634±0.02	0.66±0.01	<b>0.679±0.01</b>	0.634±0.02	0.663±0.02	0.603±0.02
SVHN	0.509±0.006	<b>0.649±0.01</b>	0.529±0.005	0.526±0.006	0.542±0.007	0.54±0.01	0.521±0.008	0.55±0.01	0.53±0.009
flower	0.599±0.02	0.662±0.02	0.553±0.02	0.629±0.02	0.626±0.02	<b>0.665±0.02</b>	0.628±0.03	0.63±0.02	0.65±0.02
GTSRB	0.586±0.01	0.886±0.01	0.782±0.01	0.98±0.003	0.981±0.003	<b>0.982±0.003</b>	0.957±0.005	0.98±0.003	0.974±0.003
STL10	0.601±0.02	0.653±0.02	0.597±0.02	0.646±0.02	0.646±0.02	<b>0.662±0.02</b>	0.641±0.02	0.651±0.02	0.574±0.02
FMNIST	0.835±0.03	0.916±0.02	0.919±0.02	0.923±0.02	0.923±0.02	<b>0.926±0.02</b>	0.918±0.02	0.924±0.02	0.924±0.02
<b>Medical images</b>									
dermammist	0.571±0.02	<b>0.639±0.02</b>	0.599±0.02	0.602±0.03	0.611±0.03	0.615±0.03	0.533±0.01	0.624±0.03	0.572±0.02
pneumoniamnist	0.812±0	0.931±0	0.921±0	0.937±0	0.944±0	0.945±0	0.925±0	0.944±0	<b>0.946±0</b>
retinamnist	0.547±0.04	<b>0.615±0.04</b>	0.592±0.03	0.579±0.04	0.584±0.04	0.604±0.04	0.605±0.03	0.64±0.04	0.591±0.04
breastmammist	0.651±0	0.759±0	0.684±0	0.739±0	<b>0.765±0</b>	0.716±0	0.725±0	0.722±0	0.712±0
bloodmnist	0.779±0.04	0.877±0.03	0.817±0.03	0.887±0.03	0.894±0.03	0.894±0.03	0.869±0.03	<b>0.897±0.02</b>	0.894±0.03
organmnist	0.812±0.03	0.889±0.02	0.889±0.02	0.847±0.04	0.892±0.02	<b>0.903±0.02</b>	0.869±0.03	0.898±0.02	0.894±0.02
organcmnist	0.811±0.03	<b>0.874±0.02</b>	0.837±0.03	0.809±0.04	0.839±0.03	0.867±0.02	0.834±0.03	0.847±0.03	0.789±0.05
organsmnist	0.685±0.02	<b>0.76±0.03</b>	0.74±0.03	0.698±0.03	0.736±0.03	<b>0.76±0.03</b>	0.729±0.04	0.748±0.03	0.684±0.04
organmnist3d	0.862±0.02	0.913±0.02	0.903±0.03	0.922±0.02	<b>0.929±0.02</b>	0.923±0.02	0.924±0.02	0.923±0.02	0.809±0.06
nodulemnist3d	0.695±0	<b>0.769±0</b>	0.743±0	0.694±0	0.708±0	0.747±0	0.706±0	0.731±0	0.751±0
fracturemnist3d	<b>0.601±0.04</b>	0.486±0.02	0.547±0.04	0.575±0.002	0.581±0.003	0.579±0.008	0.575±0.006	0.577±0.008	0.577±0.01
adrenalmnist3d	0.65±0	<b>0.771±0</b>	0.703±0	0.707±0	0.625±0	0.659±0	0.651±0	0.681±0	0.656±0
vesselmnist3d	0.56±0	0.669±0	<b>0.693±0</b>	0.623±0	0.681±0	0.663±0	0.635±0	0.625±0	0.611±0
synapsemnist3d	0.534±0	<b>0.539±0</b>	0.45±0	0.493±0	0.501±0	0.493±0	0.511±0	0.522±0	0.48±0
<b>Chemical formula</b>									
bace	0.619±0	<b>0.704±0</b>	0.684±0	0.569±0	0.678±0	0.698±0	0.634±0	0.637±0	0.694±0
BBBP	0.699±0	<b>0.747±0</b>	0.718±0	0.691±0	0.731±0	0.736±0	0.669±0	0.716±0	0.733±0
clintox	0.54±0	<b>0.569±0</b>	0.547±0	0.517±0	0.515±0	0.52±0	0.506±0	0.513±0	0.515±0
HIV	0.531±0	<b>0.562±0</b>	0.548±0	0.511±0	0.504±0	0.511±0	0.501±0	0.504±0	0.511±0

2233

2234

2235

2236

2237

2238

2239

2240

2241

2242

2243

2244

2245

2246

2247

2248

2249

2250

2251

2252

2253

2254

2255

2256

2257

2258

2259

2260

2261

2262

2263

2264

2265

2266

2267

2268

2269

2270

Table 16: AC-score (Multiclass Prediction Performance)

Dataset	CDB0	CDA	LDA	Fast SVM dual	Fast SVM primal	Fast SVM BO	SVM SGD	SVM	Fast LR
<b>Standard images</b>									
MNIST	0.888 $\pm$ 0.01	0.962 $\pm$ 0.005	0.956 $\pm$ 0.006	0.964 $\pm$ 0.005	0.964 $\pm$ 0.005	<b>0.966<math>\pm</math>0.005</b>	0.964 $\pm$ 0.005	0.965 $\pm$ 0.005	<b>0.966<math>\pm</math>0.005</b>
USPS	0.907 $\pm$ 0.01	0.970 $\pm$ 0.005	0.968 $\pm$ 0.007	0.974 $\pm$ 0.005	0.973 $\pm$ 0.005	0.973 $\pm$ 0.005	0.974 $\pm$ 0.004	0.973 $\pm$ 0.005	<b>0.975<math>\pm</math>0.004</b>
EMNIST	0.708 $\pm$ 0.02	0.884 $\pm$ 0.01	0.863 $\pm$ 0.01	0.878 $\pm$ 0.01	0.874 $\pm$ 0.01	<b>0.886<math>\pm</math>0.01</b>	0.867 $\pm$ 0.01	0.879 $\pm$ 0.01	0.855 $\pm$ 0.02
CIFAR10	0.404 $\pm$ 0.05	0.562 $\pm$ 0.03	0.482 $\pm$ 0.03	0.491 $\pm$ 0.05	0.542 $\pm$ 0.03	<b>0.579<math>\pm</math>0.03</b>	0.487 $\pm$ 0.06	0.548 $\pm$ 0.03	0.431 $\pm$ 0.08
SVHN	0.223 $\pm$ 0.05	<b>0.478<math>\pm</math>0.03</b>	0.241 $\pm$ 0.04	0.223 $\pm$ 0.06	0.242 $\pm$ 0.05	0.216 $\pm$ 0.04	0.234 $\pm$ 0.06	0.247 $\pm$ 0.05	0.224 $\pm$ 0.06
flower	0.492 $\pm$ 0.07	<b>0.597<math>\pm</math>0.05</b>	0.417 $\pm$ 0.05	0.545 $\pm$ 0.05	0.542 $\pm$ 0.04	0.591 $\pm$ 0.05	0.518 $\pm$ 0.08	0.546 $\pm$ 0.05	0.576 $\pm$ 0.04
GTSRB	0.296 $\pm$ 0.03	0.853 $\pm$ 0.02	0.762 $\pm$ 0.03	0.981 $\pm$ 0.004	0.981 $\pm$ 0.004	0.981 $\pm$ 0.004	0.956 $\pm$ 0.006	<b>0.982<math>\pm</math>0.004</b>	0.97 $\pm$ 0.004
STL10	0.425 $\pm$ 0.05	0.523 $\pm$ 0.05	0.413 $\pm$ 0.04	0.512 $\pm$ 0.05	0.51 $\pm$ 0.05	<b>0.541<math>\pm</math>0.04</b>	0.501 $\pm$ 0.05	0.521 $\pm$ 0.05	0.364 $\pm$ 0.06
FMNIST	0.801 $\pm$ 0.05	0.909 $\pm$ 0.02	0.912 $\pm$ 0.02	0.916 $\pm$ 0.02	0.915 $\pm$ 0.02	<b>0.92<math>\pm</math>0.02</b>	0.91 $\pm$ 0.02	0.917 $\pm$ 0.02	0.917 $\pm$ 0.02
<b>Medical images</b>									
dermammist	0.439 $\pm$ 0.09	<b>0.527<math>\pm</math>0.07</b>	0.352 $\pm$ 0.07	0.348 $\pm$ 0.1	0.324 $\pm$ 0.07	0.337 $\pm$ 0.09	0.131 $\pm$ 0.04	0.346 $\pm$ 0.08	0.239 $\pm$ 0.07
pneumoniammist	0.837 $\pm$ 0	0.932 $\pm$ 0	0.908 $\pm$ 0	0.94 $\pm$ 0	0.942 $\pm$ 0	0.94 $\pm$ 0	0.942 $\pm$ 0	0.94 $\pm$ 0	<b>0.943<math>\pm</math>0</b>
retinammist	0.377 $\pm$ 0.1	<b>0.506<math>\pm</math>0.07</b>	0.444 $\pm$ 0.08	0.401 $\pm$ 0.1	0.404 $\pm$ 0.1	0.433 $\pm$ 0.1	0.422 $\pm$ 0.1	0.426 $\pm$ 0.1	0.405 $\pm$ 0.1
breastammist	0.641 $\pm$ 0	<b>0.751<math>\pm</math>0</b>	0.698 $\pm$ 0	0.682 $\pm$ 0	0.732 $\pm$ 0	0.658 $\pm$ 0	0.722 $\pm$ 0	0.661 $\pm$ 0	0.59 $\pm$ 0
bloodammist	0.742 $\pm$ 0.05	0.864 $\pm$ 0.04	0.784 $\pm$ 0.04	0.865 $\pm$ 0.03	0.882 $\pm$ 0.03	0.878 $\pm$ 0.03	0.862 $\pm$ 0.04	<b>0.883<math>\pm</math>0.03</b>	0.878 $\pm$ 0.03
organammist	0.771 $\pm$ 0.05	0.872 $\pm$ 0.03	0.868 $\pm$ 0.03	0.814 $\pm$ 0.05	0.874 $\pm$ 0.03	<b>0.887<math>\pm</math>0.03</b>	0.84 $\pm$ 0.04	0.883 $\pm$ 0.03	0.877 $\pm$ 0.03
organammist	0.766 $\pm$ 0.04	<b>0.848<math>\pm</math>0.03</b>	0.797 $\pm$ 0.04	0.76 $\pm$ 0.05	0.804 $\pm$ 0.04	0.836 $\pm$ 0.03	0.788 $\pm$ 0.05	0.816 $\pm$ 0.04	0.705 $\pm$ 0.09
organsammist	0.58 $\pm$ 0.06	<b>0.69<math>\pm</math>0.05</b>	0.653 $\pm$ 0.04	0.589 $\pm$ 0.06	0.649 $\pm$ 0.05	0.677 $\pm$ 0.05	0.624 $\pm$ 0.07	0.669 $\pm$ 0.05	0.54 $\pm$ 0.1
organammnist3d	0.845 $\pm$ 0.04	0.902 $\pm$ 0.03	0.89 $\pm$ 0.03	0.914 $\pm$ 0.03	<b>0.923<math>\pm</math>0.02</b>	0.916 $\pm$ 0.02	0.917 $\pm$ 0.02	0.916 $\pm$ 0.02	0.736 $\pm$ 0.1
nodulemmnist3d	0.707 $\pm$ 0	<b>0.773<math>\pm</math>0</b>	0.693 $\pm$ 0	0.636 $\pm$ 0	0.657 $\pm$ 0	0.694 $\pm$ 0	0.623 $\pm$ 0	0.688 $\pm$ 0	0.71 $\pm$ 0
fracturemmnist3d	<b>0.569<math>\pm</math>0.09</b>	0.279 $\pm$ 0.05	0.425 $\pm$ 0.2	0.5 $\pm$ 0.07	0.508 $\pm$ 0.06	0.503 $\pm$ 0.06	0.495 $\pm$ 0.06	0.505 $\pm$ 0.05	0.482 $\pm$ 0.08
adrenalmnist3d	0.602 $\pm$ 0	<b>0.718<math>\pm</math>0</b>	0.631 $\pm$ 0	0.642 $\pm$ 0	0.52 $\pm$ 0	0.553 $\pm$ 0	0.526 $\pm$ 0	0.57 $\pm$ 0	0.528 $\pm$ 0
vesselmmnist3d	0.547 $\pm$ 0	<b>0.615<math>\pm</math>0</b>	0.58 $\pm$ 0	0.43 $\pm$ 0	0.488 $\pm$ 0	0.434 $\pm$ 0	0.376 $\pm$ 0	0.375 $\pm$ 0	0.313 $\pm$ 0
synapsemmnist3d	0.498 $\pm$ 0	<b>0.506<math>\pm</math>0</b>	0.0612 $\pm$ 0	0.189 $\pm$ 0	0.19 $\pm$ 0	0.189 $\pm$ 0	0.253 $\pm$ 0	0.239 $\pm$ 0	0.137 $\pm$ 0
<b>Chemical formula</b>									
bace	0.62 $\pm$ 0	<b>0.704<math>\pm</math>0</b>	0.678 $\pm$ 0	0.483 $\pm$ 0	0.673 $\pm$ 0	0.694 $\pm$ 0	0.583 $\pm$ 0	0.621 $\pm$ 0	0.688 $\pm$ 0
BBBP	0.693 $\pm$ 0	<b>0.715<math>\pm</math>0</b>	0.603 $\pm$ 0	0.553 $\pm$ 0	0.63 $\pm$ 0	0.632 $\pm$ 0	0.501 $\pm$ 0	0.626 $\pm$ 0	0.646 $\pm$ 0
clintox	<b>0.634<math>\pm</math>0</b>	0.365 $\pm$ 0	0.238 $\pm$ 0	0.0869 $\pm$ 0	0.0869 $\pm$ 0	0.0869 $\pm$ 0	0.0868 $\pm$ 0	0.0869 $\pm$ 0	0.0869 $\pm$ 0
HIV	<b>0.471<math>\pm</math>0</b>	0.465 $\pm$ 0	0.159 $\pm$ 0	0.0407 $\pm$ 0	0.0273 $\pm$ 0	0.0407 $\pm$ 0	0.0205 $\pm$ 0	0.0273 $\pm$ 0	0.0407 $\pm$ 0

2288

2289

2290

2291

2292

2293

2294

2295

2296

2297

2298

2299

2300

2301

2302

2303

2304

2305

2306

2307

2308

2309

2310

2311

2312

2313

2314

2315

2316

2317

2318

2319

2320

2321

## 2322 T COMPARISON WITH NATIVE MULTICLASS APPROACHES

2324 The training time complexity of CDA for a multiclass problem is on the order of  $C^2 * O(NM + N \log N)$ , where  $C$  is the number of classes,  $N$  is the number of samples per class, and  $M$  is the  
 2325 feature dimension. However, Since  $C$  is typically much smaller than  $NM$ , it is negligible, and the  
 2326 overall complexity effectively becomes  $C^2 * O(NM + N \log N)$ , similar to the binary case.  
 2327

2328 We think that exploring an inherent multiclass extension of CDA is an important direction, especially  
 2329 given that other classifiers such as LDA and SVM have their inherent multiclass approach. In the  
 2330 cases where  $C$  is large and not negligible, inherent multiclass approaches offer attractive lower  
 2331 computational complexity with respect to the number of classes ( $C$  versus  $C(C - 1)/2$  discriminants  
 2332 in pairwise schemes).

2333 In this section, we evaluated inherent multiclass LDA, SVM, and PLS-DA. The results in Table  
 2334 17 show that although these inherent multiclass methods indeed achieve faster training times, their  
 2335 predictive performance is consistently lower than that obtained by their binary counterparts combined  
 2336 with an external multiclass strategy. This makes sense since these methods are natively designed  
 2337 for binary classification such as the margin in SVM, and their optimization objective becomes less  
 2338 effective when extended to an inherent multiclass setting.

2339 Since we have evidence that the inherent multiclass approaches for LDA and SVM performed worse  
 2340 than their one-versus-one scheme, we decided to leave the investigation the multiclass CDA to future  
 2341 study.

2342 **Table 17: AUROC (Multiclass Prediction Performance)**

Dataset	CDB0	CDA	LDA	Inherent multiclass LDA	SVM	Inherent multiclass SVM	PLSDA	Inherent multiclass PLSDA
<b>Standard images</b>								
MNIST	0.897±0.01	0.963±0.005	0.958±0.006	0.926±0.009	<b>0.966±0.005</b>	0.953±0.005	0.956±0.006	0.913±0.01
USPS	0.914±0.01	0.971±0.004	0.969±0.006	0.95±0.008	<b>0.973±0.005</b>	0.967±0.007	0.968±0.006	0.939±0.01
EMNIST	0.773±0.01	0.896±0.008	0.879±0.009	0.796±0.01	0.892±0.008	0.855±0.01	0.82±0.02	0.544±0.009
CIFAR10	0.599±0.02	0.671±0.02	0.627±0.01	0.651±0.01	0.663±0.02	0.651±0.02	0.624±0.01	0.647±0.02
SVHN	0.522±0.006	<b>0.638±0.01</b>	0.531±0.007	0.541±0.007	0.558±0.01	0.52±0.003	0.528±0.007	0.532±0.008
flower	0.61±0.03	0.666±0.03	0.554±0.02	0.618±0.02	<b>0.632±0.03</b>	0.623±0.02	0.507±0.003	0.616±0.02
GTSRB	0.589±0.01	0.878±0.01	0.821±0.02	0.886±0.007	<b>0.983±0.003</b>	0.974±0.003	0.551±0.01	0.902±0.01
STL10	0.607±0.02	<b>0.655±0.02</b>	0.596±0.02	0.623±0.02	0.653±0.02	0.625±0.02	0.5±0.002	0.619±0.02
FMNIST	0.836±0.03	0.917±0.02	0.92±0.02	0.902±0.02	<b>0.924±0.02</b>	0.919±0.02	0.904±0.02	0.9±0.02
<b>Medical images</b>								
dermamnist	0.614±0.03	<b>0.658±0.03</b>	0.588±0.02	0.588±0.02	0.606±0.03	0.5±0	0.518±0.009	0.561±0.02
pneumoniamnist	0.837±0	0.933±0	0.912±8e-17	0.912±0	<b>0.941±0</b>	0.5±0	0.913±6e-17	0.91±0
retinamnist	0.575±0.04	<b>0.622±0.04</b>	0.592±0.03	0.57±0.02	0.603±0.04	0.5±0	0.517±0.009	0.5±0.009
breastmnist	0.66±0	<b>0.763±8e-17</b>	0.703±0	0.656±6e-17	0.709±0	0.5±0	0.467±3e-17	0.523±0
bloodmnist	0.789±0.04	0.88±0.03	0.817±0.03	0.859±0.03	<b>0.895±0.03</b>	0.5±0	0.716±0.05	0.826±0.04
organamnist	0.815±0.03	0.888±0.02	0.885±0.03	0.851±0.03	<b>0.897±0.02</b>	0.5±0	0.878±0.03	0.803±0.04
organcmnist	0.809±0.03	<b>0.869±0.03</b>	0.833±0.03	0.84±0.03	0.847±0.03	0.5±0	0.827±0.03	0.812±0.03
organismnist	0.694±0.03	<b>0.761±0.03</b>	0.735±0.03	0.725±0.02	0.746±0.03	0.5±0	0.73±0.03	0.684±0.03
organmnist3d	0.867±0.03	0.913±0.02	0.903±0.03	0.844±0.03	<b>0.925±0.02</b>	0.5±0	0.505±0.008	0.498±0.005
nodelemnist3d	0.715±0	<b>0.781±0</b>	0.732±8e-17	0.722±0	0.724±0	0.5±0	0.508±6e-17	0.448±0
fracturemnist3d	<b>0.622±0.04</b>	0.518±0.01	0.554±0.04	0.52±0.03	0.576±0.009	0.5±0	0.478±0.03	0.506±0.002
adrenalmnist3d	0.653±8e-17	<b>0.756±8e-17</b>	0.692±0	0.671±6e-17	0.665±6e-17	0.5±0	0.51±6e-17	0.487±0
vesselmnist3d	0.605±8e-17	<b>0.685±0</b>	0.681±8e-17	0.712±0	0.6±0	0.5±0	0.521±6e-17	0.555±0
synapsemnist3d	0.539±8e-17	<b>0.544±8e-17</b>	0.508±0	0.53±6e-17	0.539±0	0.5±0	0.515±0	0.488±0
<b>Chemical formula</b>								
bace	0.621±8e-17	<b>0.705±0</b>	0.684±8e-17	0.696±6e-17	0.637±6e-17	0.699±0	0.497±4e-17	0.508±0
BBBP	0.711±8e-17	<b>0.743±0</b>	0.693±0	0.691±0	0.697±0	0.678±6e-17	0.506±0	0.547±0
clintox	<b>0.65±0</b>	0.575±0	0.543±0	0.562±0	0.514±6e-17	0.549±0	0.621±6e-17	0.584±6e-17
HIV	0.6±0	<b>0.616±8e-17</b>	0.537±0	0.536±0	0.506±0	0.511±0	0.51±6e-17	0.492±3e-17

2376 **U RELATION BETWEEN CDA AND NEURAL NETWORK**  
23772378 **U.1 COMPARISON BETWEEN CDA WITH NEURAL NETWORK**  
2379

2380 Given that neural networks are prevalent, especially deep learning architectures such as ResNet, we  
2381 made a comparison between linear CDA and them. Specifically, we compared CDA with ResNet-18,  
2382 and included a single-hidden-layer MLP as the baseline for the simplest neural network. We tested  
2383 on 6 3D medical image datasets of MedMNIST. The results are shown in Appendix Table. 18. The  
2384 parameters of MLP and ResNet-18 are: 100 training epochs; SGDM optimizer; initial learning rate  
2385 0.01 with decay of 50% every 30 epochs. For MLP, we used ReLU activation function; the number  
2386 of hidden-layer neurons was set to approximately  $\sqrt{\# \text{samples} \times \# \text{features}}$ . We can see that even  
2387 compared with the more complex architecture ResNet, CDA still outperforms on the adrenalmnist3d  
2388 dataset. In addition, CDA demonstrates a better performance than MLP, outperforming on 4 out of 6  
2389 datasets.

2390 **Table 18: Test set multiclass AUROC on MedMNIST3D datasets.**

Method	CDA	MLP	ResNet-18
organmnist3d	0.913	0.936	<b>0.977</b>
nodelemnist3d	0.781	0.766	<b>0.850</b>
fracturemnist3d	0.518	0.564	<b>0.611</b>
adrenalmnist3d	<b>0.756</b>	0.635	0.737
vesselmnist3d	0.685	0.674	<b>0.769</b>
synapsemnist3d	0.544	0.507	<b>0.656</b>

2398 **U.2 COMBINING CDA WITH NEURAL NETWORK**  
2399

2400 We conducted two experiments using more sophisticated, learned features. First, we used CDA to  
2401 initialize the final linear layer of a ResNet-18 by taking an ImageNet-pretrained ResNet-18 and  
2402 performing transfer learning on SVHN. Instead of randomly initializing the final linear layer, we  
2403 initialized it using class-wise averaged CDA weights. This led to clear improvements over the  
2404 baseline, yielding higher test accuracy and faster training, as measured by area-across-epochs (AAE).  
2405 Second, we evaluated Gaussian kernel CDA as a nonlinear model and compared it to a single-hidden-  
2406 layer MLP (512 input features  $\rightarrow$  45 hidden units  $\rightarrow$  10 output neurons). Because kernel CDA  
2407 requires kernel matrix computations that scale quadratically with the number of samples, we used  
2408 the same reduced dataset (24k/99k) employed in our first manuscript. Kernel CDA outperformed  
2409 the MLP baseline, and a CDA-initialized MLP achieved similar test performance to the randomly  
2410 initialized MLP while training much faster, as shown by both AAE and the training curve comparison  
2411 in Figure 15.

2412 These experiments demonstrate that CDA is well-performing and flexible: it can act as a strong  
2413 initializer in neural networks—whether for a simple linear layer or an MLP—improving both  
2414 convergence speed and final performance, and it can be extended to kernelized nonlinear variants that  
2415 outperform standard nonlinear baselines.

2416 When the data is complex with strong nonlinear relations, it is also feasible to combine linear CDA  
2417 with prevalent deep learning architectures by leveraging deep features. We validated this combined  
2418 approach on SVHN by extracting features from the penultimate layer of an ImageNet-pretrained  
2419 ResNet-18 and training linear CDA on these features. For prediction, we used the pretrained ResNet  
2420 weights together with the trained CDA weights. As shown in Appendix Table 19, this combination  
2421 significantly outperforms applying linear CDA directly on the raw data, illustrating the strong potential  
2422 of CDA for handling complex real-world datasets with substantial nonlinear structure.

2423  
2424  
2425  
2426  
2427  
2428  
2429

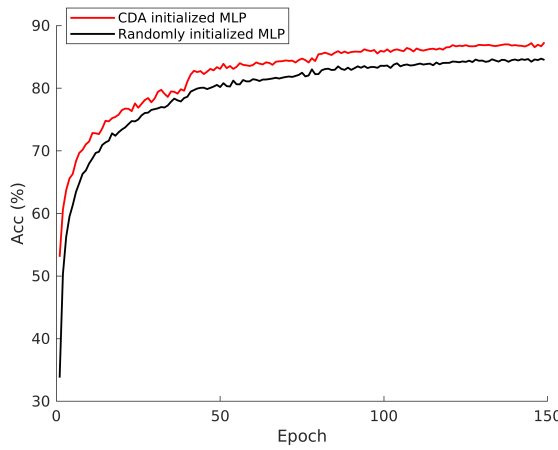
2430  
2431  
2432  
2433  
2434  
2435  
2436

2437 Table 19: Test set multiclass prediction performance on the SVHN dataset (ResNet-18 pretrained  
2438 feature extractor + classifier).

Method	AUROC	AUPR	Fscore	ACscore	Acc	AAE
CDA initialized linear layer	<b>0.79</b>	<b>0.797</b>	<b>0.795</b>	<b>0.748</b>	<b>0.664</b>	<b>0.637</b>
Randomly initialized linear layer	0.78	0.795	0.789	0.73	0.653	0.621
Gaussian CDA	<b>0.815</b>	<b>0.816</b>	<b>0.815</b>	<b>0.783</b>	<b>0.683</b>	-
CDA initialized MLP	0.796	0.799	0.798	0.757	0.674	0.824
Randomly initialized MLP	0.795	0.798	0.798	0.755	0.666	0.797

2445 Hyperparameters: 150 epochs; Batch size = 128; Initial LR = 0.005 with 50% decay every 40 epochs; L2  
2446 regularization =  $10^{-4}$ . For nonlinear method tests (the last 3), we take a subset=24000/99289 as total data due to  
2447 time limit to perform kernel method on full dataset

2448  
2449  
2450  
2451  
2452  
2453  
2454  
2455  
2456  
2457  
2458  
2459  
2460  
2461  
2462



2477 Figure 15: Training curve comparison between CDA initialized MLP and randomly initialized MLP.  
2478

2479  
2480  
2481  
2482  
2483

2484 **V COMPUTATION CONDITIONS**  
24852486 The simulations were performed on a Lenovo P620 workstation (a AMD Ryzen Threadripper PRO  
2487 3995WX, 64 CPU cores at maximum 4.308GHz, 256GB memory) with single-thread computing.  
2488 The large-scale tests on single-cell data were performed on a server (two AMD EPYC 7H12 CPUs,  
2489 each with 64 CPU cores at maximum 2.6GHz, 4096 GB memory) with single-thread computing.  
2490 MATLAB 2023b was used as the platform to run the main algorithms. The "tic" and "toc" functions  
2491 in Matlab were used to measure the computation time.  
24922493 **W LICENSING**  
24942495 The code packages libSVM and liblinear are with BSD 3-Clause license. Matlab is with a paid  
2496 proprietary license.  
24972498 **X CODE AVAILABILITY**  
24992500 We released the Matlab and Python code for the CDA algorithm, on [https://anonymous.4open.science/r/Centroid\\_discriminant\\_Analysis-5444](https://anonymous.4open.science/r/Centroid_discriminant_Analysis-5444). Kernel method is cur-  
2501 rently supported on the Matlab version.  
25022503 **Y CLAIM OF THE LLM USAGE**  
25042505 We used LLM-based tools to improve the language and flow; the principles, core logic, and innovations  
2506 are entirely the authors'.  
2507  
2508  
2509  
2510  
2511  
2512  
2513  
2514  
2515  
2516  
2517  
2518  
2519  
2520  
2521  
2522  
2523  
2524  
2525  
2526  
2527  
2528  
2529  
2530  
2531  
2532  
2533  
2534  
2535  
2536  
2537